Engineering Synechococcus sp. UTEX 2973 and Devising Carbon Dioxide Uptake Strategies for Amino Acid and Bioplastic Production

by

Zachary Anthony Dookeran

A Dissertation Presented in Partial Fulfillment
of the Requirements for the Degree
Doctor of Philosophy

Approved February 2022 by the
Graduate Supervisory Committee:

David R. Nielsen, Chair
Xuan Wang
Brent L. Nannenga
Arul M. Varman
Christie A. M. Peebles

ARIZONA STATE UNIVERSITY

May 2022

ABSTRACT

Amino acids and related targets are typically produced by well-characterized heterotrophs including *Corynebacterium glutamicum* and *Escherichia coli*. Recent efforts have sought to supplant these sugar-intensive processes through the metabolic engineering of cyanobacteria, which instead can directly utilize atmospheric carbon dioxide (CO_2) and sunlight. One of the most promising among recently discovered photoautotrophic strains is *Synechococcus elongatus* UTEX 2973 (hereafter UTEX 2973), which has been reported to have doubling times as low as 1.5 hours. While encouraging, there are still major challenges preventing the widespread industrial acceptance of engineered cyanobacteria, chief among them is the scarcity of genetic tools and parts with which to engineer production strains. Here, UTEX 2973 was engineered to overproduce L-lysine through the heterologous expression of feedback-resistant copies of aspartokinase lysC and the L-lysine exporter ybjE from *Escherichia coli*, as aided by the characterization of novel combinations of genetic parts and expression sites. At maximum, using a plasmid-based expression system, a L-lysine titer of 556 ± 62.3 mg/L was attained after 120 hours, surpassing a prior report of photoautotrophic L-lysine bioproduction. Modular extension of the pathway then led to the novel photosynthetic production of the corresponding diamine cadaverine (55.3 ± 6.7 mg/L by 96 hours) and dicarboxylate glutarate (67.5 ± 2.2 mg/L by 96 hours). Lastly, mass transfer experiments were carried out to determine if the solubility of CO_2 in and its rate of mass transfer to BG-11 media could be improved by supplementing it with

various amines, including cadaverine. Ultimately, however, cyanobacteria grown in the presence of all tested amines was worse than in BG-11 alone, demonstrating the need for additional tolerance engineering to successfully implement this strategy.

ACKNOWLEDGMENTS

There are literally too many people to name, this block of text is undoubtedly leaving out so many important people in my life over the last seven and a half years. Thank you, obviously, to David Nielsen for taking a chance on me when it felt like nobody else would, for giving me the room to grow as a scientist and a thinker, and for being there to guide my studies when I inevitably ended up lost on some goose chase. Thank you to Drs. Xuan Wang, Arul Varman, Brent Nannenga, and Christie Peebles for being on my committee and for your constructive criticism over the years. Thank you to all of my colleagues, too many of which to name; those who moved on before me in the Nielsen lab: Daniel Herschel, John Hagstrom, Alexander Mayhob and Lizbeth Nieves, as well as Drs. Brian Thompson, Kyle Staggs, Michael Machas, and Andrew Flores; those who I left behind: Amanda Godar, Arren Liu, Cody Kamoku, Sydney Parrish, Dr. Stefan Tekel and especially Dr. Christopher Jones, who regularly challenged my preconceptions and opinions. Thank you to the undergraduates who have graced the Nielsen lab including but certainly not limited to Cameron McAllister, Omar Abed, Christopher Gregson, Gavin Steeber, Brendan Brookhouser, Cheyanna Cooper, and Ashley Straub. Thank you to members of the Wang lab including Rodrigo Martinez, Moses Onyeabor, Rebecca Condruti and Drs. Gavin Kurgan and Steven Holland. Thank you to members of the Varman lab including Apurv Mhatre, Nima Hajinajaf, and Dr. Aditya Sarnaik. Thank you to members of the Nannenga lab including Kyle Swain and Dr. Guanhong Bu. Thank you to Dr. Willem Vermaas and members of his lab

including Wes Swenson, Christopher Ashe, Anna Keilty and Drs. Shuqin Li, Tyson Burch and Daniel Brune. Thank you to Dr. Kaushal Rege and all those in his lab over the years including Rajesh Nitiyanandan, Deepanjan Ghosh, and Drs. Sai Pavan, Karthik Pushpavanam, Subhadeep Dutta, Russell Urie, Sheba Goklany, and Matt Christensen. Thank you to Dr. Huimin Zhao, who gave me my start in the world of synthetic biology, and members of his lab, including but not limited to Ran Chao, Ryan Cobb, and Drs. Sam Hamedi Rad, Dawn Eriksen, Xueyang Feng, Daniel Coursolle, and Jiazhang Lian. Thank you to even more individuals yet including Dr. So Hirata, Dr. Yuji Aso, Fred Peña, Carina Prell, Arnaud Taton, Dr. Susan Golden, Michelle Liberton, Dr. Abhinav Acharya and Sahil Inamdar.

Thank you to Timmy Marrinan for introducing me to literally all of my friends in the state of Arizona, and thank you to those many friends. Thank you to the entire Codex DNA team for rooting me on as I finished up my PhD whilst working full-time.

Thank you to my parents, Drs. Keith Dookeran and Janine Yasmin Khan, who continually pushed me to reach the heights I now currently sit atop. Thank you to my dogs Padme and Siegfried, who oscillated between making my hectic life even harder and being the only bright spot on some of my worst days.

Above all thank you to Jessica Lily Wong, my amazing partner who I unequivocally do not deserve. I am both shocked that you put up with me all this time and grateful to have your support through something that I could never have accomplished by myself.

TABLE OF CONTENTS

Page

CHAPTER Page

LIST OF TABLES

LIST OF FIGURES

Figure Page

CHAPTER 1

RECENT PROGRESS TOWARDS THE INDUSTRIALIZATION OF PHOTOAUTOTROPHIC BIOPRODUCTION PLATFORMS

ABSTRACT

Cyanobacteria, which photosynthesize by assimilating sunlight and atmospheric CO_2, provide an appealing contrast to traditional industrial microbes which consume energy-intensive and costly carbohydrate feedstocks. Photoautotrophic implementation within the biotechnology sector, however, is dependent upon overcoming several key, technical challenges. Mainly, there is a paucity of genetic parts and tools to engineer cyanobacteria when compared to well-established model organisms such as *Escherichia coli*. For instance, there are currently few validated neutral sites and shuttle vectors with which to express gene constructs. Expansion of the cyanobacterial “toolbox” will improve the design-build-test cycle and lead to more effective strain mutations. New photoautotrophic strains have emerged which possess superior growth traits, reaching higher thresholds for CO_2 and light limitations. These newer strains, while encouraging for scale-up in bioindustry, are even more limited in the set of tools with which they can be manipulated. This chapter covers these challenges in more detail, while describing the genetic elements available and opportunities for improvement of photosynthetic bioproduction platforms.

1.1 Introduction

Photoautotrophic cyanobacteria, which directly utilize atmospheric CO_2 and sunlight as substrates, offer an opportunity to supplant conventional industrial bioprocesses which rely upon by sugar-intensive, heterotrophic organisms. To date, photoautotrophic biocatalysts have been developed to produce a wide range of chemicals (Table 1.01), matching many of the successes of conventional chasses: alcohols[1–3], fatty acids[4,5], and various alkenes[6–9] among them. Further targets include the aromatic amino acids L-phenylalanine, L-tyrosine, and L-tryptophan, all of which were derived from the well-characterized shikimate pathway[10,11] of *Synechocystis* sp. PCC 6803 (hereafter PCC 6803). Another biogenic amino acid, L-lysine, has also been produced through the heterologous expression of key pathway genes[12] in *Synechococcus* sp. PCC 7002 (hereafter PCC 7002). Amino acids can furthermore potentially act as precursors for bioplastic monomers, as seen with the decarboxylation of L-lysine to cadaverine and L-arginine to putrescine. Other monomer targets are reached independent of amino acids and have already been produced by photoautotrophs. Recent successes include PCC 6803-based production of ethylene[13], L-lactate[14,15], 3-hydroxypropionic acid[16], and 3-hydroxybutyric acid[17], and the production of L-lactate[18] in *Synechococcus elongatus* PCC 7942 (hereafter PCC 7942), succinic acid[19], and 3-hydroxypropionic acid[20]. Cyanobacteria have even been engineered to uptake xylose in a photomixotrophic fashion towards the production of 3-hydroxypropionic acid[21]. As the capabilities of cyanobacterial chasses towards amino acid precursor

production improves, it stands to reason that the list of photosynthesized bioplastic monomers and other valuable targets will grow as well.

Table 1.01 Comparison of the Photosynthetic Production of Various Amino Acids and Bioplastic Monomers by Engineered Strains of Cyanobacteria

	Product	Host	Conditions (CO2, Temp., LI)	Final Titer (mg/L)	Product-to-Biomass Yield (mg/gDCW)	Duration (days)	Reference
Amino Acids	L-lysine	PCC 7002	1% CO_2, 37°C, 200 µE/m^2/s	454.7	164.5	20	Korosh et al 2017[12]
	L-phenylalanine	PCC 6803	3% CO_2, 30°C, 50 µE/m^2/s	579.8	904	10	Brey et al 2020[10]
	L-tyrosine	PCC 6803	3% CO_2, 30°C, 50 µE/m^2/s	41.1	64	10	Brey et al 2020[10]
	L-tryptophan	PCC 6803	3% CO_2, 30°C, 240 µE/m^2/s	212	57.5	10	Deshpande et al 2020[11]

	Product	Host	Conditions (CO2, Temp., LI)	Final Titer (mg/L)	Product-to-Biomass Yield (mg/gDCW)	Duration (days)	Reference
Bioplastic Monomers	3-hydroxybuyrate	PCC 6803	Air, 30°C, 120 µE/m^2/s	533.4	n.d.	21	Wang et al 2013[17]
	3-hydroxypropionic acid	PCC 6803	Air, 30°C, 50 µE/m^2/s	837.2	359.3	6	Wang et al 2016[16]
	3-hydroxypropionic acid	PCC 7942	Air, 30°C, 50 µE/m^2/s	665	n.d.	12	Lan et al 2015[20]
	3-hydroxypropionic acid	UTEX 2973	Air + 6 g/L xylose, 41°C, 200 µE/m^2/s	120	n.d.	5	Yao et al 2022[21]
	Succinic acid	PCC 7942	Air, 30°C, 30 µE/m^2/s	430	n.d.	8	Lan and Wei 2016[19]
	L-lactate	PCC 6803	Air, 30°C, 30 µE/m^2/s	288.3	34.1	17	Angermayr et al 2012[14]
	L-lactate	PCC 7942	Air, 30°C, 18h L / 6h D	56.3	n.d.	4	Niederholtmeyer et al 2010[18]
	Ethylene	PCC 6803	5% CO_2, 30°C, 50 µE/m^2/s	7.125/h	n.d.	2	Ungerer et al 2012[13]

Despite the inherent advantages that would be afforded by cyanobacterial biorefineries, one challenge facing the conventional, “model” host strains (e.g., PCC 6803, PCC 7002, PCC 7942) is their relatively slow growth rates (owing to limitations in the supply of light and/or carbon), which ultimately also translates into low rates of productivity. Efforts to engineer more efficient photosynthetic activity in cyanobacteria range from the active transport systems delivering CO_2 and bicarbonate into the cell, the carboxysome responsible for concentrating CO_2 levels, and the enzyme ribulose biphosphate carboxylase-oxygenase (hereafter RubisCO) localized inside said carboxysome, which directly fixes carbon into central metabolism (Figure 1.01). Overexpressing RuBisCO or downstream genes in the Calvin-Benson-Bassham cycle has led to improved photosynthetic titers of isobutyraldehyde[22], ethanol[23], and free fatty acids[24]. Protein engineering efforts to improve RuBisCO activity have proved difficult, as there is invariably a trade-off between higher catalytic rates and stronger specificity for CO_2 over O_2[25]. Upstream of RuBisCO, it is unclear how important carboxysome engineering is towards photosynthesis of valuable products; it was demonstrated in PCC 7002[26] that the carboxysome is not a requirement for cyanobacterial fitness or bioproduction so long as cultures are subjected to a high CO_2 media environment. Furthermore, only a single study has successfully improved C_i uptake through engineering of bicarbonate transporters, and this achievement occurred under somewhat dubious media conditions where wild-type PCC 6803 grew poorly under air and standard light intensity[27].

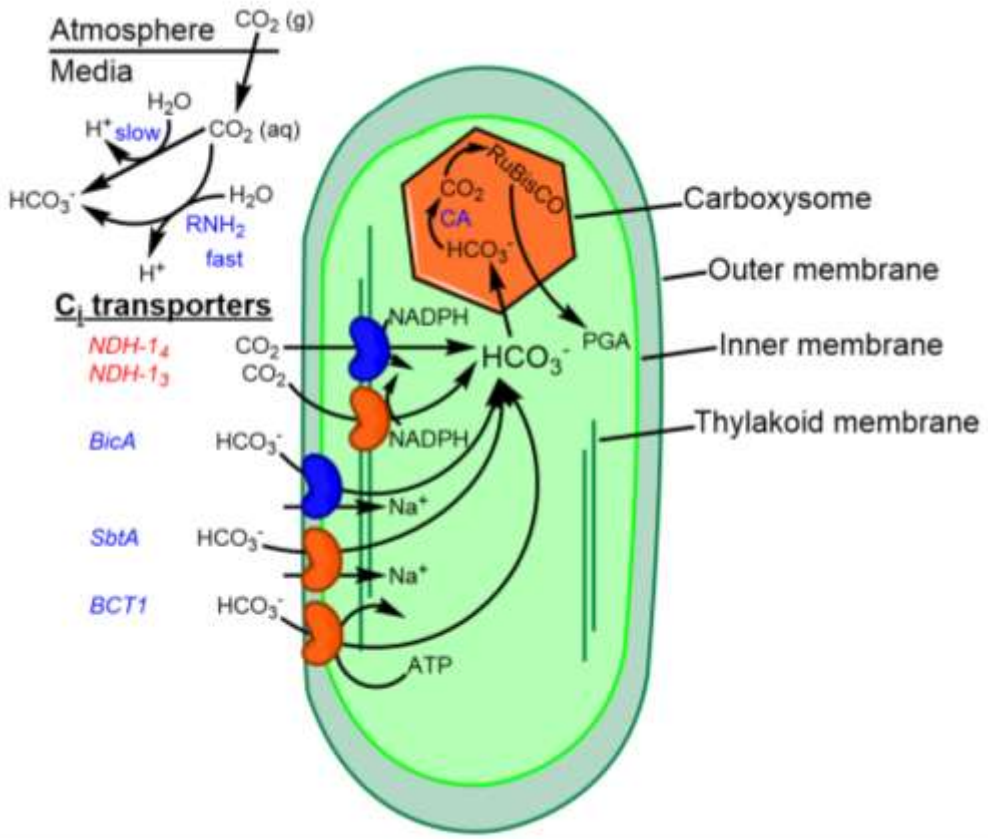

Figure 1.01 Inorganic Carbon Flux from Atmosphere to Metabolism in Cyanobacteria

Diagram illustrating the mass transfer of atmospheric CO_2 i) into aqueous media where it either slowly equilibrates to HCO_3^- or is catalyzed by the addition of an amine specie; ii) the C_i transporters deliver HCO_3^- into the cytosol; iii) carbonic anhydrase (CA) reverts HCO_3^- to CO_2 inside of the carboxysome, subsequently converted to phosphoglycerate (PGA) by RuBisCO and able to cross back out of the carboxysomal shell. Induced transporters are shown in orange, and constitutive ones are shown in blue. Figure adapted from G. D. Price 2011[28].

Taken together, the difficulties experienced by researchers attempting to improve carbon flux of model cyanobacteria through rational design methods indicates that solutions may lie with other photoautotrophic chasses entirely. Recently discovered and/or characterized strains of cyanobacteria have been reported that demonstrate faster growth rates than their more well-characterized

counterparts, notably including *Synechoccocus elongatus* sp. UTEX 2973[29] (hereafter UTEX 2973) and *Synechococcus* sp. PCC 11901 (hereafter PCC 11901)[30]. Among these, UTEX 2973, a freshwater cyanobacterium, is closely related to both *S. elongatus* sp. PCC 6301 and PCC 7942, allowing many genetic parts/tools and physiological insights to be readily translated over from these organisms. At the same time, UTEX 2973 metabolizes carbon more efficiently, as it avoids a key bottleneck present in both PCC 6803[31] and PCC 7942[32] with regards to pyruvate synthesis, through the decoupling of pyruvate kinase inhibition from high rates of photosynthesis[33]. UTEX 2973's phenotypic improvements have been demonstrated to benefit from commensurate improvements to the delivery of CO_2 into the culture media[34]. Such findings indicate that physicochemical strategies to increase dissolved carbon could play an important role in optimizing growth, including mechanisms to more efficiency sparge CO_2 into the culture medium[35], maintaining higher pHs to encourage conversion of aqueous CO_2 to bicarbonate[36] (the carbon species preferred for uptake by cyanobacteria), and employing amine species as bicarbonate catalysts31. Although so far only to a limited extent, UTEX 2973 has already been shown to be capable of serving as a robust host for engineering the photosynthetic production of various biochemicals, including 3-hydroxypropionic acid[21], hapalindoles[38] and sucrose[39,40]. Importantly, in contrast to PCC 7002, whose doubling time has been reported as 4.1 hours[29], UTEX 2973 has a doubling time as fast as just 1.5 h under optimal conditions[41].

1.2 Obstacles Related to the use of Fast-Growing Cyanobacteria for Industrial Bioproduction

At a minimum, metabolic engineering of cyanobacteria requires the ability to introduce and control the expression of various biosynthetic genes of interest. That said, different cyanobacterial species can differ considerably with respect to suitable methodologies and available parts for gene expression[42]. For instance, in most cases, metabolic engineering of cyanobacteria typically involves the chromosomal integration of desired genetic elements. This contrasts most lab scale work with more ubiquitous strains like *E. coli*, where utilization of plasmid-based constructs allows for comparatively faster design-build-test cycles[43] and enhanced expression levels (due to increased copy number[44]). For a given strain of cyanobacteria, there are typically a handful of validated "neutral sites" that are commonly used for integrating expression cassettes[42]. However, the disruption of these ORFs, despite their unknown function, can lead to negative outcomes for the engineered strain, as it is likely that evolution finds the entirety of the cyanobacterial genome advantageous depending on the conditions. Furthermore, parallel engineering of multiple integrated constructs can lead to a scarcity of available validated neutral sites and/or unique antibiotic cassettes. Sections 1.2.1 and 1.2.2 next provide an overview of known cyanobacterial neutral sites and expression plasmids, respectively.

1.2.1 Currently Validated Neutral Sites in Model Cyanobacteria

There exist a number of commonly employed neutral sites in model cyanobacteria that serve as genomic loci for the integration of expression cassettes. As seen in Table 1.01, these differ between strains and many do in fact code for proteins; although most have unknown functions and/or cause no change in phenotype when disrupted under standard experimental conditions.

Table 1.02 List of Common Neutral Sites Utilized to Engineer Model Cyanobacteria.

	Neutral site	Notes	Reference
PCC 6803	*slr0168*	Protein of unknown function	Sergeyenko and Los 2000[45]
	sll0410	Downstream of *ndhB*	Kopf et al 2014[46]
	slr2030-31	Intergenic region; *slr2031* has role under nitrogen/sulfur starvation conditions	Aoki et al 2011[47]
	slr0646	Putative carboxypeptidase	Marbouty et al 2009[48]
	slr0271		Pinto et al 2015[49]
	slr0397		Pinto et al 2015
PCC 7002	*SYNPCC7002_A0159*	Omega-3 acyl-lipid desaturase, functional at 18°C	Sakamoto et al 1997[50]
	SYNPCC7002_A2842	Pseudogene *glpK*	Begemann et al 2013[51]
	SYNPCC7002_A0935-36	Intergenic region	Davies et al 2014[52]
	SYNPCC7002_A0932-33	Non-coding region	Ruffing et al 2016[53]
	SYNPCC7002_A1202-2304	Non-coding region	Ruffing et al 2016
	SYNPCC7002_A0026-27	Non-coding region	Wang et al 2019[54]
PCC 7942	*NS1*		Bustos and Golden 1992[55]
	NS2		Andersson et al 2000[56]
	NS3		Niederholtmeyer et al 2010[18]

For its part, PCC 7942 has three neutral sites that are used in the large majority of reported studies, aptly annotated as NS1[55], NS2[56], and NS3[18]. These neutral sites, despite their long history of use, have largely escaped critical interrogation in the way of PCC 6803 or PCC 7002, an especially impressive feat for the former site, which was acknowledged to have been discovered by an undergraduate researcher around 30 years ago[55]. Similar to other model organisms, integration of cassettes into these neutral sites often presents no phenotypic change to PCC 7942 under standard conditions[57]. UTEX 2973, being a close relative, has been engineered by several studies to express genes in NS3 successfully[39,40].

1.2.2 Currently Validated Expression Plasmids in Model Cyanobacteria

Apart from chromosomal integration at specific neutral sites, there do exist a handful of common, broad-host-range plasmids that can also be employed in cyanobacteria. Perhaps the most common of these is RSF1010, an incQ group plasmid identified originally in *E. coli*[58]. Broad-range-host plasmids from the incQ family have long held an interest to cyanobacterial researchers[59], as they possess host-independent replication machinery and thus can affect heterologous gene expression even in under-characterized organisms[60]. More recently, efforts have been made to streamline the engineering and use of RSF1010-based vectors across diverse model cyanobacterial strains[61], including the versatile CYANO-VECTOR Assembly Portal[62,63], through which improvements have been made in copy number and conjugation efficiency.

Aside from broad-host-range vectors, there are also a number of shuttle vectors which have been developed using various origins of replication derived from endogenous plasmids. For example, an eYFP cassette was expressed in PCC 6803 on the small endogenous plasmid pCC5.2 at a strength 8- to 14-times that observed when the same cassette was inserted into putative non-transcribing chromosomal loci[64]. On the other hand, plasmid mutations were maintained at a reduced frequency to the chromosome in the absence of antibiotic selection. Recent work has demonstrated that merodiploid integration into an essential cyanobacteria gene can result in minimal fitness loss, while quickly reverting to the endogenous gene once selection is removed[65]. Similar behavior with pCC5.2 points to its essentiality and by extension its potential inadequacy as a common shuttle vector. The creation of antibiotic-dependent shuttle vector expression systems has since been expanded to PCC 6803's other two small endogenous plasmids60, pCA2.4 and pCB2.4, widening the potential regions with which desired gene cassettes can be stably maintained.

Efforts have also been made to exploit PCC 7002's smallest (and highest copy number) endogenous plasmid pAQ1 for use as a shuttle vector. However, pAQ1 has been determined to be essential, with attempts to cure it having failed[67]. Therefore, steps must therefore be taken to ensure homologous integrations into pAQ1 remain stable. The shuttle vector pAQ-EX1[68], for example, contains the putative origin of the PCC 7002 plasmid as well as the origin and ampicillin cassette from the common *E. coli* vector pUC19.

PCC 7942 has options for shuttle vectors not available to other model photoautotrophs, making it, and by extension UTEX 2973, powerful platforms for the testing of transient expression cassettes. The above plasmid pAQ-EX1 was found to be stably transformed and maintained in PCC 7942 owing to the latter organism not having its own excluding pAQ1 origin[69]. The shuttle vector pAM4788 further represented a major breakthrough in episomal photoautotrophic expression due to its pairing of the small endogenous pANS backbone with a toxin-antitoxin cassette from PCC 6803 (again taking advantage of that particular system not being native to PCC 7942). This plasmid was stably expressed in the absence of antibiotics even after 5 weeks of subculturing[70], representing one of the best attempts made yet at a plasmid-based expression platform that can rival those routinely employed in heterotrophs.

1.3 Tools for Controlling Gene Expression in Model Cyanobacteria

In addition to expanding the availability of reliable locales for incorporating gene cassettes in model cyanobacterial strains, there has also been a recent expansion in the number and diversity of genetic elements available for controlling their expression. Many promoters used in photoautotrophs are tied to endogenous, light-dependent processes and thus act in a constitutive manner when culturing under continuous illumination. These include P_{psbA2} (from photosystem II) and P_{cpcB} (involved in C-phycocyanin beta subunit biosynthesis) from PCC 6803, the latter of which has been successfully ported over for use in PCC 7002[67,71,72] and PCC 7942[73], as well as adapted into a “super-strong”

variant, P_{cpc560}[74]. The promoter associated with expression of carbon-fixing RuBisCo, P_{rbcL}, also functions constitutively under high light conditions, and is commonly utilized in literature. Direct comparison by Liu and Pakrasi[66] determined P_{cpcB} to be roughly an order of magnitude stronger than either P_{psbA2} or P_{rbcL}. Heterologous constitutive promoters have been tested to mixed results, with *E. coli*'s P_{trc10} and the bacteriophage-derived $P_{\lambda cI}$ demonstrating strong expression of a fluorescent reporter[61,66] while others including P_{luxR} having proven ineffective., There are also many other promising constitutive native promoters available that are not associated with light or carbon metabolism, including P_{sll514} and $P_{sll1626}$ in PCC 6803[66].

By contrast, PCC 7002 suffers from an overall lack of genetic parts, as evidenced by the long and continuing role played by PCC 6803's *cpcB* promoter as a well characterized constitutive promoter[71]. A range of strong constitutive synthetic promoters ported from *E. coli* have additionally been demonstrated to work in PCC 7002, with P_{J23119} displaying the strongest expression among them[71].

Meanwhile, in applications where the desired product may be toxic or burdensome on cell growth, there are several inducible systems that function in photoautotrophs. Englund and colleagues[75] characterized a range of promoters in PCC 6803 driving the expression of metal efflux pumps and determined that the nickel-associated P_{nrsB} (first interrogated by Peca and colleagues[76]) demonstrates a good fold range of strength when activated by Ni^{2+} as well as inducer specificity lacking in other metal-induced promoters. One of PCC 6803's

major shortcomings with respect to synthetic biological parts is the insensitivity of IPTG-inducible promoters when expressed heterologously[15,77], owing to structural differences between the RNA polymerases and σ factor sets employed by *E. coli* versus cyanobacteria[78]. Promoter engineering has somewhat overcome PCC 6803's disadvantage through experimenting with dual *lacO* sites and the spacing between them[79]. While tetracycline-regulated expression systems have been shown to work in PCC 6803[80], the light-sensitivity of the inducer molecule anhydrous tetracycline makes it a poor strategy for promoter control in photoautotrophs[72,81]. Recently an IPTG-inducible T7-RNA polymerase gene expression system was demonstrated as a powerful tool in PCC 7002, able to generate protein at two-thirds of total cellular protein and displaying a 60-fold dynamic range, albeit at the expense of biomass[82]. An aTc-inducible system is also viable in PCC 7002 using the tightly-regulated P_{EZtet}, as well as trans-acting small RNA systems to attenuate gene expression[72].

PCC 7942 shares many parts with its freshwater relative PCC 6803, including light-inducible and light-attenuated promoters such as P_{cpcB1}, P_{cpc560}, P_{psbA2} from both PCC 7942 and 6803, P_{psbA3}77, P_{cpcB1*}, and P_{psaA}[38], constitutive synthetic promoters such as P_{trc} and P_{J23119}[38], small molecule inducible promoters such as the IPTG/*lacI*^{q} system[38], and translational control elements such as theophylline-[84,85] and adenine-[83] inducible riboswitches.

It stands to reason that many of the genetic parts validated in PCC 7942 should be portable to UTEX 2973, given that the latter strain differs by just 55 single nucleotides polymorphisms and indels[29]. While largely true, there have

been notable differences in expression via the same promoter in each organism under similar conditions, as demonstrated when studying heterologous expression via P_{psbA} from *Amaranthus hybridus*[83,86]. In addition to better understanding the subtleties of this promoter context-dependency, there are expression sites in UTEX 2973 that remain underrepresented and unexplored in literature, including the previously mentioned NS3 and stable plasmids such as pAQ1-EX and pAM4788. Interrogation of these sites with respect to promoter parts would contribute significantly to the “toolbox” of UTEX 2973 genetic elements. The additional validation of untested genetic elements would be similarly useful to the cyanobacteria research community.

CHAPTER 2

ENGINEERING L-LYSINE OVERPRODUCTION IN THE FAST-GROWING CYANOBACTERIUM *SYNECHOCOCCUS* SP. UTEX 2973

ABSTRACT

Synechococcus sp. UTEX 2973 was systematically engineered to overproduce and secrete the amino acid L-lysine. To facilitate metabolic engineering efforts, it was first demonstrated that pAM4788, a shuttle vector previously engineered for *S. elongatus* PCC 7942, was also stably maintained in UTEX 2973. Next, the relative activities of a subset of previously uncharacterized promoters were investigated using *yemGFP* as a reporter, while also comparing the effects of both chromosomal (from neutral site NS3) and episomal (from pAM4788) expression. Using these parts, L-lysine overproduction in UTEX 2973 was engineered by introducing a feedback resistant (fbr) copy of aspartate kinase (encoded by $lysC^{fbr}$) and a L-lysine exporter (encoded by *ybjE*), both from *E. coli*. While chromosomal expression resulted in L-lysine production up to just 325.3 ± 14.8 mg/L after 120 hours, this was then further increased to 556.3 ± 62.3 mg/L via plasmid-based expression; also surpassing prior reports of photoautotrophic L-lysine bioproduction. In particular, it was noted that low expression of $lysC^{fbr}$ was ultimately required to maximize L-lysine titers and preserve strain fitness, suggesting that increased flux into the L-lysine pathways was a significant competitor for available, growth-essential resources. Meanwhile, cell growth and production were severely inhibited in the absence of

ybjE co-expression, indicating that native lysine export was limiting in UTEX 2973 and also necessary to maintain fitness.

2.1 Introduction

The discovery and characterization of *C. glutamicum* from biologic material samples[87,88] paved the way for industrial production of most canonical amino acids. Classical mutagenesis methods later yielded strains capable of accumulating significant titers of L-lysine[89], the likes of which would come to dominate the industry for roughly four decades. Elucidation of *C. glutamicum* metabolism later enabled a shift towards defined mutations[90,91], with the performance of rationally engineered L-lysine producing strains eventually surpassing that of their mutagenized predecessors[92,93]. The improved understanding of L-lysine metabolism in *C. glutamicum* has ultimately led to the identification of specific beneficial mutations. Key among these are point mutations in aspartokinase, encoded by *lysC*[94], which provide relief from feedback inhibition caused by L-lysine and L-threonine. Aspartokinase represents the first committed step in the pathway used to ultimately convert L-aspartate to L-lysine (Figure 2.01), making it a key node for controlling metabolite flux. Expression of a mutant, feedback-resistant copy of aspartokinase can be seen as single the most important feature of current industrial L-lysine producers[89].

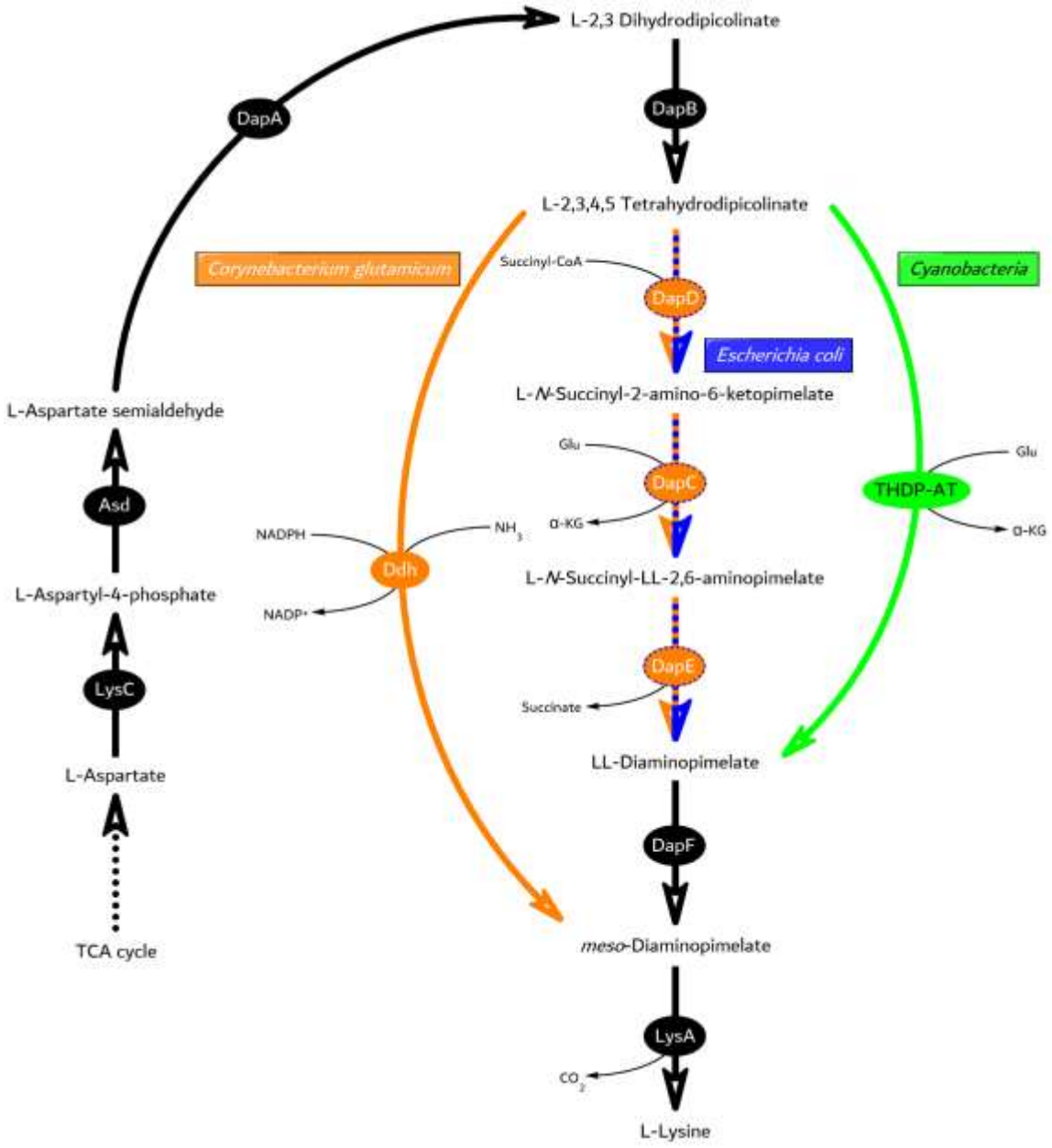

Figure 2.01 Selected L-Lysine Bioproduction Routes in Prokaryotes.
The set of metabolic pathways from L-aspartate to L-lysine differ between common industrial bacteria. *C. glutamicum* (orange) possesses the dehydrogenase pathway that converts L-2,3,4,5 tetrahydrodipicolinate (THDP) to *meso*-diaminopimelate via diaminopimelate dehydrogenase (Ddh), and shares the multistep succinylase pathway with *E. coli* (blue). Cyanobacteria (green) instead convert THDP to LL-diaminopimelate using the aminotransferase pathway via THDP-aminotransferase. Enzymes shared commonly by all prokaryotes mentioned are shown in black. Not pictured is the acetylase pathway, which is similar in its multistep nature to the succinylase version.

Further downstream in the L-lysine pathway, additional reactions have also been identified as secondary flux control points. For example, overexpression of the genes *dapA*, *dapC*, and *dapF* (which are unique to *C. glutamicum*'s succinylase pathway) were found to have various beneficial impacts on L-lysine production[95]. However, it's been noted that these steps are likely not limiting in the pathway[96], and the importance of their engineering is secondary to the *lysC* node. For instance, when expressing second gene copies of the entire *C. glutamicum ddh*-dependent L-lysine pathway, only a 15% improvement in yield was achieved[97]. Such diminishing returns have been demonstrated in *E. coli* as well. Modeling by Contador and colleagues[98] predicted the importance of feedback inhibited *lysC* and *dapA*, while downplaying the production improvements associated with overexpression of pathway genes such as *asd* and *lysA* (Figure 2.01). The importance of *lysC*'s conservation as a flux-control point was demonstrated when a separate study overexpressed feedback-resistant copies of *lysC* and *dapA* in *E. coli*[99], roughly improving the L-lysine titer 1.5-fold over the control strain. Further expression of additional genes from the L-lysine pathway, including *asd*, *dapB*, *lysA* and the *C. glutamicum*'s *ddh* (Figure 2.01), offered only another 1.3-fold titer increase to 36 g/L in flask experiments and 125.6 g/L in fed-batch. Interestingly, incrementally worse optical densities were also observed as more genes were expressed, indicating the fitness trade-off of increasing the metabolic burden.

Following its biosynthesis, L-lysine is then excreted from the cell, which is facilitated in *C. glutamicum* by the native L-lysine exporter encoded by *lysE*[91,100,101]. Deletion of *LysE* has been shown to prevent L-lysine excretion[102]. Meanwhile, overexpression of an additional *lysE* copy in the native host has contributed to improved L-lysine titers, suggesting that low export rates can represent an additional bottleneck. Enhancing L-lysine export has also been shown to be critical for other heterotrophic production platforms. For example, the methylotrophic bacterium *Methylophilus methylotrophus* AS1 was able to excrete an order of magnitude more L-lysine when heterologously expressing both *lysE* and feedback resistant *dapA* (relative control strains expressing just one of the two genes)[103]. This also indicate that enhancing export alone is not necessarily sufficient to maximize titers.

Upstream of the L-lysine biosynthesis pathway, ample provision of the essential precursor phosphoenolpyruvate (PEP) is also a strong determinant of L-lysine bioproduction. For example, in their recombineered L-lysine overproducing *C. glutamicum* strain, Xu and colleagues[104] found that avoiding overconsumption of ATP through heterologous expression of an ADP-dependent glucokinase likely led to an abundance of AMP that in turn induced expression of pyruvate kinase (Pyk), the enzyme responsible for converting PEP to pyruvate and regenerating ATP from ADP in the process. Improved assimilation of PEP and pyruvate into the TCA cycle, which can be facilitated by PEP carboxylase (Ppc), pyruvate carboxykinase (Pyc) and pyruvate dehydrogenase (Pdhc), has similarly been investigated with respect to improving L-lysine production since,

ostensibly, increased carbon flux into the TCA cycle should improve the production of downstream metabolites including L-lysine. Buchholz and colleagues[97] furthermore demonstrated the inverse to be true in *C. glutamicum* by replacing the native promoter of *aceE*, a gene coding for a subunit of Pdhc, with a mutated *dapA* promoter library to knockdown its expression. In this case, reduced flux into the TCA cycle led to increased titers of 2-ketoisovalerate and L-valine; two metabolites reached by a pathway that directly competes with L-lysine biosynthesis for pyruvate. Kind and colleagues99 'hijacked' carbon flux through the TCA cycle by simply deleting succinyl-CoA synthetase, forcing the mutant strain to convert succinyl-CoA to succinate instead via the succinylase pathway (Figure 2.01) and drive biosynthesis towards L-lysine. Similar to the L-lysine pathway nodes, heterotrophic species beyond *C. glutamicum* also display a benefit from engineering of central carbon metabolism. Engineered *E. coli* expressing *ppc* on a plasmid achieved a titer of 134.9 ± 2.3 g/L L-lysine after 72 h under culture-optimized nitrogen conditions[106], in line with modeling prediction by Contador and colleagues[98]. An *E. coli* strain with feedback resistant copies of *lysC* and *dapA* was additionally engineered to express *ppc*, resulting in a statistically significant improvement to titer and productivity[99].

Current industrial L-lysine production occurs from carbohydrate substrates (starches, sucrose, raw sugar, and molasses) that directly compete with human nutrition. To address this, strains have been developed with the ability to produce L-lysine from diverse, non-model feedstocks[107–111] (xylose, arabinose, hemicellulose, cellobiose, and mannitol) however, more must still be done. In

contrast to heterotrophic production, photosynthetic L-lysine production, in which carbon and energy are furnished by atmospheric CO_2 and sunlight, respectively, would allow for the implementation of industrial processes largely divorced from food supply. Importantly, shifting away from typical sugar sources towards open pond systems in which cyanobacteria are grown to scale would liberate arable land for other uses. Current industrial L-lysine production represents an attractive target for disruption by photoautotrophs engineered to recapitulate the key metabolic features of previously-optimized heterotrophs. Korosh and colleagues[12] were the first to demonstrate photosynthetic L-lysine production, utilizing PCC 7002. As could be expected, proof-of-principle cyanobacterial L-lysine productivity (0.003 g/L/h), even in the best case, pales in comparison to the record set by an optimized industrial *C. glutamicum* strain utilizing sugar98 (5.53 g/L/h). Rough calculations done in the study suggest that, even in ideal weather conditions, each acre of arable land contributing to sugar production for conversion into L-lysine requires, at minimum, 3.3 acres of open pond to achieve the same production with photoautotrophs. Improving on the efficiency on this cyanobacterial success will translate to a smaller footprint for a potential industrialized L-lysine photosynthetic process.

The breakthrough in photosynthetic L-lysine production was informed by the large body of work already discussed for *C. glutamicum* and other heterotrophs. Korosh and colleagues[12] introduced feedback-resistant and codon-optimized copies of *lysC* and dihydrodipicolinate synthase (*dapA*) (Figure 2.01) from *Xenorhabdus bovienii* and PCC 7942, respectively, expressing each from

the PCC 7002 chromosome via inducible tetracycline promoters. The well-characterized L-lysine exporter *ybjE* from *E. coli*[112], meanwhile, was also tested in various permutations with the L-lysine pathway genes, as well as a copy of *ppc* from PCC 7942 demonstrating feedback resistance to L-aspartate. Their results determined that the best photosynthetic production occurred when *lysC* and *ybjE* were solely co-expressed[12], confirming that that feedback-resistant aspartokinase and export node are key even in photoautotrophic chasses. The former is critical to drive flux into the L-lysine pathway without feedback inhibition, while the latter is necessary owing to PCC 7002's complete lack of native homologs of known L-lysine exporter genes. In fact, integration of deregulated *lysC* alone failed to generate mutant colonies, indicating that failure to relieve L-lysine bottlenecks through excretion is especially toxic in photoautotrophs.
Just as the work discussed above recapitulated the successes of *C. glutamicum* in PCC 7002, it is likely that faster-growing cyanobacterial host platforms can also recreate that success while potentially improving on L-lysine productivity, owing to their faster assimilation of CO_2 and other nutrients. Selecting a different chassis with improvements in carbon uptake and utilization could be seen as an analog to the beneficial central carbon metabolism mutations made in *C. glutamicum*. As discussed in Chapter 1, UTEX 2973 fits this description while still managing to be a genetically tractable organism with a decent set of expression parts and systems.

In this study, it was first sought to engineer UTEX 2973 for L-lysine overproduction by analogously deregulating the main pathway bottleneck and

introducing a heterologous exporter. These efforts, along with final bioproduction performance, were aided via the characterization of a subset of versatile promoter systems as well as a novel episomal expression strategy.

2.2 Methods and Materials

2.2.1 Chemicals

All enzymes were purchased from New England Biolabs (Ipswich, MA). Cadaverine was purchased from TCI America (Portland, OR). All other chemicals were purchased at the highest available purities from Sigma-Aldrich (St. Louis, MO) or Santa Cruz Biotechnology (Dallas, TX), unless otherwise indicated.

2.2.2 Strains and Culture Conditions

UTEX 2973 was obtained from the UTEX Culture Collection of Algae at the University of Texas at Austin. Culturing in liquid media and on solid agar plates was performed using BG-11 medium buffered with 10 mM TES/NaOH, pH 8.2 (where agar plates were also supplemented with 3 g/L sodium thiosulfate) at 38°C under continuous light at an intensity of ~200 µmol photon m^{-2} s^{-1}, unless otherwise specified. Where necessary, plasmids were maintained in UTEX 2973 via addition of 50 µg/mL kanamycin. Liquid cultures were grown while shaking at 200 rpm in 250 mL non-baffled flasks containing 25 mL media and seeded to an initial cell density as determined by optical density at 750 nm (OD_{750}) of 0.1. Culture growth at 1% CO_2 was carried out in a Caron Plant Growth Chamber Model 7300 (Marietta, OH) set to maximum humidity (~63%). Where appropriate, expression of relevant pathway genes via the inducible P_{trc2O}-*lacI*/O and P_{conII}-

Riboswitch F systems was achieved by the addition of IPTG (at up to 500 µM) and/or theophylline (at up to 2 mM), respectively.

2.2.3 Plasmid Construction

All plasmids constructed and/or used in this study are summarized in Tables 2.01 and 2.02. Plasmids constructed for this study were assembled via Gibson assembly[113]. All oligonucleotide primers (IDT, Coralville, IA) used in plasmid assembly and sequencing are summarized in Appendix A. The shuttle vector pAM4788-Km^R was constructed by amplifying and assembling a fragment from pAM4788 of *Synechococcus elongatus* sp. PCC 7942[70] together with a fragment containing the Km^R cassette from pEERM1[114]. Plasmid pSL3137 served as the template for the P_{trc2O} promoter and the T_{rrnB} terminator. Plasmid pCJ049 served as template for the T_{T7}-*lacI*^{WF} cassette used to construct IPTG-inducible plasmids[82]. Plasmid pCDF-*lysC*^{fbr}-*dapA*^{fbr} served as the template for the feedback resistant copy of aspartatokinase (encoded by *lysC*^{fbr}), originally from *E. coli* MG1655[115]. Genomic DNA (gDNA) from UTEX 2973 served as the template for the P_{cpcB1*} promoter, the RBS_{cpcA1} intergenic region, and the T_{psbC} terminator, as well as the upstream and downstream regions of the NS3 neutral site. *E. coli* MG1655 gDNA served as the template for genes encoding the L-lysine exporter (*ybjE*), phosphoenolpyruvate carboxykinase (*pck*), and the phosphoenolpyruvate carboxylase (*ppc*). *C. glutamicum* ATCC 13032 gDNA served as the template for pyruvate carboxylase (*pyc*) and the cadaverine antiporter (*cadB*). All plasmids were screened first by colony PCR, followed by restriction digest mapping and final verification via DNA sequencing.

Table 2.01 List of Plasmids Constructed and Used in this Study to Characterize the Relative Behaviors of Different Expression Control Systems in UTEX 2973.

Plasmid	Genotype
pZD-LGC-01	pANS; *yemGFP*-T_{rrnB2}; Km^R
pZD-LGC-02	pANS; P_{cpcB1*}-*yemGFP*-T_{rrnB2}; Km^R
pZD-LGC-03	pANS; P_{J23119}-*yemGFP*-T_{rrnB2}; Km^R
pZD-LGC-04	pANS; P_{trc2O}-*yemGFP*-T_{T7}-P_{MB2}-$lacI^{WF}$; Km^R
pZD-LGC-05	pANS; P_{conII}-Riboswitch-F-*yemGFP*-T_{T7}-P_{MB2}-$lacI^{WF}$; Km^R
pZD-LGC-06	NS3::P_{tac}-*yemGFP*-T_{rrnB2}; Km^R
pZD-LGC-07	NS3::*yemGFP*-T_{rrnB2}; Km^R
pZD-LGC-08	NS3::P_{cpcB1*}-*yemGFP*-T_{rrnB2}; Km^R
pZD-LGC-09	NS3::P_{J23119}-*yemGFP*-T_{rrnB2}; Km^R
pZD-LGC-10	NS3::P_{trc2O}-*yemGFP*-T_{T7}-P_{MB2}-$lacI^{WF}$; Km^R
pZD-LGC-11	NS3::P_{conII}-Riboswitch-F-*yemGFP*-T_{T7}-$lacI^{WF}$; Km^R

Table 2.02 List of Plasmids Constructed and Used in this Study to Engineer the Production and/or Export of L-lysine.

Plasmid	Genotype
pZD-LGC-13	NS3::P_{trc2O}-$lysC^{fbr}$-T_{T7}-P_{MB2}-$lacI^{WF}$; P_{cpcB1*}-*ybjE*-T_{psbC}; Km^R
pZD-LGC-14	pANS; P_{trc2O}-$lysC^{fbr}$-T_{T7}-P_{MB2}-$lacI^{WF}$; Km^R
pZD-LGC-15	pANS; P_{cpcB1*}-*ybjE*-T_{rrnB2}; Km^R
pZD-LGC-16	pANS; P_{trc2O}-*yemGFP*-T_{T7}-P_{MB2}-$lacI^{WF}$; P_{cpcB1*}-*ybjE*-T_{psbC}; Km^R
pZD-LGC-17	pANS; P_{trc2O}-$lysC^{fbr}$-T_{T7}-P_{MB2}-$lacI^{WF}$; P_{cpcB1*}-*ybjE*-RBS_{cpcA1}-*yemGFP*-T_{psbC}; Km^R
pZD-LGC-18	pANS; P_{trc2O}-$lysC^{fbr}$-T_{T7}-P_{MB2}-$lacI^{WF}$; P_{cpcB1*}-*ybjE*-RBS_{cpcA1}-*pck*- T_{psbC}; Km^R
pZD-LGC-19	pANS; P_{trc2O}-$lysC^{fbr}$-T_{T7}-P_{MB2}-$lacI^{WF}$; P_{cpcB1*}-*ybjE*- RBS_{cpcA1}-*ppc*- T_{psbC}; Km^R
pZD-LGC-20	pANS; P_{trc2O}-$lysC^{fbr}$-T_{T7}-P_{MB2}-$lacI^{WF}$; P_{cpcB1*}-*ybjE*- RBS_{cpcA1}-*pyc*- T_{psbC}; Km^R
pZD-LGC-21	pANS; P_{trc2O}-$lysC^{fbr}$-T_{T7}-P_{MB2}-$lacI^{WF}$; P_{cpcB1*}-*ybjE*-P_{J23119}-*pyc*-T_{psbC}; Km^R

The plasmid pZD-LGC-01, a derivative of pAM4788-Km^R possessing no promoter, was assembled by amplifying pAM4788-Km^R as template with the primer pair ZDC-081 and ZDC-004, as well as the pair ZDC-001 and ZDC-080. The plasmid pZD-LGC-02, a derivative of pAM4788-Km^R possessing the strong constitutive promoter P$_{cpcB1*}$, was assembled by amplifying the template pAM4788-Km^R with primers ZDC-016 and ZDC-012, and the P$_{cpcB1}$ promoter region from UTEX 2973 gDNA with primers ZDC-005 and ZDC-006. The resulting promoter fragment was amplified again with ZDC-005 and ZDC-008 to create the truncated P$_{cpcB1*}$ described by Knoot and colleagues[38]. The plasmid pZD-LGC-03, a derivative of pAM4788-Km^R possessing the synthetic strong promoter P$_{J23119}$, was assembled by amplifying pAM4788-Km^R as template with the primer pair ZDC-242 and ZDC-004, as well as the pair ZDC-001 and ZDC-243. The plasmid pZD-LGC-04, a derivative of pAM4788-Km^R possessing an IPTG-inducible P$_{trc2O}$-*lacI^{WF}* promoter system, was assembled by amplifying the template pAM4788-Km^R with primers ZDC-060 and ZDC-048, the promoter P$_{trc2O}$ from pSL3137[66] with primers ZDC-045 and ZDC-046, the yemGFP gene from pAM4788 with primers ZDC-047 and ZDC-057, and the T$_{T7}$-*lacI^{WF}* region from pCJ049[82]. The plasmid pZD-LGC-05, a derivative of pAM4788-Km^R possessing a theophylline-inducible P$_{conII}$-Riboswitch-F system, was assembled by amplifying pZD-LGC-04 as template with the primer pair ZDC-220 and ZDC-004, as well as ZDC-001 and ZDC-221. The plasmid pZD-LGC-06, a version of pAM4788-Km^R with the backbone swapped for a suicide vector integrating into NS3[18], was assembled by amplifying the template pAM4788-Km^R with primers ZDC-131 and

ZDC-167, NS3 I from UTEX 2973 gDNA with primers ZDC-168 and ZDC-134, the ori-bom region from pAM4788 with primers ZDC-135 and ZDC-136, and NS3 II also from UTEX 2973 gDNA with primers ZDC-129 and ZDC-130. The plasmid pZD-LGC-07, a suicide vector version of pZD-LGC-01 that integrates into NS3, was assembled by amplifying the template pZD-LGC-06 with primers ZDC-168 and ZDC-130, and the promoter-less Km^R-*yemGFP* region of pZD-LGC-01 with primers ZDC-131 and ZDC-167. The plasmid pZD-LGC-08, a suicide vector version of pZD-LGC-02 that integrates into NS3, was assembled by amplifying the template pZD-LGC-02 with primers ZDC-131 and ZDC-167, and the previous fragment from pZD-LGC-06. The plasmid pZD-LGC-09, a suicide vector version of PZD-LGC-03 that integrates into NS3, was assembled by amplifying the template pZD-LGC-03 with primers ZDC-131 and ZDC-167, and the previous fragment from pZD-LGC-06. The plasmid pZD-LGC-10, a suicide vector version of pZD-LGC-04 that integrates into NS3, was assembled by amplifying the template pZD-LGC-06 with primers ZDC-166 and ZDC-130, and the Km^R-P_{trc2O}-*yemGFP-lacI*^{WF} region of pZD-LGC-04 with primers ZDC-131 and ZDC-165. The plasmid pZD-LGC-11, a suicide vector version of pZD-LGC-05 that integrates into NS3, was assembled by amplifying the template pZD-LGC-05 with primers ZDC-131 and ZDC-165, and the previous fragment from pZD-LGC-06. The plasmid pZD-LGC-14, a derivative of pZD-LGC-04 expressing the feedback-resistant L-lysine decarboxylase $lysC^{fbr}$, was assembled by amplifying the template pZD-LGC-04 with primers ZDC-088 and ZDC-089, and *lysC*^{fbr} from pCDF-*lysC*^{fbr}-*dapA*^{fbr}109 with primers ZDC-086 and ZDC-087. The plasmid pZD-

LGC-15, a derivative of pZD-LGC-02 expressing the L-lysine exporter *ybjE*, was assembled by amplifying the template pZD-LGC-02 with primers ZDC-025 and ZDC-094, and *ybjE* from *E. coli* MG1655 gDNA with primers ZDC-097 and ZDC-024. The plasmid pZD-LGC-13, a derivative of pAM4788-Km^R expressing two cassettes containing a L-lysine production pathway, was assembled by amplifying the template pZD-LGC-14 with primers ZDC-072 and ZDC-071, the native terminator T_{psbC} from UTEX 2973 gDNA with primers ZDC-070 and ZDC-096, and the P_{cpcB1*}-*ybjE* cassette from pZD-LGC-15 with primers ZDC-095 and ZDC-067. The plasmid pZD-LGC-12, a suicide vector that integrates the L-lysine production pathway into NS3, was assembled by amplifying the template pZD-LGC-06 with primers ZDC-133 and ZDC-130, and the L-lysine pathway from pZD-LGC-13 with primers ZDC-131 and ZDC-132. The plasmid pZD-LGC-16, a version of pZD-LGC-13 where the $lysC^{fbr}$ gene has been replaced with *yemGFP*, was assembled by amplifying the template pZD-LGC-04 with primers ZDC-072 and ZDC-057, and the T_{T7}-$lacI^{WF}$+P_{cpcB1*}-*ybjE*-T_{psbC} region of pZD-LGC-13 with primers ZDC-058 and ZDC-067. The plasmid pZD-LGC-25, a derivative of pZD-LGC-13 additionally expressing the cadaverine antiporter gene *cadB* as part of a bicistronic operon under P_{cpcB1*}, was assembled by amplifying the template pZD-LGC-13 with primers ZDC-105 and ZDC-104, and *cadB* from *E. coli* MG1655 gDNA with primers ZDC-103 and ZDC-102. The plasmid pZD-LGC-17, a derivative of pZD-LGC-25 where *cadB* has been replaced with *yemGFP*, was assembled by amplifying the template pZD-LGC-25 with primers ZDC-219 and ZDC-218, and *yemGFP* from pAM4788 with primers ZDC-217 and ZDC-216. The

plasmid pZD-LGC-18, a derivative of pZD-LGC-25 where *cadB* has been replaced with the phosphoenolpyruvate carboxykinase *pck*, was assembled by amplifying the template pZD-LGC-25 with primers ZDC-143 and ZDC-142, and *pck* from *E. coli* MG1655 gDNA with primers ZDC-141 and ZDC-140. The plasmid pZD-LGC-19, a derivative of pZD-LGC-25 where *cadB* has been replaced with the phosphoenolpyruvate carboxylase *ppc*, was assembled by amplifying the template pZD-LGC-25 with primers ZDC-199 and ZDC-198, and *ppc* from *E. coli* MG1655 gDNA with primers ZDC-197 and ZDC-196. The plasmid pZD-LGC-20, a derivative of pZD-LGC-25 where *cadB* has been replaced with the pyruvate carboxylase *pyc*, was assembled by amplifying the template pZD-LGC-25 with primers ZDC-207 and ZDC-206, and *pyc* from *C. glutamicum* ATCC 13032 gDNA with primers ZDC-205 and ZDC-204. The plasmid pZD-LGC-24, a derivative of pZD-LGC-03 where *yemGFP* has been replaced by *cadB*, was assembled by amplifying the template pZD-LGC-03 with primers ZDC-246 and ZDC-247, and *cadB* from *E. coli* MG1655 gDNA with primers ZDC-244 and ZDC-245. The plasmid pZD-LGC-26, a derivative of pZD-LGC-25 no longer expressing $lysC^{fbr}$, was assembled by amplifying the template pAM4788-Km^R with primers ZDC-072 and ZDC-229, and the P_{cpcB1*}-*cadB*-T_{psbC} cassette from pZD-LGC-25 with primers ZDC-228 and ZDC-067. The plasmid pZD-LGC-27, a derivative of pZD-LGC-26 where the intergenic region RBS_{cpcA1} has been replaced by the P_{J23119} was assembled by amplifying the backbone pZD-LGC-26 with the primers ZDC-254 and ZDC-104, and the P_{J23119}-*cadB* cassette from pZD-LGC-24 with primers ZDC-103 and ZDC-253. The plasmid

pZD-LGC-21, a derivative of pZD-LGC-20, where the intergenic region RBS_{cpcA1} has been replaced by the P_{J23119}, was assembled by amplifying the template pZD-LGC-27 with primers ZDC-264 and ZDC-002, and the two cassettes from pZD-LGC-20 sans P_{cpcB1*}-*ybjE*-RBS_{cpcA1} with primers ZDC-003 and ZDC-263.

2.2.4 Genetic Modification of UTEX 2973

All constructed shuttle and integration vectors were delivered to UTEX 2973 via conjugation, in this case using a tripartite mating procedure adapted from Yu and colleagues[29]. Briefly, UTEX 2973 was inoculated in 50 mL BG-11 media (as described above) while two strains of *E. coli* – DH5α, harboring the conjugal plasmid pRL443, and DH5α MCR, harboring both the helper plasmid pRL623 and the desired cargo plasmid – were simultaneously inoculated into separate tubes containing 5 mL LB media with appropriate antibiotics. Following overnight growth, by which time UTEX 2973 had reached approximately early-exponential phase (OD_{750} = 0.4-0.8), both *E. coli* cultures were pelleted by centrifugation at 3,000·*g* for 5 min before then decanting the supernatant and resuspending each pellet in 5 mL fresh LB media containing no antibiotics. This procedure was repeated twice more. Meanwhile, UTEX 2973 was harvested by pelleting at 2,000·*g* for 10 min, before decanting the supernatant and resuspending the cells in 5 mL of fresh BG-11. In a sterile 1.5 mL tube, 250 µL of resuspended DH5α carrying pRL443 was then mixed with 250 µL of resuspended DH5α MCR carrying pRL623 and the cargo plasmid. Next, 500 µL of resuspended UTEX 2973 was added to the same tube, after which it was then tightly capped and inverted several times to mix. Following this, 200 µL of the

tripartite mating mixture was pipetted directly onto a BG-11 + 5% LB agar plate containing no antibiotics, spread evenly across the face of the agar using glass beads and then allowed to air dry. The plate was then incubated as described above, except that light intensity was set to 10-40 µmol photon m^{-2} s^{-1}. After 16-24 hours, a sterile metal spatula was used to separate and lift the BG-11 agar from the petri dish to allow 600 µL fresh BG-11 liquid media with kanamycin to be pipetted into the bottom of the dish (i.e., below the agar). The agar was then reseated into the petri dish, allowing kanamycin to diffuse through the agar where it would reach an approximate final concentration of 50 µg/mL. Exconjugants typically appeared after 3-4 days, at which point they were picked and streaked onto a fresh BG-11 plate containing 50 µg/mL kanamycin.

2.2.5 Fluorescence Measurements

Relative expression levels were determined by measuring the whole cell fluorescence of yemGFP-expressing strains of UTEX 2973 12 hours after inoculation (i.e., in early to mid-exponential phase), as described above. At this point, OD_{750} was measured (which ranged from 0.3-0.7) and 100 µL of culture was transferred to a 96-well black-bottom Costar plate. Fluorescence was then measured in an Infinite M Nano+ Tecan microplate reader using excitation and emission wavelengths of 489 and 520 nm, respectively.

2.2.6 Sample Preparation for Intracellular Metabolite Analysis

To assay for the intracellular accumulation of select metabolites of interest, cells were first harvested by centrifugation at 3,000·*g* for 5 minutes, before then resuspending and washing the pellet three times using the same

volume of sterile deionized H_2O in order to remove any extracellular products. The final cell pellet was then stored at -80°C overnight before being dried via lyophilization (Labconco FreeZone® 2.5, LABCONCO). Fully dried pellets were weighed before lysis was performed using Bugbuster™ Master Mix solution (Novagen), with sample incubated on a shaking platform at room temperature for 20 minutes. After centrifugation at 12,000·*g* for 20 minutes, 30 µL of the clarified solution was derivatized for analysis, as described below.

2.2.7 Determination of UTEX 2973 Biomass

Cell growth was measured by OD_{750} using a Thermo Spectronic BioMate 3 UV-Vis spectrophotometer and correlated with cell dry weight. To do so, three flasks of wild-type UTEX 2973 were cultured as described above, with cell biomass being harvested at different time points during exponential growth. Cells were concentrated by centrifugation after which pellets were dried by lyophilization (as outlined above) and weighed. The resulting correlation between OD_{750} and cell dry weight is shown in Figure 2.02.

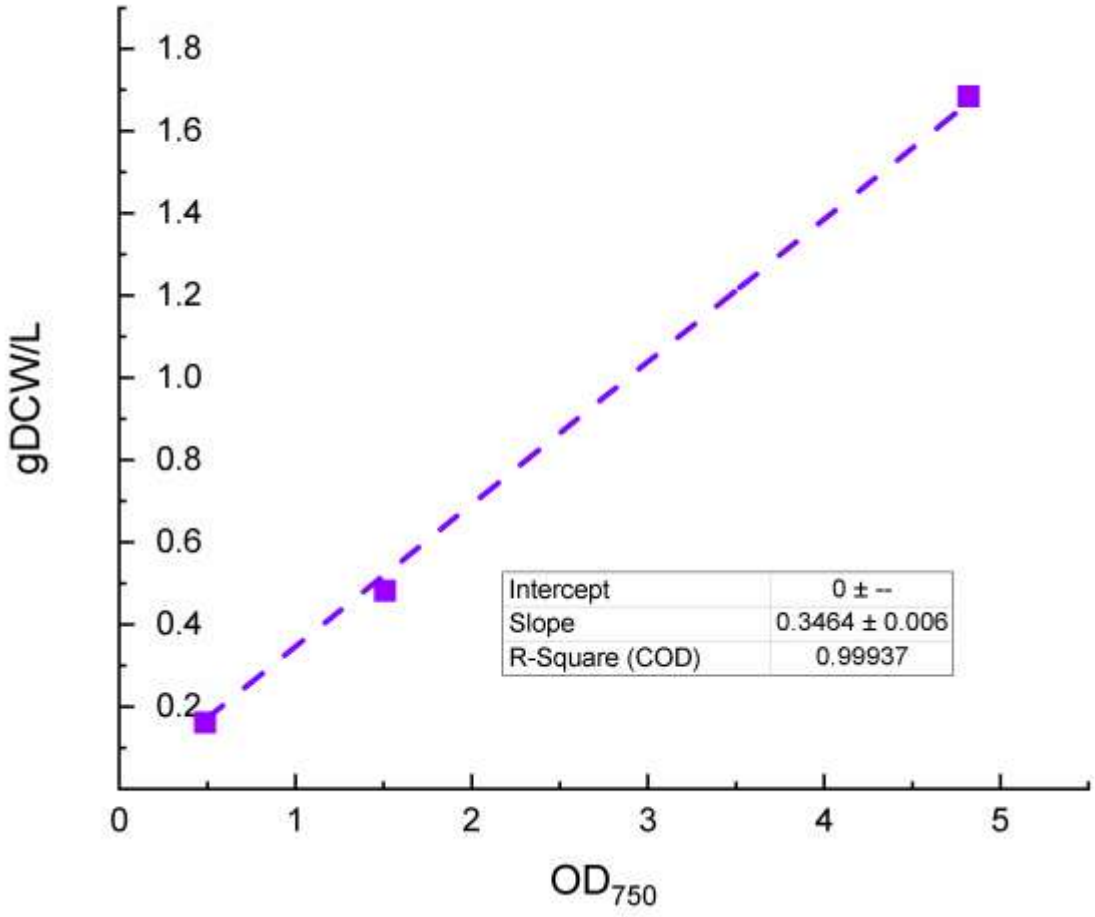

Figure 2.02 Calibration Used to Correlate Biomass Measurements in OD_{750} with g-DCW/L.
Linear correlation obtained when relating OD_{750} with g-DCW/L for wild-type UTEX 2973. Flasks were harvested at 12, 24, and 48 hours, and freeze dried to determine dry cell weight (DCW).

2.2.8 Analytical Methods

Periodically throughout each culture, aqueous samples were removed for amino acid analysis via high-performance liquid chromatograph (HPLC) using a method adapted from that of Kim and colleagues[116]. First, 50 µL culture removed and centrifuged at 12,000·*g* for 10 minutes to remove cells (note: an equal volume of fresh BG-11 medium buffered with 10 mM TES/NaOH, pH 8.2 was

added back to the culture to maintain a constant volume). Next, 30 µL of the resulting supernatant was added to an HPLC sample vial containing 189 µL deionized H_2O, 18 µL of 0.5 M borate buffer solution (pH 9.0; Alfa Aesar), 60 µL methanol, and 3 µL diethyl ethoxymethylenemalonate (DEEMM). The vial was then tightly capped and allowed to stand at room temperature for 2 hours before HPLC analysis. Analysis was carried out using an Agilent 1100 Series HPLC equipped with a diode array detector set to 284 nm. The derivatized sample (5 µL) was injected and separated using a C18 column (Agilent Hypersil GOLD column, 4.6 x 250 mm, 5 µm particle size) maintained at 35°C using a mobile phase flowing at 1 mL/min and consisting of acetonitrile (A) and 25 mM aqueous sodium acetate buffer, pH 4.8 (B) according to the following gradient program: 0-2 minutes, 20-25% A; 2-32 minutes, 25-60% A; 32-40 minutes, 60-20% A. Under these conditions, L-aspartate, L-lysine, and eluted at 3.6 and 12.7 min, respectively.

2.3 Results and Discussion

2.3.1 Expanding the Gene Expression Toolbox of UTEX 2973

Despite its promising phenotypic traits, and in contrast to both commonly employed heterotrophic chasses (e.g., *E. coli*, *C. glutamicum*) and even other more established cyanobacterial strains (e.g., PCC 7002, *Synechocystis* sp. PCC 6803), UTEX 2973 currently suffers from a relative shortage of well-characterized genetic parts which, in turn, limits metabolic engineering efforts. However, since the genome of UTEX 2973 differs from that of its parent PCC 7942 by just 55

single nucleotide polymorphisms and indels[29], this has fortuitously enabled a range of promoters and other translational control systems to be effectively ported over[38,83]. That said, it has also been previously shown (e.g., in the case of P_{psbA} from *Amaranthus hybridus* chloroplasts) that relative promoter strengths can be quite variable between UTEX 2973[83] and PCC 7942[86]. Moreover, genetic parts can often also display context-dependent activities, including with respect to the specific expression site employed[114]. In UTEX 2973, most parts characterization has to date been confined to one of either neutral site NS1 or NS2. Finally, although copy number variation has been shown to hold an outsized influence over total gene expression levels in other microorganisms[44,117,118], its relative influences have yet to be thoroughly examined in UTEX 2973 due to the lack of an available self-replicating shuttle vector. With these limitations in mind, this study first sought to characterize the relative activities of a tractable subset of promoters and a riboswitch from both the less commonly employed neutral site NS3 as well as the as yet unexplored (to our knowledge) pAM4788 shuttle vector (derived from the endogenous pANS small plasmid of PCC 7942).

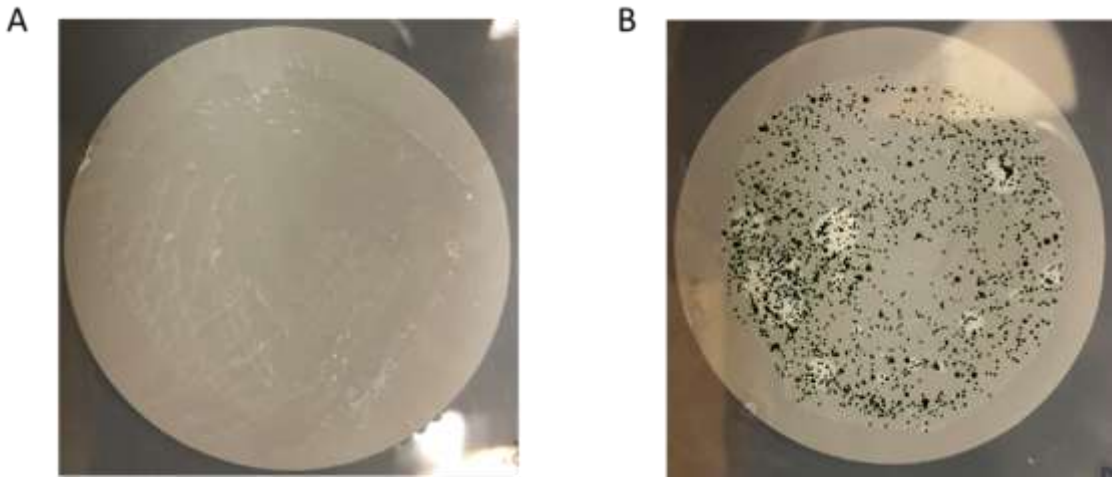

Figure 2.03 Comparison of Plates Containing UTEX 2973 Exconjugants. UTEX 2973 exconjugants harboring pAM4788-Km^R, obtained through the outlined procedure, plated onto BG-11 + 5% LB plates containing 50 µg/mL kanamycin, and topped with cellulose filters for visibility. The negative control lacked the conjugal plasmid pRL443 during tripartite mating (A), in contrast to the normal conjugation (B).

It was confirmed that pAM4788-Km^R could be transformed into and stably maintained in UTEX 2973 (Figure 2.03); a largely expected result since UTEX 2973 also carries the pANS small plasmid and it is identical to the copy from PCC 794264. An example of the typical growth profile of wild-type UTEX 2973 in liquid under the standard conditions can be seen in Figure 2.04.

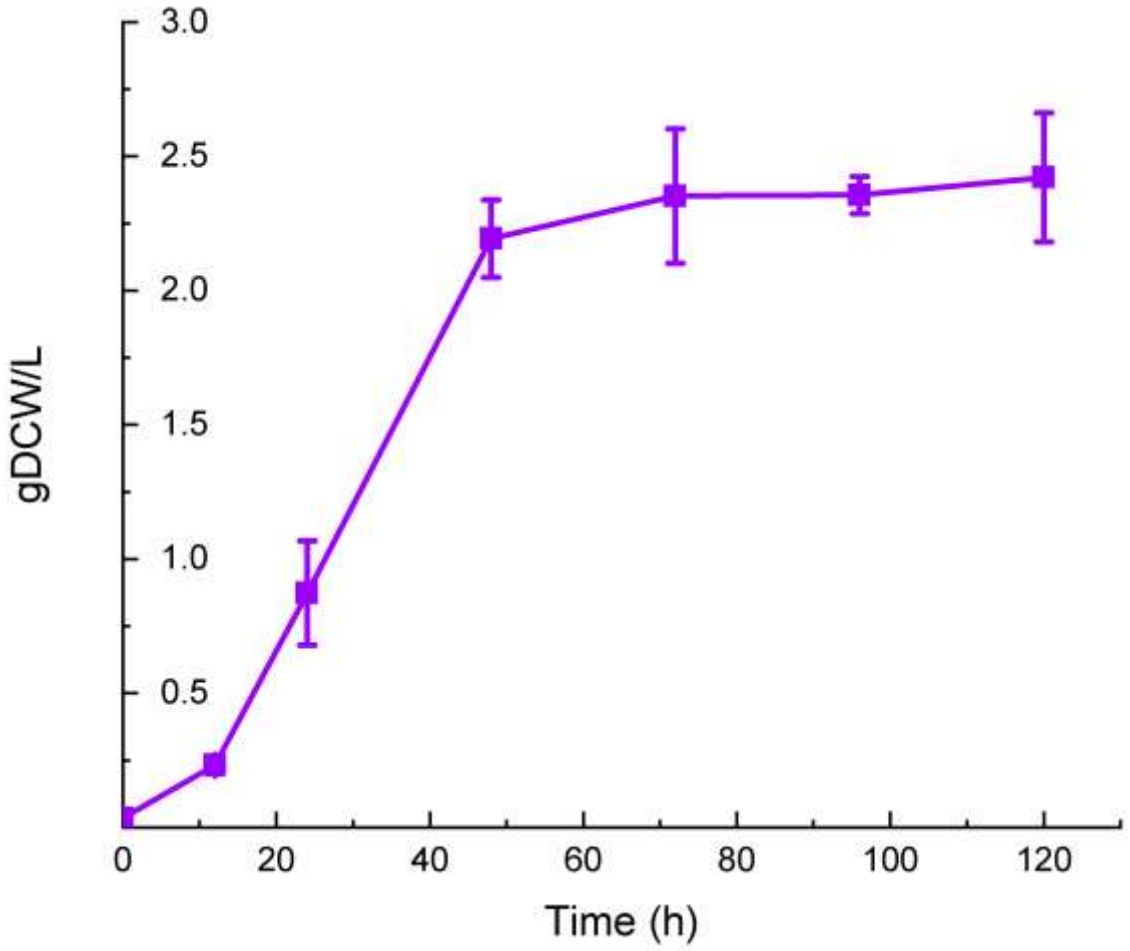

Figure 2.04 Growth of Wild-Type UTEX 2973 Under Standard Conditions. Biomass accumulation of wild-type UTEX 2973 strains over the course of 120 hours when grown in shake flasks containing 25 mL BG-11 at the specified standard conditions. Error bars represent standard error from biological triplicates.

Next, *yemGFP* production levels were compared for a small subset of gene expression systems in order to characterize their relative strengths under both chromosomal (NS3) and episomal (pAM4788-Km^R) conditions. As seen in Figure 2.05, all of the tested systems were found to be functional from both loci, including the constitutive P_{tac}, P_{cpcB1*}, and P_{J22119} promoters, as well as well the IPTG-inducible P_{trc2O}-*lacI*/O promoter system and the theophylline-inducible

P_{conII}-Riboswitch F; with the latter two uniquely providing titratable control as a function of inducer concentration. Overall, while chromosomal expression provided a higher dynamic range than episomal expression (roughly 186- vs. 113-fold), the highest overall levels of *yemGFP* production were seen in the latter case (Figure 2.05). For example, using P_{tac} (originally present on pAM4788-Km^R), roughly 2.3-fold higher normalized fluorescence levels were achieved when *yemGFP* was expressed from pAM4788-Km^R vs. NS3. A similar magnitude of difference was also observed in the case of P_{cpcB1*}. Although this ratio could be taken to reflect the relative pAM4788-Km^R versus chromosome copies in UTEX 2973, it is notably less than the reported ratio (of about 10) for pANS in PCC 7942[70]. Meanwhile, although similar maximum expression levels were achieved for the inducible P_{trc2O}-*lacI*/O system at the highest IPTG induction level (i.e., 500 µM IPTG) under both chromosomal and episomal conditions, at all lower induction levels at least a 2.2-fold difference was again observed. Furthermore, in the absence of IPTG, a statistically significant increase in fluorescence relative to the no promoter control was only observed in the episomal case, suggesting that higher gene copy number also increased the net effect of 'leaky' expression (i.e., a less tight OFF state). In contrast, meanwhile, statistically significant differences in chromosomal vs. episomal *yemGFP* expression via the P_{conII}-Riboswitch F system were only observed at 0.5 mM theophylline (where the difference was still only <2-fold). This result is consistent with past reports where, as observed for other RNA-based genetic switches, regulation has predominantly been shown to be controlled by the concentration of the conformation-changing

molecule (i.e., inducer) and not mRNA abundance[84,85,119]. Importantly, this behavior also resulted in the P_{conII}-Riboswitch F providing the tightest OFF state when employed on pAM4788-Km^R, with fluorescence levels being indistinguishable from even the no promoter control. The opposite was also true, however, when the P_{conII}-Riboswitch F was used on the chromosome, with higher levels of fluorescence being observed relative to both the no promoter control as well as the P_{trc2O}-*lacI*/O system in the absence of IPTG. Overall, where dynamic (i.e., inducible) control of expression is needed in UTEX 2973, these findings indicate a trade-off between a tight OFF state and overall expression, both of which benefited from the increased copy number provided by episomal expression, though in an opposite manner between the two expression systems examined.

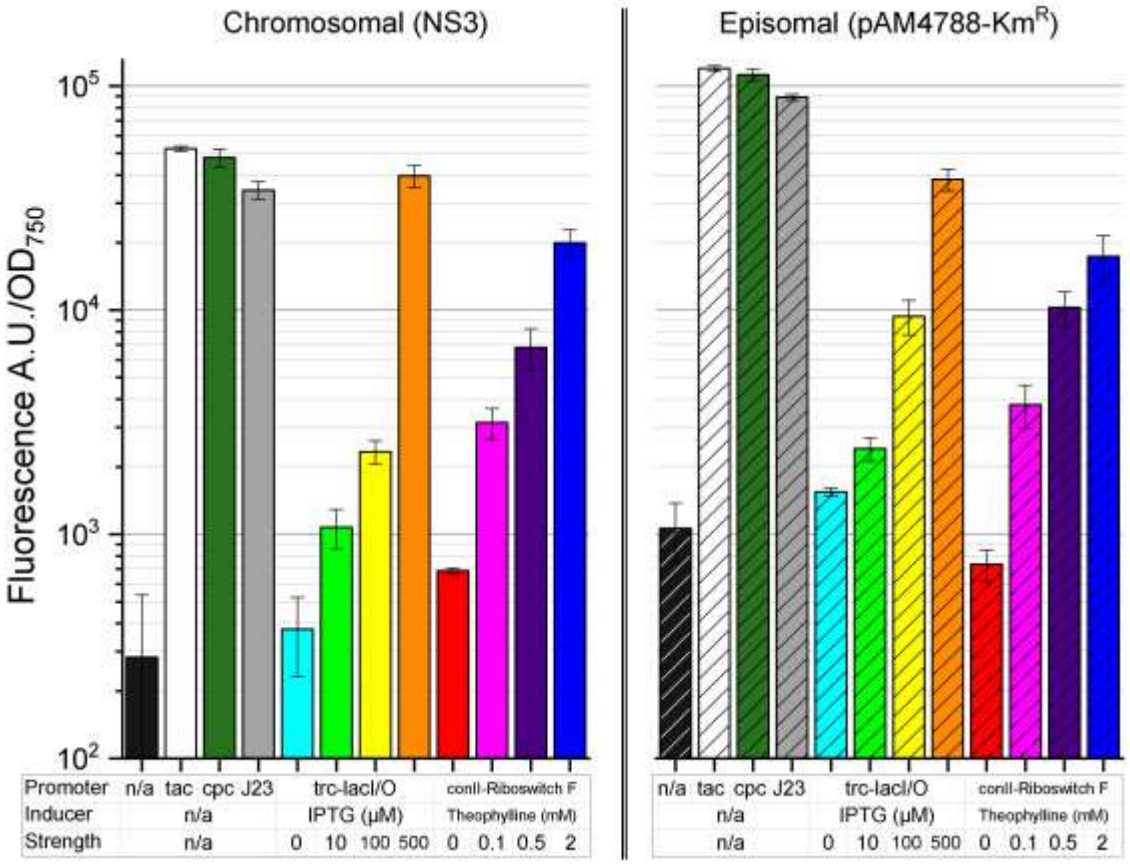

Figure 2.05 Characterization of the Relative Behaviors of Different Expression Control Systems and the Influence of their Chromosomal versus Episomal Application.
Arbitrary fluorescence units normalized by OD_{750} for different promoters and a riboswitch when chromosomally integrated at NS3 (left, solid bars) or expressed on the self-replicating plasmid pAM4788-Km^R (right, striped bars) into UTEX 2973. The tested systems include: no promoter (control; charcoal); tac promoter (white); cpcB1* promoter (denoted as 'cpc', dark green); J23119 promoter (denoted as 'J23', grey); the P_{trc2O}-*lacI/O* system with 0 μM (cyan), 10 μM (bright green), 100 μM (yellow), and 500 μM IPTG (orange); P_{conII}-Riboswitch F with 0 mM (red), 0.1 mM (pink), 0.5 mM (purple), and 2.0 mM theophylline (blue). Error bars represent standard error from biological triplicates.

2.3.2 Chromosomal Expression of a Heterologous L-lysine Pathway in UTEX 2973

Equipped with the above characterized parts and following the general metabolic engineering template first established in PCC 7002 by Korosh and

colleagues[12], this study next sought to engineer UTEX 2973 for L-lysine over-production by: i) relieving allosteric inhibition caused by L-lysine upon aspartate kinase and ii) enhancing L-lysine export (Figure 2.06).

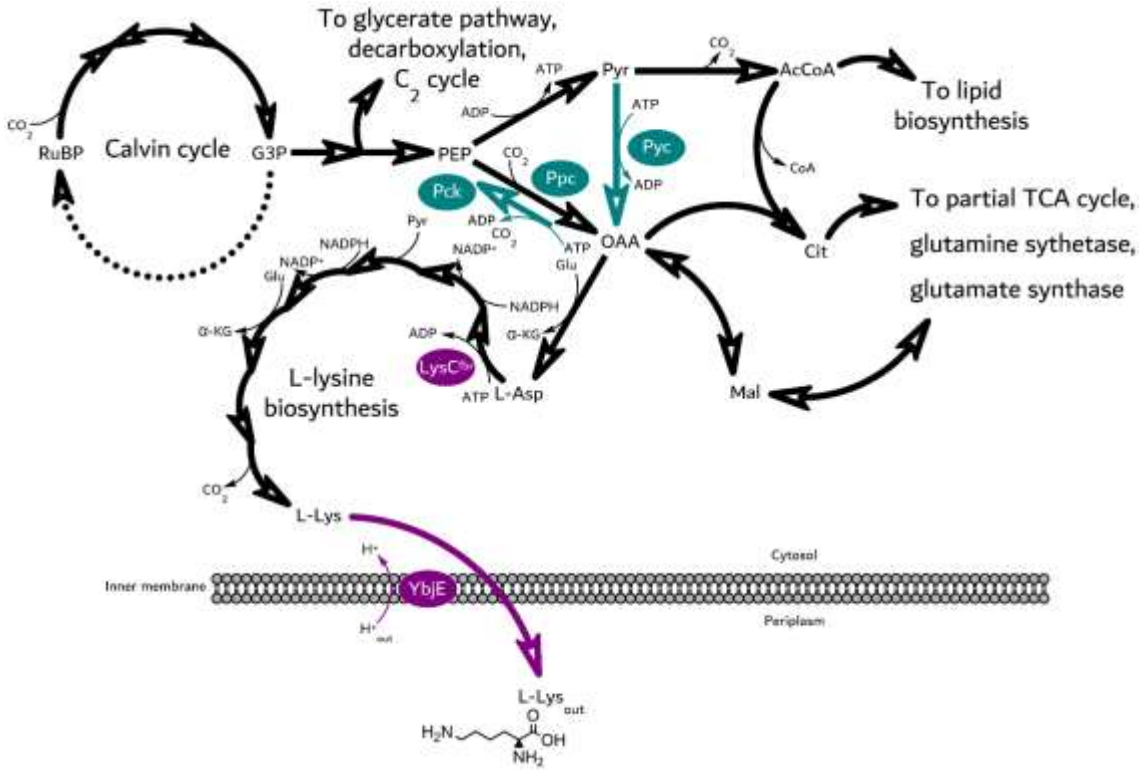

Figure 2.06 Central Carbon and L-Lysine Biosynthesis Metabolism in UTEX 2973.
Central carbon metabolism, L-lysine biosynthesis and the introduction of heterologous genes in UTEX 2973. Genes over-expressed to increase L-lysine production and export genes are shown in purple, including *lysC*^{fbr}, feedback-resistant aspartate kinase; and *ybjE*, L-lysine exporter. Genes over-expressed to increase production of oxaloacetate are shown in teal, including *pck*, pyruvate carboxykinase; *ppc*, phosphoenolpyruvate carboxylase; and *pyc*, pyruvate carboxylase. Metabolites shown include RuBP, RuBisCO; G3P, glyceraldehyde 3-phosphate; PEP, phosphoenolpyruvate; Pyr, pyruvate; AcCoA, acetyl-coenzyme A; Cit, citrate; OAA, oxaloacetic acid; Mal, malate; L-Asp, L-aspartate; L-Lys, L-lysine.

Plasmid pZD-LGC-12 was accordingly constructed by cloning *lysC*^{fbr} under control of the IPTG-inducible P_{trc2O}-*lacI*/O promoter system and *ybjE* under control of the strong and constitutive P_{cpcB1*} promoter. Homology arms surrounding the cassette were also included to enable integration into NS3. Once fully segregated, the resulting strain (UTEX 2973 NS3::*lysC*^{fbr}+*ybjE*) was tested for its ability to over-produce L-lysine by culturing it at different IPTG induction levels (0, 10, or 100 µM; Figure 2.07C). Ultimately, maximum production was achieved using 10 µM IPTG where, after 120 hours, the final L-lysine titer reached 325.3 ± 14.8 mg/L. At 100 µM IPTG, meanwhile, biomass levels were significantly reduced (Figure 2.07A). In all cases, despite generally increasing L-lysine titers over the entire culture duration, cell density declined as cultivation continued past 48 hours. For example, even at the optimal level of 10 µM IPTG, although the culture reached a maximum biomass density of 1.64 ± 0.08 g-DCW/L by 48 hours, it ultimately fell to 1.00 ± 0.08 g-DCW/L by the end of the culture (120 hours). For comparison, wild-type UTEX 2973 under the same conditions does not typically exhibit such collapse (Figure 2.04), suggesting that this behavior indeed results as a consequence of L-lysine overproduction.

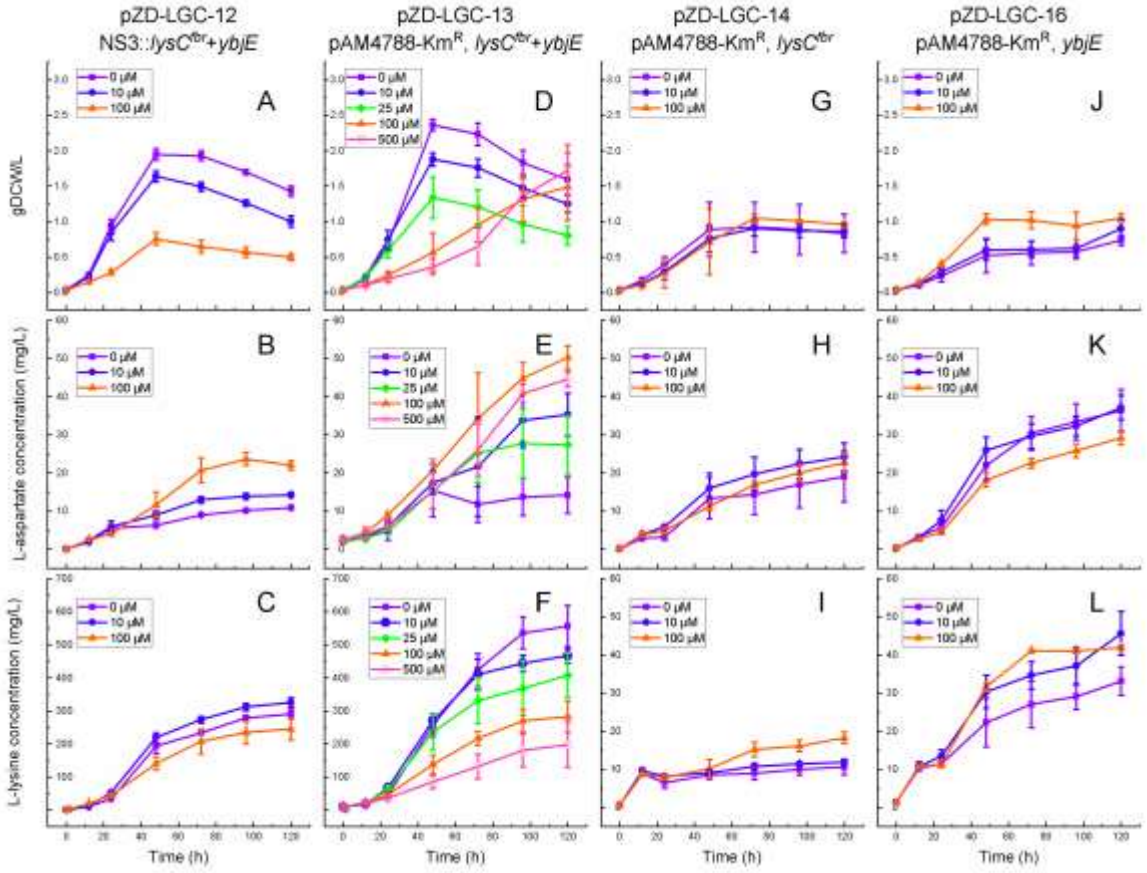

Figure 2.07 Comparison of L-lysine Production via Chromosomal and Episomal Pathway Expression in UTEX 2973.
Comparing cell growth (top row), extracellular L-aspartate accumulation (middle row), and extracellular L-lysine accumulation (bottom row) by engineered UTEX 2973 strains over the course of 120 hours when grown in shake flasks containing 25 mL BG-11 and varying concentrations of IPTG. From left column to right: strains conjugated with pZD-LGC-12 for chromosomal expression of *lysC*^{fbr}*+ybjE* (A-C), pZD-LGC-13 for episomal expression of *lysC*^{fbr}*+ybjE* (D-F), pZD-LGC-14 for episomal expression of *lysC*^{fbr} (G-I), and pZD-LGC-15 for episomal expression of *ybjE* (J-L). IPTG concentrations used were 0 μM (purple squares), 10 μM (blue circles), 25 μM (green diamonds), 100 μM (orange triangles), and 500 μM (pink bullseye). Error bars represent standard error from biological triplicates.

The observation that excessive *lysC*^{fbr} expression (i.e., >10 mM IPTG) negatively impacted both growth and L-lysine production could suggest that increased competition for precursor L-aspartate (the immediate precursor to L-

lysine) and/or its central metabolic precursor oxaloacetate (OAA) was responsible. However, in addition to growth and L-lysine production losses, increased *lysC*^{fbr} expression was actually found to correspond with greater extracellular accumulation of L-aspartate (Figure 2.07B). Notably, in addition to supporting the lowest L-lysine titer, the highest *lysC*^{fbr} induction level (i.e., 100 µM IPTG) also yielded the most L-aspartate, reaching 22.0 ± 1.2 mg/L by 120 hours; roughly 2-fold higher than with 10 µM IPTG. As this would seemingly suggest that essential precursors were not critically drained, it seems more plausible that, as demonstrated in other bacteria, the negative effects of high *lysC*^{fbr} induction are instead associated with a more generalized disruption of a stringently regulated amino acid network[12,120].

Lastly, it is noted that this initial strain employing chromosomal co-expression of *lysC*^{fbr} and *ybjE* represents a design analogous to the PCC 7002-derived L-lysine over-producer developed by Korosh and colleagues[12]. For comparison, under its own unique optimal expression conditions, that strain was capable of producing up to 254.4 ± 17.5 mg/L L-lysine by 96 hours (in this case using standard Media A$^+$, 1% CO_2 and ~200 µmol photon m^{-2} s^{-1}), which is slightly below the 312.3 ± 10.9 mg/L produced here in the same time by UTEX 2973 NS3::*lysC*^{fbr}+*ybjE*. Thus, the average volumetric productivity here was increased by 41% (3.8 vs. 2.7 mg/L-h) as a result of alternatively employing fast-growing UTEX 2973. Indeed, the initial volumetric growth rate (i.e., over the first 48 hours) of UTEX 2973 NS3::*lysC*^{fbr}+*ybjE* was nearly 2-fold faster than that of the PCC 7002 L-lysine over-producer under the respective conditions examined,

reaching an average of 34 mg-DCW/L-h. That said, the PCC 7002 L-lysine over-producer did not display the same decline in biomass as observed here (i.e., beyond 48 hours), suggesting unknown genotypic differences were responsible. This is further reflected by the fact that, while maximal L-lysine production by UTEX 2973 required low and optimized *lysC*^{fbr} expression, maximal expression was instead required in PCC 7002. Although differences in expression systems surely played a role (in PCC 7002, *lysC*^{fbr} was expressed via the tetracycline-inducible P_{EZtet} promoter), this study hypothesizes that key central metabolic differences between UTEX 2973 and PCC 7002 also contributed to the contrasting phenotypes. In particular, while there is no known α-ketoglutarate dehydrogenase encoded in cyanobacterial genomes[121] (responsible for converting α-ketoglutarate to succinyl-CoA as part of a complete TCA cycle[122]), individual cyanobacteria address this void in different ways[123]. For instance, *Synechocystis* sp. PCC 6803 maintains a functional γ-aminobutyric acid (GABA) shunt[124] whereas PCC 7002 utilizes α-ketoglutarate decarboxylase and succinic semialdehyde dehydrogenase in the absence of 2-oxoglutarate dehydrogenase[125,126]. The situation is furthermore different in UTEX 2973, as genes associated with both such routes are missing and thus so is its ability to operate a complete TCA cycle. Instead, past labeling data suggest that UTEX 2973 may use a linear pathway to convert OAA to citrate and α-ketoglutarate, and furthermore must convert a portion of L-aspartate to fumarate (via *RS11515* and *RS01375*; which can then be converted to the TCA organic acids malate and succinate) via purine metabolism[33]. These differences may increase the

sensitivity of UTEX 2973 to changes in its endogenous OAA and L-aspartate pools and, as such, also the confound influence of increased aspartate kinase activity, which in turn may impose greater stress on central carbon metabolism relative to PCC 7002.

2.3.3 Comparison of Chromosomal and Episomal Expression of the L-lysine Pathway

To improve upon the performance of UTEX 2973 NS3::*lysC*^{fbr}+*ybjE* , this study investigated whether an episomal expression strategy could instead be employed to increase L-lysine production, ideally while reducing (or eliminating) the need to supply costly IPTG. A single cassette featuring P_{trc2O}-*lysC*^{fbr}-T_{T7}-P_{MB2}-*lacI*^{WF} and P_{cpcB1*}-*ybjE*-T_{psbC} was cloned from pZD-LGC-12 and into the pAM4788-Km^{R} shuttle vector, resulting in pZD-LGC-13. UTEX 2973 harboring pZD-LGC-13 was then analogously cultivated under a range of IPTG concentrations (Figure 2.07D-F). As expected, episomal expression of *lysC*^{fbr} reduced the requirement for IPTG induction, with maximal L-lysine production now occurring in its complete absence (i.e., 'leaky expression' by the P_{trc2O}-*lacI*/O system). In this case, the maximal L-lysine titer was increased to 556.3 ± 62.3 mg/L after 120 hours; a 71% improvement relative to UTEX 2973 NS3::*lysC*^{fbr}+*ybjE* with 10 mM IPTG. As before, increasing beyond the optimal IPTG level reduced both growth and L-lysine production as well as resulted in increased accumulation of L-aspartate, in this case reaching a maximum of 50.3 ± 3.1 mg/L at 100 µM IPTG. Furthermore, a prolonged lag phase also emerged

at IPTG concentrations above 25 µM, likely as a result of excessive metabolic burden.

2.3.4 Confirmation of the Key 'Bottlenecks' in the Photosynthetic L-lysine Pathway

While the results thus far have confirmed that the general metabolic engineering strategy developed previously for PCC 7002[12] was sufficient and similarly effective for engineering L-lysine over-production by UTEX 2973, the essentiality of *lysC*^{fbr} and/or *ybjE* over-expression for achieving this phenotype was not yet explicitly determined. Although aspartate kinase has been predicted in UTEX 2973 (encoded by *RS11150*), its regulatory behavior and potential role as a pathway bottleneck have not yet been investigated. Meanwhile, although there are currently only three known L-lysine-specific exporters, including YbjE from *E. coli*[112], LysE from *C. glutamicum*[91,100,101], and the recently discovered MglE from *Xenopus oocyte*[127], none show significant homology with any protein in UTEX 2973 and no other native L-lysine exporters have otherwise been identified (directly or inferred). Accordingly, a series of control strains were constructed to individually examine the roles and importance of both *lysC*^{fbr} and *ybjE* expression on L-lysine production in UTEX 2973. As seen in Figure 2.07G-I, when *lysC*^{fbr} alone was episomally expressed via P_{trc2O}-*lacI*/O (using pZD-LGC-14) with up to 100 µM IPTG, both cell growth (reaching a maximum of 1.05 ± 0.06 g-DCW/L by 72 hours) and L-lysine production (reaching a maximum of just 18.3 ± 1.5 mg/L by 120 hours) were significantly reduced. Thus, with L-lysine export being significantly disrupted in the absence of *ybjE* co-expression, its

intracellular accumulation was likely responsible for the significant fitness defect. Meanwhile, when *ybjE* alone was episomally expressed via P_{cpcB1*} (pZD-LGC-16), both cell growth (peaking at 1.05 ± 0.06 g-DCW/L by 120 hours) and L-lysine production (reaching just 45.7 ± 5.8 mg/L by 120 hours) were again similarly reduced (note: IPTG was added to maintain identical culture conditions; Figure 2.07J-L). Furthermore, this strain also secreted and accumulated significant levels of L-aspartate, reaching as high as 37.1 ± 3.2 mg/L; an observation that may suggest that *ybjE* itself displays some activity on L-aspartate. Reduced fitness in this case, meanwhile, was likely instead due to export losses of a more limited endogenous L-lysine pool. Lastly, the function and importance of *ybjE* (as well as other factors) was further examined by analyzing the constructed strains with respect to changes in intra- vs. extracellular levels of L-lysine and L-aspartate (both on a per-cell-mass basis) following 120 hours of culturing (Figure 2.08). While levels of intracellular L-lysine remained relatively constant across all strains expressing either $lysC^{fbr}$ or *ybjE* (~0.8-2.1 mg/g-DCW), extracellular L-lysine was significantly increased when both $lysC^{fbr}$ and *ybjE* were co-expressed (with extracellular:intracellular L-lysine ratios peaking at 138.7 and 197.2 for chromosomal and episomal expression, respectively). In contrast, when just either $lysC^{fbr}$ or *ybjE* were expressed, this ratio reached a maximum of just 52.2 (i.e., when *ybjE* was expressed alone). For comparison, the control expressing neither gene achieved a ratio of 16.6 for L-lysine. Extracellular:intracellular ratios of L-aspartate followed an opposite trend to that of L-lysine, being reduced to minimum levels when $lysC^{fbr}$ and *ybjE* were co-expressed (reaching just 2.5 and

3.4 for chromosomal and episomal expression, respectively); levels that remained similar to the empty vector control. As yet another comparison, a previous study measured cytosolic and secreted sucrose in salt-stressed UTEX 2973 engineered with the sucrose export gene *cscB*[40]. After 144 hours, the extracellular:intracellular ratio of sucrose reached roughly 50, similar to the *ybjE* control in this work. A strain of *C. glutamicum* engineered with its endogenous L-lysine export gene *lysE* under the control of an L-lysine-ON riboswitch only reached an extracellular:intracellular ratio of 1.4[128]. Notably, this strain was not fully optimized as an L-lysine overproducing platform, with a fairly modest titer of 6.1 g/L L-lysine. Overall, *lysC*^{fbr} and *ybjE* co-expression was critical for L-lysine production in UTEX 2973, as significant flux to L-lysine was not possible without *lysC*^{fbr}, whereas effective export of L-lysine was not possible without *ybjE*.

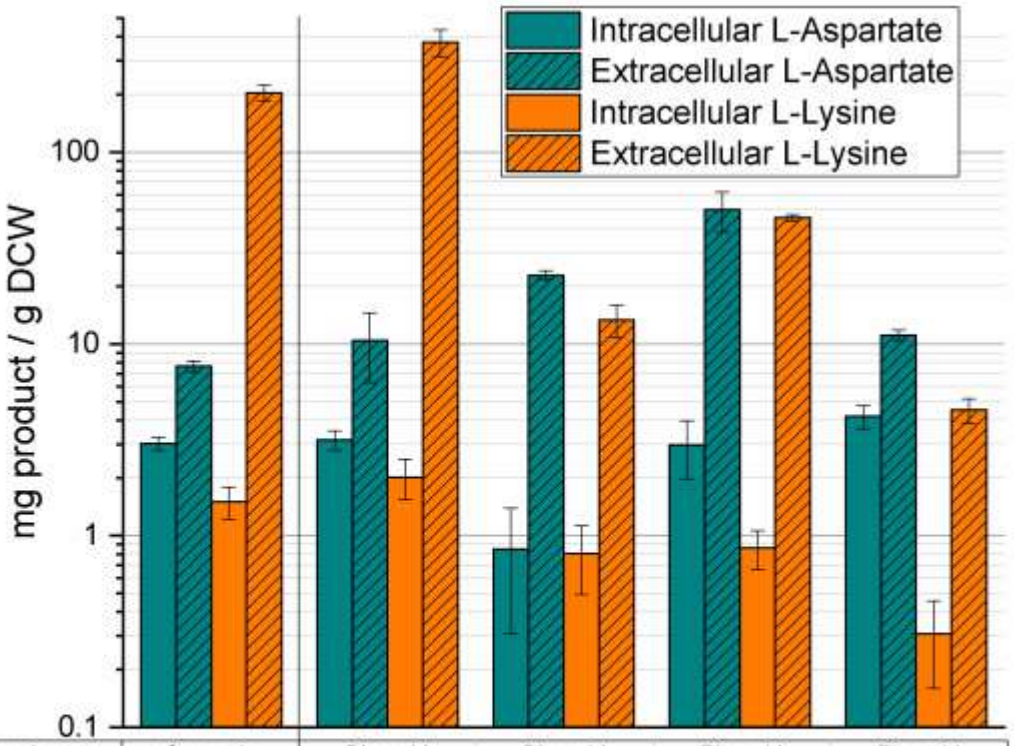

Expression	Genomic	Plasmid	Plasmid	Plasmid	Plasmid
P_{trc10}-*lysC*^{fbr}-lacI	+	+	+	-	-
P_{cpcB1}-*ybjE*	+	+	-	+	-
IPTG (μM)	10	0	0	0	0
Final gDCW/L	1.00±0.07	1.25±0.11	0.83±0.27	0.74±0.07	1.68±0.21

Figure 2.08 Comparison of Intracellular versus Extracellular L-lysine Accumulation by Different UTEX 2973 Mutants.
Intracellular (solid bars) and extracellular (striped bars) concentrations of L-aspartate (teal) and L-lysine (orange) were determined per unit biomass for selected UTEX 2973 mutants after 120 hours. Error bars represent standard error from biological triplicates.

2.3.5 Engineering Central Carbon Metabolism to Improve Precursor Flux to the L-lysine Pathway

This study lastly sought to examine if L-lysine production could be further improved by increasing metabolite flux towards OAA, thereby providing a greater 'push' into the L-lysine pathway. Pyruvate carboxykinase (encoded by *pck*) and phosphoenolpyruvate carboxylase (encoded by *ppc*) from *E. coli* as well as

pyruvate carboxylase (encoded by *pyc*) from *C. glutamicum* are all central metabolic enzymes whose over-expression has been extensively examined in heterotrophs as a means to boost production of various biochemicals derived from OAA[104,129] (Figure 2.09). Among these, Pyc notably catalyzes the direct conversion of pyruvate to OAA; a reaction not known to natively occur in UTEX 2973 (Figure 2.06). Each of *pck*, *ppc*, and *pyc* were individually co-expressed alongside *lysC*^{fbr} and *ybjE* to examine their potential effect on photosynthetic L-lysine production. However, when compared to Figure 2.07F, in all cases, maximum final L-lysine titers were reduced relative to UTEX 2973 harboring pZD-LGC-13 (by 23.6 to 55.2%). Though unsuccessful for improving L-lysine production, this outcome reinforces the past observation that, in UTEX 2973, native PEP carboxylase already drives significant flux to OAA[33], which places additional importance on *lysC*^{fbr} as the pathway bottleneck rather than another upstream step. ^{13}C labelling of CO_2 for metabolic flux analysis, the technique employed by Abernathy and colleagues[33] to elucidate carbon flow in UTEX 2973, can similarly be used in future studies to quantitively demonstrate central carbon metabolism flux in mutant strains overproducing L-lysine.

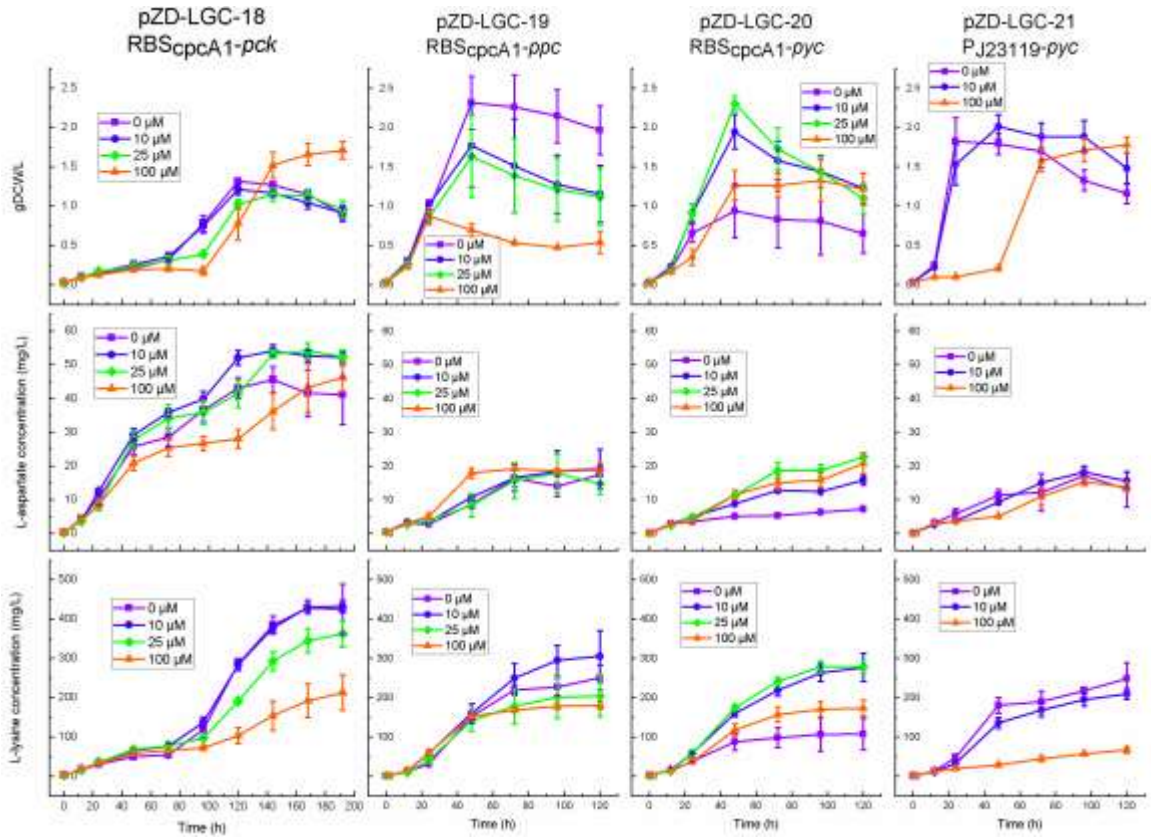

Figure 2.09. Comparing the Influence of Different Strategies for Increasing Flux to OAA during L-lysine Production by UTEX 2973.
Accumulation of biomass (top row), L-aspartate (middle row), and L-lysine (bottom row) by UTEX 2973 mutants over 120 hours in shake flasks containing 25 mL BG-11 at varying concentrations of IPTG. From left to right are strains harboring: pZD-LGC-18, pZD-LGC-19, pZD-LGC-20, and pZD-LGC-21. IPTG concentrations used were 0 μM (purple squares), 10 μM (blue circles), 25 μM (green diamonds), and 100 μM (orange triangles). Error bars represent standard error from biological triplicates.

2.4 Future Work

Based on rough calculations of the expected amount of nitrogen present in the standard BG-11 used (Appendix B), it appears that nitrogen starvation might account for the crash in biomass observed in Figure 2.07A and D. Preliminary attempts to supplement with ammonium sulfate led to poorer growth compared to

strains grown in normal control media (Appendix C). However, changes made to the light source in this experiment serve to confound the specific effect of the additional nitrogen source. Further experiments under standard light conditions and exploring more species of nitrogen would serve to better determine whether UTEX 2973 biomass can be rescued when overexpressing feedback-resistant L-lysine pathway genes.

Cyanobacterial L-lysine production benefits from the expression of THDP-acetyltransferase (*THDP-AT*), which catalyzes the conversion of THDP directly to LL-diaminopimelate (Figure 2.01). By contrast, *E. coli*'s succinylase-based pathway accomplishes the same using three enzymes. In the vein of this observation, a potentially complementary gene to express in addition to the current work's cassette would be *ddh* from *C. glutamicum*, which converts THDP yet one more step further than *THDP-AT* to *meso*-diaminopimelate. Xu and colleagues[99] previously demonstrated the benefit of heterologous *ddh* expression to improve L-lysine overproduction titers in *E. coli*.

Finally, assaying of pZD-LGC-12 and pZD-LGC-13 under light-dark cycling conditions is necessary to determine the feasibility of industrial scale-up with these mutants. Productions strains grown in open- and raceway-pond systems will not be subject to continuous light. A study involving another UTEX 2973 mutant engineered to produce 3-hydroxypropionic acid found that light-dark cycles caused a roughly 50% drop in biomass and 60% drop in production, despite additional mutations that allowed the strain in question to consume xylose supplied to the culture[21]. Similar understanding of production loss in this

work would help to illuminate the true productivity of photosynthetic L-lysine relative to the established heterotrophic industry.

CHAPTER 3

PRODUCTION OF BIOPLASTIC MONOMERS IN THE FAST-GROWING CYANOBACTERIUM *SYNECHOCOCCUS* SP. UTEX 2973

ABSTRACT

The L-lysine overproducing UTEX 2973 strain developed in Chapter 2 was next further engineered for the photosynthetic biosynthesis of both cadaverine and glutarate; two 5-carbon, bioplastics monomers. Cadaverine production was achieved through a single step catalyzed by L-lysine decarboxylase, encoded by *E. coli cadA*. However, since cadaverine demonstrated significant toxicity towards UTEX 2973, the additional introduction of an efflux system was also investigated to improve tolerance. Several known, heterologous cadaverine exporters were accordingly screened in UTEX 2973, which was then grown in the presence of exogenous cadaverine at different concentrations. Ultimately, the ATP-binding cassette transporter encoded by *sapBCDF* from *E. coli* demonstrated the best performance and was subsequently co-expressed along with feedback-resistant aspartokinase $lysC^{fbr}$ and lysine decarboxylase *cadA* (all from *E. coli* as well). By this approach, cadaverine was produced at up to 55.3 ± 6.7 mg/L by 96 hours. Glutarate, by contrast, was not found to be inhibitory to UTEX 2973 and was (at least to a limited extent) natively capable of crossing the cell membrane. Heterologously expressing the operons *davDT* and *davBA* (both from *Pseudomonas putida*) in tandem with $lysC^{fbr}$ enabled glutarate production at final titers reaching 67.5 ± 2.2 mg/L by 96 hours. In the future, overcoming

remaining pathway and/or transport bottlenecks will be important to improving upon the production performance of both molecules.

3.1 Introduction

Bioplastics represent a diverse and growing class of renewable products whose overall market was projected to reach $5.08 billion in 2021[130]. One class of bioplastics, polyamides, have potential uses in a wide range of industries, including aeronautics and automobiles, machining, packing, and cosmetics[131,132]. The market for traditional, petroleum-derived polyamides currently stands at 6.6 million tons produced per year[133], indicating huge potential for growth of bio-based competitors in the coming years. Using biogenic L-lysine as a starting point, it is possible to target multiple potential polyamide monomers via heterologously expressed metabolic pathways. This includes both the diamine cadaverine, as well as the dicarboxylate glutarate (which can further be used in polyester production).

From lysine, cadaverine overproduction is straightforward to engineer, as it involves just a single step: lysine decarboxylase[134] (Figure 3.01). While *C. glutamicum* would once again appear the most obvious choice for a molecule that requires L-lysine as a precursor, this organism lacks a native lysine decarboxylase. There are two lysine decarboxylases native to *E. coli*, the inducible *cadA* and constitutively-expressed *ldcC*[133]. Most cadaverine production literature involves the use of CadA, as LdcC demonstrates lower activity and worse stability by comparison[135,136]. Using this strategy, a record titer of 103.78

g/L cadaverine has been reached through the provision of glucose[137] (similar titers have also been achieved using xylose as feedstock[129]).

The biosynthetic route from L-lysine to glutarate is somewhat more complex by comparison. As previously demonstrated by Revelles and colleagues, the *davDT* operon from *Pseudomonas putida* KT2440 encodes glutarate-semialdehyde dehydrogenase and 5-aminovalerate aminotransferase which together can catalyze the conversion of 5-aminovalerate (5-AMV; itself a useful biomonomer) to glutarate through the intermediate glutarate semialdehyde[138]. Subsequent annotation of the *davBA* operon[139], which encodes lysine 2-monooxygenase and 5-aminopentanamidase, converting L-lysine to 5-aminovaleramide and subsequently 5-AMV, revealed a completed pathway for converting L-lysine to glutarate (Figure 3.01). Heterologous expression of this pathway was achieved simultaneously by several groups, demonstrating that *E. coli* could be engineered to target either species, with titers reaching up to 1.7 g/L glutarate[115,140] (and 3.6 g/L 5-AMV expressing just *davDT*). *C. glutamicum*, a much more prodigious chassis for L-lysine accumulation, has also been extensively engineered to produce glutarate at up to a remarkable 105.3 g/L over the course of just 69 hours[129]. The main discoveries of that work reflect earlier described works relating to photoautotrophic L-lysine production, including the cruciality of relieving intermediate accumulation and efficiently exporting final products in order to affect optimal bioproduction[12,129,141,142]. In particular, a recently discovered native dicarboxylate exporter gene, *ynfM*[143], was expressed chromosomally under a strong promoter to roughly double the final titer[129].

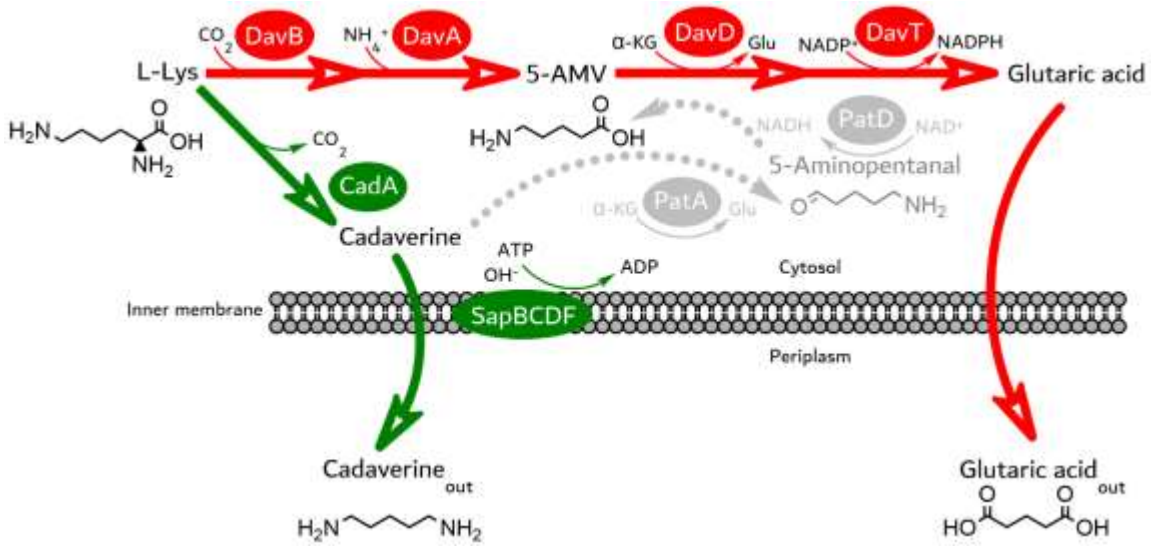

Figure 3.01. Engineered Pathways towards Cadaverine and Glutarate Biosynthesis in UTEX 2973.
Pathways engineered in this work for the biosynthesis of the biomonomers cadaverine and glutarate using L-lysine as a starting point. Cadaverine production genes are shown in dark green and include *cadA*, lysine decarboxylase; and *sapBCDF*, polyamine exporter. Glutarate production genes are shown in red and include *davB*, lysine 2-monooxygenase; *davA*, 5-aminopentanamidase; *davD*, glutarate-semialdehyde dehydrogenase; and *davT*, 5-aminovalerate aminotransferase. The *E. coli* degradation pathway linking cadaverine and 5-aminovalerate is shown in light gray and was not heterologously expressed in this work. Metabolites shown include L-Lys, lysine; and 5-AMV, 5-aminovalerate.

As was the approach with engineering photosynthetic L-lysine overproduction in Chapter 2, here the goal was to recapitulate these established, heterotrophic pathways for the first time in a photoautotrophic host, namely UTEX 2973. This work builds from the results and strains developed in Chapter 2, specifically leveraging the engineered UTEX 2973-based L-lysine overproduction strain as a starting point.

3.2 Methods and Materials

3.2.1 Chemicals

All enzymes were purchased from New England Biolabs (Ipswich, MA). Cadaverine was purchased from TCI America (Portland, OR). All other chemicals were purchased at the highest available purities from Sigma-Aldrich (St. Louis, MO) or Santa Cruz Biotechnology (Dallas, TX), unless otherwise indicated.

3.2.2 Strains and Culture Conditions

UTEX 2973 was obtained from the UTEX Culture Collection of Algae at the University of Texas at Austin. Culturing in liquid media and on solid agar plates was performed using BG-11 medium buffered with 10 mM TES/NaOH, pH 8.2 (where agar plates were also supplemented with 3 g/L sodium thiosulfate) at 38°C under continuous light at an intensity of ~200 µmol photon m^{-2} s^{-1}, unless otherwise specified. Where necessary, plasmids were maintained in UTEX 2973 via addition of 50 µg/mL kanamycin. Liquid cultures were grown while shaking at 200 rpm in 250 mL non-baffled flasks containing 25 mL media and seeded to an initial cell density as determined by optical density at 750 nm (OD_{750}) of 0.1. Culture growth at 1% CO_2 was carried out in a Caron Plant Growth Chamber Model 7300 (Marietta, OH) set to maximum humidity (~63%). Where appropriate, expression of relevant pathway genes and/or transporters was achieved via addition of IPTG (for the *lac*-derived promoter system) and/or theophylline (for the Riboswitch F-derived promoter system) at final concentrations of up to 500 µM and 2 mM, respectively.

3.2.3 Plasmid Construction

All plasmids constructed and/or used in this study are summarized in Table 3.01. Plasmids constructed for this study were assembled via the Gibson assembly[113]. All oligonucleotide primers (IDT, Coralville, IA) used in plasmid assembly and sequencing are summarized in Appendix A. *E. coli* MG1655 gDNA served as the template for genes encoding cadaverine antiporter (*cadB*), the cadaverine export system (*sapBCDF*), and lysine decarboxylase (*cadA*). *C. glutamicum* ATCC 13032 gDNA served as the template for genes encoding cadaverine exporter (*cgmA*), and dicarboxylic acid exporter (*ynfM*). *Pseudomonas putida* KT2440 gDNA served as the template for the native operons encoding lysine 2-monooxygenase and 5-aminopentanamidase (*davBA*) as well as glutarate semialdehyde dehydrogenase and 5-aminovalerate aminotransferase (*davDT*). All plasmids were screened first by colony PCR, followed by restriction digest mapping and final verification via DNA sequencing. The plasmid pZD-LGC-25, a derivative of pZD-LGC-13 additionally expressing the cadaverine antiporter *cadB* as part of a bicistronic operon under P_{cpcB1*}, was assembled by amplifying the template pZD-LGC-13 with primers ZDC-105 and ZDC-104, and *cadB* from *E. coli* MG1655 gDNA with primers ZDC-103 and ZDC-102. The plasmid pZD-LGC-24, a derivative of pZD-LGC-03 where *yemGFP* has been replaced by *cadB*, was assembled by amplifying the template pZD-LGC-03 with primers ZDC-246 and ZDC-247, and *cadB* from *E. coli* MG1655 gDNA with primers ZDC-244 and ZDC-245. The plasmid pZD-LGC-26, a derivative of pZD-

LGC-25 no longer expressing *lysC*^{fbr}, was assembled by amplifying the template pAM4788-Km^{R} with primers ZDC-072 and ZDC-229, and the P$_{cpcB1*}$-*cadB*-T$_{psbC}$ cassette from pZD-LGC-25 with primers ZDC-228 and ZDC-067. The plasmid pZD-LGC-27, a derivative of pZD-LGC-26 where the intergenic region RBS$_{cpcA1}$ has been replaced by the P$_{J23119}$ promoter was assembled by amplifying the backbone pZD-LGC-26 with the primers ZDC-254 and ZDC-104, and the P$_{23119}$-cadB cassette from pZD-LGC-24 with primers ZDC-103 and ZDC-253. The plasmid pZD-LGC-22, a derivative of pZD-LGC-027 where *ybjE*-P$_{J23119}$-*cadB* has been replaced by the cadaverine exporter *cgmA*, was assembled by amplifying the template pZD-LGC-027 with primers ZDC-093 and ZDC-092, and *cgmA* from *C. glutamicum* gDNA with primers ZDC-091 and ZDC-090. The plasmid pZD-LGC-23, a derivative of pZD-LGC-027 where *ybjE*-P$_{J23119}$-*cadB* has been replaced by the putative cadaverine exporter *sapBCDF*, was assembled by amplifying the template pZD-LGC-027 with primers ZDC-233 and ZDC-232, and *sapBCDF* from *E. coli* MG1655 gDNA with primers ZDC-231 and ZDC-230. The plasmid pZD-LGC-028, a derivative of pZD-LGC-13 with an extra terminator T$_{rrnB}$ directly behind *lysC*^{fbr} in the cassette, was assembled by amplifying the template pZD-LGC-13 with the primers ZDC-123 and ZDC-109, and T$_{rrnB}$ from pSL3137 with the primers ZDC-110 and ZDC-122. The plasmid pZD-029, a derivative of pZD-LGC-11 where *yemGFP* has been replaced with the lysine decarboxylase *cadA*, was assembled by amplifying the template pZD-LGC-11 with the primers ZDC-050 and ZDC-225, and *cadA* from *E. coli* MG1655 gDNA with primers ZDC-224 and ZDC-049. The plasmid pZD-LGC-30, a derivative of pZD-LGC-23

additionally expressing a cadaverine production pathway, was assembled by amplifying the template pZD-LGC-28 with primers ZDC-233 and ZDC-227, the P_{conII}-Riboswitch-F-*cadA*-T_{T7}-*lacI*^{WF} cassette from pZD-LGC-29 with primers ZDC-226 and ZDC-071, and the *sapBCDF*-T_{psbC} cassette from pZD-LGC-23 with primers ZDC-070 and ZDC-230. The plasmid pZD-LGC-31, a derivative of pZD-LGC-25 where *cadB* has been replaced with glutarate semialdehyde dehydrogenase / 5-aminovalerate aminotransferase operon *davDT*, was assembled by amplifying the template pZD-LGC-25 with the primers ZDC-105 and ZDC-182, and *davDT* from *P. putida* KT2440 gDNA with primers ZDC-181 and ZDC-180. The plasmid pZD-LGC-32, a derivative of pZD-LGC-31 where the glutaric acid production pathway is completed by the replacement of *ybjE* with lysine 2-monooxygenase / 5-aminopentanamidase operon *davBA*, was assembled by amplifying the template pZD-LGC-31 with the primers ZDC-183 and ZDC-180, and *davBA* from *P. putida* KT2440 gDNA with primers ZDC-179 and ZDC-178. The plasmid pZD-LGC-33, a derivative of pZD-LGC-32 where the intergenic region RBS_{cpcA1} has been replaced by the P_{J23119} promoter was assembled by amplifying the backbone pZD-LGC-32 with ZDC-256 and ZDC-248 an the promote with ZDC-251 and ZDC-255. The plasmid pZD-LGC-34, a derivative of pZD-LGC-32 with the putative glutaric acid exporter *ynfM* under the control of P_{conII}-Riboswitch-F was assembled by amplifying the template pZD-LGC-32 with the primers ZDC-259 and ZDC-178, the pANS origin backbone and *lysC*^{fbr} stretching from P_{cpcB1*} on one end to P_{conII}-Riboswitch-F on the other from

pZD-LGC-30 with primers ZDC-183 and ZDC-260, and *ynfM* from *C. glutamicum* ATCC 13032 gDNA with primers ZDC-257 and ZDC-258.

Table 3.01 List of Plasmids Constructed and Used in this Study to Engineer the Production and/or Export of Cadaverine and Glutarate.

Plasmid	Genotype
pZD-LGC-22	pANS; P_{cpcB1*}-*cgmA*-T_{psbC}; Km^R
pZD-LGC-23	pANS; P_{cpcB1*}-*sapBCDF*- T_{psbC}; Km^R
pZD-LGC-24	pANS; P_{J23119}-*cadB*-T_{rrnB2}; Km^R
pZD-LGC-25	pANS; P_{trc2O}-*lysC*^{fbr}-T_{T7}-P_{MB2}-*lacI*^{WF}; P_{cpcB1*}-*ybjE*-RBS_{cpcA1}-*cadB*-T_{psbC}; Km^R
pZD-LGC-26	pANS; P_{cpcB1*}-*ybjE*- RBS_{cpcA1}-*cadB*- T_{psbC}; Km^R
pZD-LGC-27	pANS; P_{cpcB1*}-*ybjE*-P_{J23119}-*cadB*- T_{psbC}; Km^R
pZD-LGC-28	pANS; P_{trc2O}-*lysC*^{fbr}- T_{rrnB2}-T_{T7}-P_{MB2}-*lacI*^{WF}; P_{cpcB1*}-*ybjE*-T_{psbC}; Km^R
pZD-LGC-29	pANS; P_{conII}-Riboswitch-F-*cadA*-T_{T7}-P_{MB2}-*lacI*^{WF}; Km^R
pZD-LGC-30	pANS; P_{trc2O}-*lysC*^{fbr}- T_{rrnB2}-P_{conII}-Riboswitch-F-*cadA*-T_{T7}-P_{MB2}-*lacI*^{WF}; P_{cpcB1*}-*sapBCDF*- T_{psbC}; Km^R
pZD-LGC-31	pANS; P_{trc2O}-*lysC*^{fbr}-T_{T7}-P_{MB2}-*lacI*^{WF}; P_{cpcB1*}-*ybjE*- RBS_{cpcA1}-*davDT*- T_{psbC}; Km^R
pZD-LGC-32	pANS; P_{trc2O}-*lysC*^{fbr}-T_{T7}-P_{MB2}-*lacI*^{WF}; P_{cpcB1*}-*davBA*- RBS_{cpcA1}-*davDT*- T_{psbC}; Km^R
pZD-LGC-33	pANS; P_{trc2O}-*lysC*^{fbr}-T_{T7}-P_{MB2}-*lacI*^{WF}; P_{cpcB1*}-*davBA*-P_{J23119}-*davDT*-T_{psbC}; Km^R
pZD-LGC-34	pANS; P_{trc2O}-*lysC*^{fbr}- T_{rrnB2}-P_{conII}-Riboswitch-F-*ynfM*-T_{T7}-P_{MB2}-*lacI*^{WF}; P_{cpcB1*}-*ybjE*-RBS_{cpcA1}-*davDT*- T_{psbC}; Km^R

3.2.4 Genetic Modification of UTEX 2973

Conjugation was performed to deliver all constructed shuttle and integration vectors via a tripartite mating procedure adapted from Yu and colleagues[29]. An elaborated method can be found in Section 2.2.5.

3.2.5 Sample Preparation for Intracellular Metabolite Analysis

Cells were prepared for intracellular analysis in a manner identical to the method elaborated upon in Section 2.2.6.

3.2.6 Analytical Methods

Periodically throughout each culture, aqueous samples were removed for amino acid analysis via high-performance liquid chromatograph (HPLC) following a diethyl ethoxymethylenemalonate (DEEMM) derivatization method adapted from that of Kim and colleagues[116]. An elaborated method can be found in Section 2.2.9. Under the conditions of DEEMM derivative analysis, L-aspartate, 5-AMV, L-lysine, and cadaverine eluted at 3.6, 9.3, 12.7 and 26.3 min, respectively.

Where appropriate, culture samples were likewise analyzed for glutaric acid via HPLC. In this case, 250 µL culture was collected and cells were removed by pelleting before 200 µL of supernatant was then added to an HPLC vial containing 200 µL deionized H_2O. Analysis was carried out using an Agilent 1100 Series HPLC equipped with a refractive index detector maintained at 35°C. Moreover, in this case, separation was performed using a Bio-Rad Aminex HPX-87H column (7.8 mm x 300 mm, 9 µm particle size) maintained at 35°C and mobile phase consisting of 5 mM H_2SO_4 solution at a constant flow rate of 0.77 mL/min. Under these conditions, glutaric acid eluted at 11.0 min. An external calibration curve for glutarate was also generated using solutions prepared from an authentic standard.

3.3 Results and Discussion

3.3.1 Toxicity Assay of UTEX 2973 in the Presence of Cadaverine

In preliminary work, several plasmid constructs constitutively expressing *lysC*^{fbr} and *cadA* in tandem were conjugated into UTEX 2973 but yielded no exconjugants (data not shown). This result indicated the possible toxicity of cadaverine towards UTEX 2973. Similar loss of fitness in the presence of cadaverine was also observed for PCC 6803 (see Chapter 4; Figure 4.05), suggesting that cadaverine was likely broadly inhibitory to cyanobacteria. Interestingly, however, cadaverine toxicity was never noted to be a particular concern for either *E. coli* or *C. glutamicum*, indicating that this behavior was specific to cyanobacterial species in some regard. Phenotypically, the presence of the thylakoid membrane sets cyanobacteria apart from typical heterotrophs[29,144]. This physiological difference may lead to intercalation of cadaverine[145]. Another potential culprit (and difference from *E. coli* or *C. glutamicum*) is the lack of a native cadaverine exporter in model cyanobacteria strains. To begin troubleshooting cadaverine production in UTEX 2973, its toxicity was next more specifically characterized by growing the wild-type strain in the presence of increasing concentrations of exogenous cadaverine (Figure 3.02). Wild-type UTEX 2973 demonstrated decent tolerance up to working concentrations of 110 mg/L cadaverine, however, levels above this proved deleterious to cell growth. Cadaverine export, based off of these results, was hypothesized to not only be useful to relieving upstream flux bottlenecks but as an essential mechanism in the engineering of tolerance.

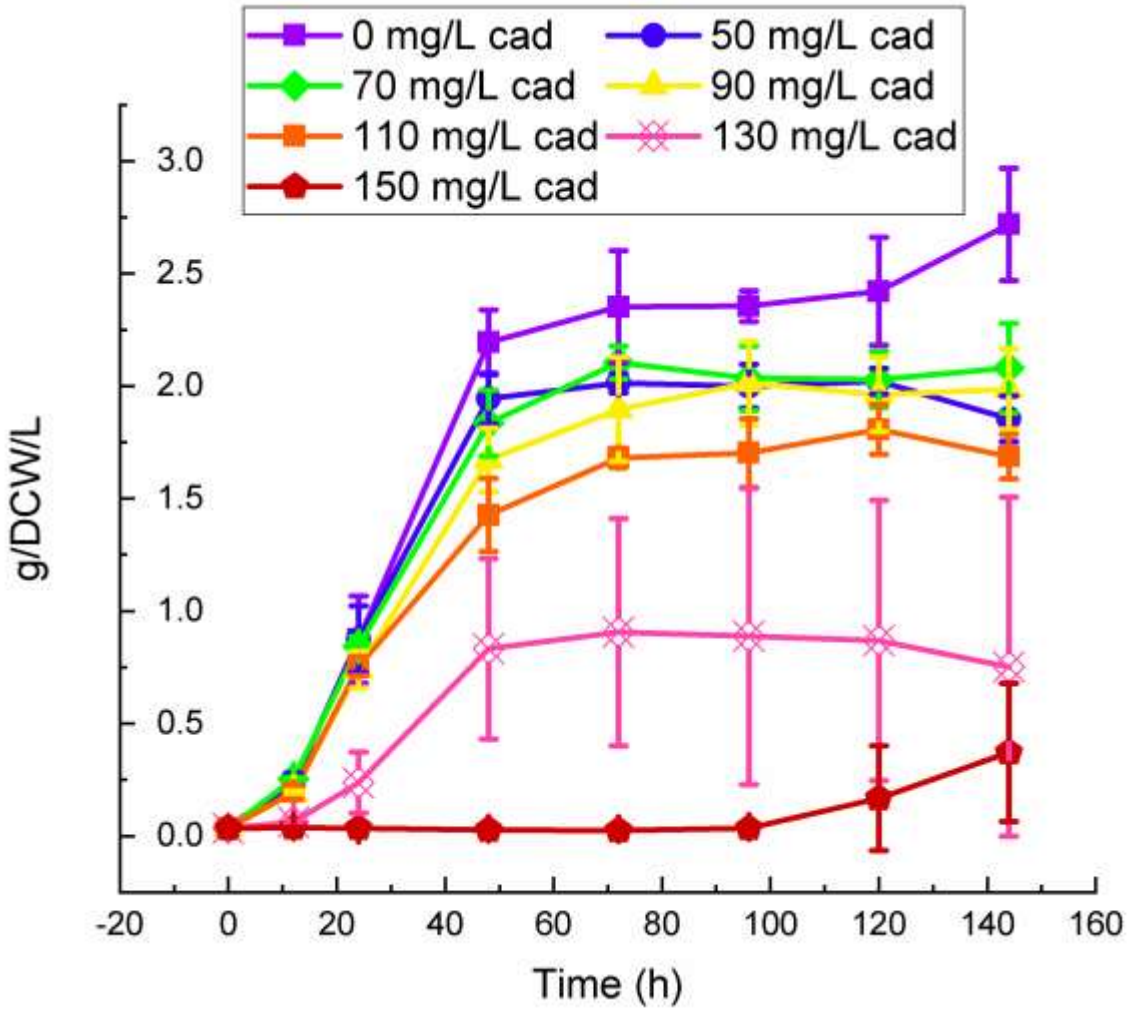

Figure 3.02. Growth of UTEX 2973 in the Presence of Varying Concentrations of Cadaverine.
UTEX 2973, grown under standard conditions (BG-11 media, 38°C, 200 µmol photons/m^2/s, 1% CO_2, maximum humidity) over 144 hours with increasing amounts of cadaverine added to the media. From lowest to highest concentration: 0 mg/L (purple squares), 50 mg/L (blue circles), 70 mg/L (green diamonds), 90 mg/L (yellow triangles), 110 mg/L (orange squares), 130 mg/L (pink bullseyes), 150 mg/L (red pentagons). Error bars represent standard error from biological triplicates.

3.3.2 Engineering Cadaverine Tolerance in UTEX 2973

While it may be the case that a potential polyamide-specific transporter remains undiscovered, a BLAST search of known cadaverine transporters

against the genome of UTEX 2973 revealed no candidates. Among known cadaverine transporters are *E. coli*'s lysine:cadaverine antiporter, *cadB*[146]; *C. glutamicum*'s cadaverine-exporting facilitator permease, *cgmA*[147]; and *E. coli*'s putrescine/cadaverine ATP-binding cassette transporter, *sapBCDF*[142,148]. Regardless of the reason, realization of photoautotrophic cadaverine production necessitates simultaneous engineering of cadaverine tolerance. Since active efflux can itself constitute an effective tolerance mechanism[127,149,150], this work first sought to address prospective challenges by evaluating the heterologous function of a series of different cadaverine exporters and their impact on the ability of UTEX 2973 to tolerate exogenously supplied cadaverine over a range of concentrations (Figure 3.03). The specific exporters of interest included *cgmA* (pZD-LGC-22) and *sapBCDF* (pZD-LGC-23). Furthermore, the lysine:cadaverine antiporter encoded by *cadB* from *E. coli* was also investigated, in this case by co-expressing it together with *ybjE* (pZD-LGC-27) while additionally supplementing the medium with 860 mg/L L-lysine (twice the molar equivalent of the maximal cadaverine concentration used; i.e., 300 mg/L) to provide the biochemical driving force needed for cadaverine export. A control plasmid expressing *yemGFP* (pZD-LGC-02) was also constructed and used for comparison. In all cases, exposure to 300 mg/L cadaverine proved severe, with near-complete loss of growth (i.e., 75-85% reduction relative to growth of the same strain at 0 mg/L cadaverine) within 48 to 72 hours. Overall, while cadaverine was relatively toxic to UTEX 2973, strains expressing the *sapBCDF* cassette generally displayed the highest tolerance, especially when faced with concentrations in the range of 150-200

mg/L. The *ybjE/cadB* antiporter, meanwhile, fared the worst, displaying poorer cadaverine tolerance than even the control strain; likely as a result of the increased burden associated with co-expressing two membrane proteins. Based on these outcomes, *sapBCDF* was selected to be advanced in support of engineering cadaverine biosynthesis.

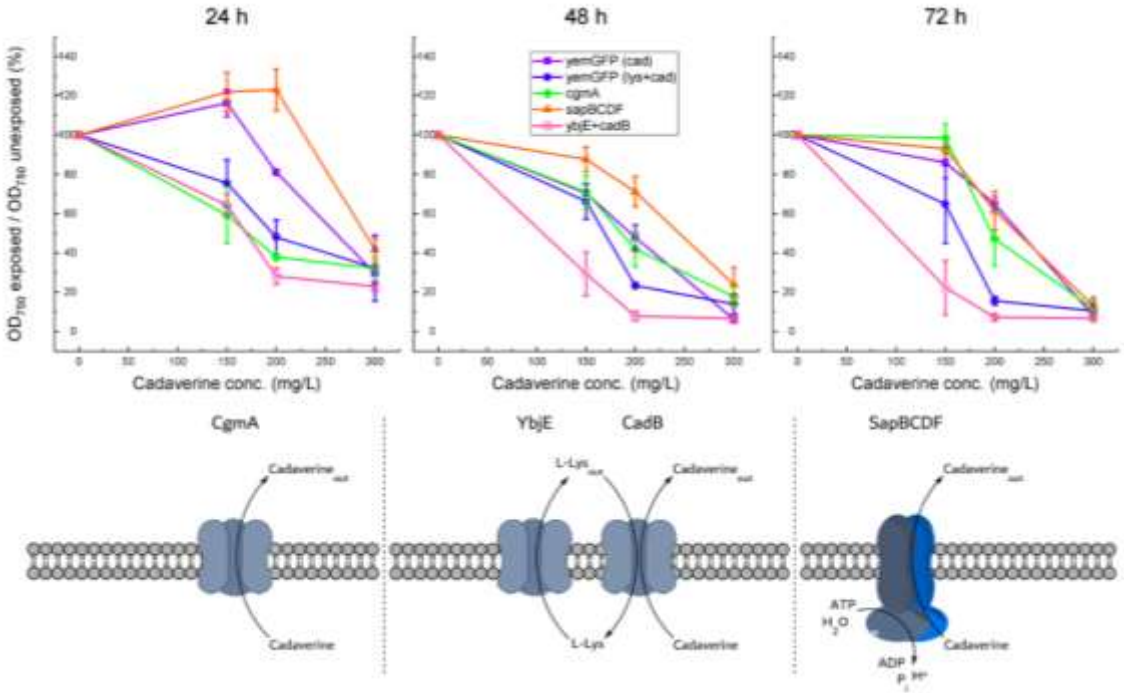

Figure 3.03. Comparison of Exporter Expression in UTEX 2973 in the Presence of Cadaverine.
Above: comparing the growth of UTEX 2973 strains expressing different cadaverine export systems when exposed to increasing cadaverine concentrations versus unexposed. Tested exporters and controls were yemGFP in the presence of cadaverine (purple squares), yemGFP in the presence of both lysine and cadaverine (blue circles), cgmA in the presence of cadaverine (green diamonds), sapBCDF in the presence of cadaverine (orange triangles), and ybjE and cadB in the presence of cadaverine (pink bullseyes). Error bars represent standard error from biological triplicates. Below: modes of cadaverine export by each of the evaluated systems including (from left to right): CgmA, CadB with YbjE, and SapBCDF.

3.3.3 Engineering Direct Cadaverine Production in UTEX 2973

To explore de novo cadaverine production by UTEX 2973, pZD-LGC-30 was next constructed to co-express *lysC*^{fbr} (via P_{trc2O}-*lacI/O*), *cadA* (via P_{conII}-Riboswitch F), and *sapBCDF* (via P_{cpcB1*}). Following conjugation, UTEX 2973 harboring pZD-LGC-30 was then cultivated in BG-11 media containing no IPTG and a range of theophylline concentrations. Here, as seen in Figure 3.04, while cadaverine production was possible in all cases, a maximum final titer of 59.7 ± 10.0 mg/L was achieved by 120 hours when using 0.5 mM theophylline. Minor co-accumulation of L-lysine was also observed in all cultures (reaching ~6-8 mg/L), though this behavior was consistent with the empty vector control (Figure 3.05) and remained insensitive to the *cadA* induction level. While providing no theophylline led to the best growth (reaching up to 1.79 ± 0.14 g-DCW/L), this also resulted in the lowest final cadaverine titers (24.4 ± 9.8 mg/L). It should also be noted that, although no proteomic analysis was performed to confirm expression of the pathway genes, no cadaverine was detected over 120 hours for either wild-type UTEX 2973 or the lysine-producing strain (i.e., carrying pZD-LGC-13; not shown). In general, when compared with the L-lysine producing strains, fitness losses displayed during cadaverine production were of a similar magnitude as those displayed by the L-lysine control strain expressing just *lysC*^{fbr} alone (i.e., no *ybjE*; Figure 2.07G-I). This could suggest that fitness losses during cadaverine production were again a result of intracellular L-lysine build-up, as

would be caused in this case by its inefficient conversion to and/or export of cadaverine. That said, further increased in *cadA* expression (i.e., using 2 mM theophylline) led to reduced cadaverine production (45.0 ± 10.9 mg/L) along with an even a greater decline in fitness (with the maximum biomass concentration reaching just 0.76 ± 0.18 g-DCW/L; Figure 3.04). Thus, it appears most likely that the fitness defect in this case was instead due to inefficient cadaverine export which, in turn, may have caused a metabolite 'backlog' that, due to intracellular L-lysine and/or cadaverine accumulation, led to growth inhibition. Indeed, the extracellular:intracellular cadaverine ratio was found to be 2.6-times higher when using 0.5 mM theophylline (i.e., stronger *cadA* expression) relative to 2.0 mM theophylline (34.7 vs. 13.1; Figure 3.06). Thus, further engineering of an effective cadaverine exporter and/or optimization of its expression is expected to be critical for future improvements in photosynthetic cadaverine production.

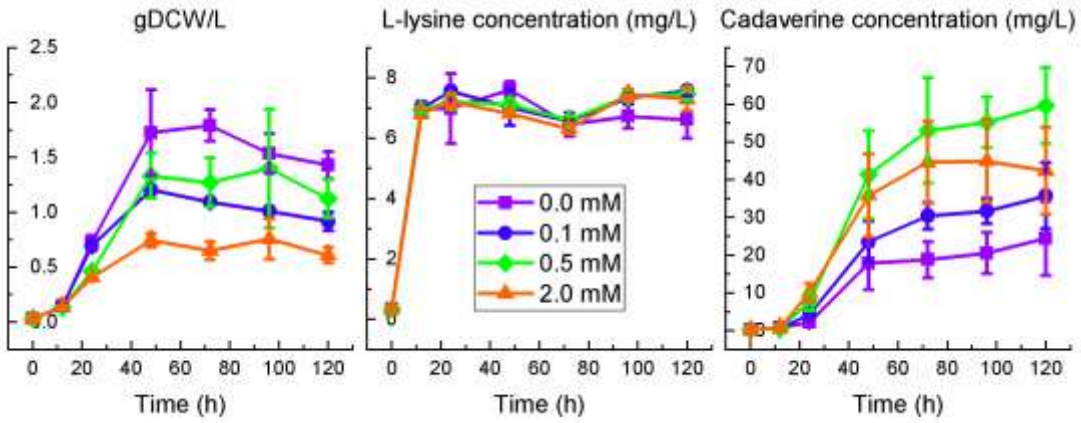

Figure 3.04. Cadaverine Production by Engineered UTEX 2973.
Accumulation of biomass (left), lysine (middle), and cadaverine (right) over 120 hours by UTEX 2973 harboring pZD-LGC-30 in shake flasks containing 25 mL BG-11 at varying concentrations of theophylline. Theophylline concentrations

used were 0 mM (purple squares), 0.1 mM (blue circles), 0.5 mM (green diamonds) and 2.0 mM (orange triangles). Error bars represent standard error from biological triplicates.

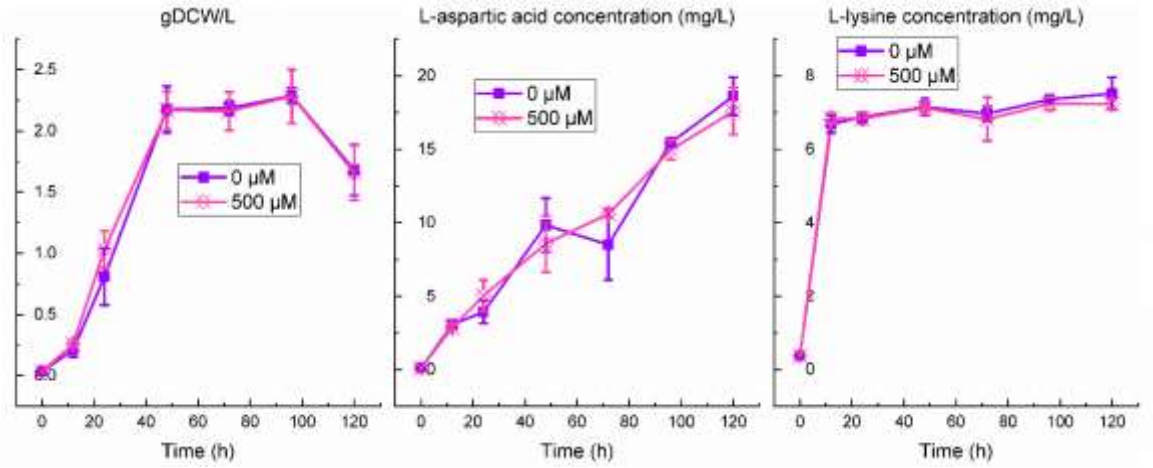

Figure 3.05. Extracellular Accumulation of L-aspartate and L-lysine by UTEX 2973 Harboring pZD-LGC-04.

Accumulation of biomass (left), L-aspartate (middle), and L-lysine (right) by UTEX 2973 harboring pZD-LGC-04 over 120 hours in shake flasks containing 25 mL BG-11 at varying concentrations of IPTG. IPTG concentrations used were 0 μM (purple squares), and 500 μM (pink bullseyes). Error bars represent standard error from biological triplicates.

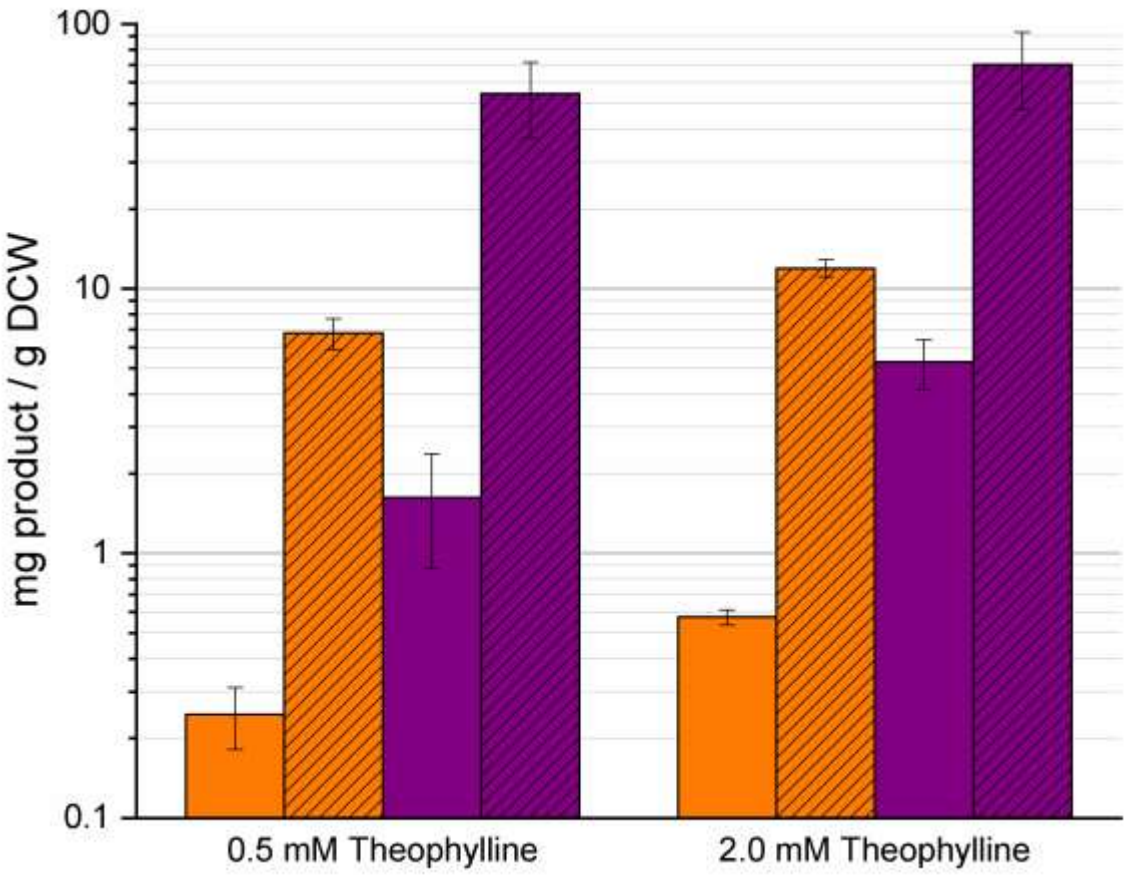

Figure 3.06. Comparing Intracellular versus Extracellular Accumulation of Cadaverine by UTEX 2973.
Intracellular (solid bars) and extracellular (striped bars) concentrations of L-lysine (orange) and cadaverine (purple) normalized per unit biomass measured after 120 hours when culturing UTEX 2973 harboring pZD-LGC-32 in the presence of 0.5 or 2.0 mM theophylline. Error bars represent standard error from biological triplicates.

3.3.4 Engineering Direct Glutarate Production in UTEX 2973

To further explore the photosynthetic production of L-lysine-derived biochemicals, UTEX 2973 was lastly engineered to produce glutarate via an alternative extension of the L-lysine pathway. Like cadaverine, the 5-carbon dicarboxylate glutarate is also of interest for bioplastic production. As previously demonstrated in other hosts[115,140–142], glutarate can be produced from L-lysine

via the intermediate 5-aminovalerate (5-AMV) using the *davBA* and *davDT* operons from *P. putida*. Although cyanobacterial production of glutarate has not previously been demonstrated, production of its 4-carbon analog succinate has been. Specifically, Lan and Wei showed that succinate could be overproduced by PCC 7942 without any apparent inhibitory effects, and also that it was naturally secreted (although the associated secretion mechanism remains unclear)[19]. Considering its structural similarity with succinate, it was postulated that the same might also hold true for glutarate. Accordingly, plasmid pZD-LGC-32 was constructed where, in place of *ybjE* on pZD-LGC-13, an expression cassette including both the *davBA* and *davDT* operons was included. As with cadaverine production, glutarate was not detected over 120 hours for either wild-type UTEX 2973 or the lysine-producing strain (i.e., carrying pZD-LGC-13; not shown). Carrying pZD-LGC-32, UTEX 2973 was found to produce glutarate at a maximum titer of 68.6 ± 7.1 mg/L by 96 hours (Figure 3.07). Meanwhile, as was the case for cadaverine production, in the absence of *ybjE* expression, extracellular L-lysine accumulation was modest and again ~8 mg/L. Similar to L-lysine production, “leaky” expression of $lysC^{fbr}$ (i.e., 0 mM IPTG) supported the highest glutarate production, whereas cell growth was again reduced with increasing IPTG concentrations (also like L-lysine production; Figure 2.07A, D). Glutarate production, on the other hand, was mostly insensitive to the IPTG induction level, suggesting that the current flux bottleneck likely resides downstream of aspartate kinase. Notably, as seen in Figure 3.07, 5-AMV accumulated to higher levels at lower IPTG concentrations (conditions promoting

greater L-lysine production); an outcome that implicates inefficient glutarate export and/or sub-optimal expression of the *davDT* operon as the most probable bottlenecks. To investigate the latter possibility, *davDT* was cloned under the strong P_{J23119} promoter. Unfortunately, however, the resulting plasmid (pZD-LGC-33) could not be successfully conjugated into UTEX 2973 (data not shown), suggesting that this was somehow a lethal arrangement.

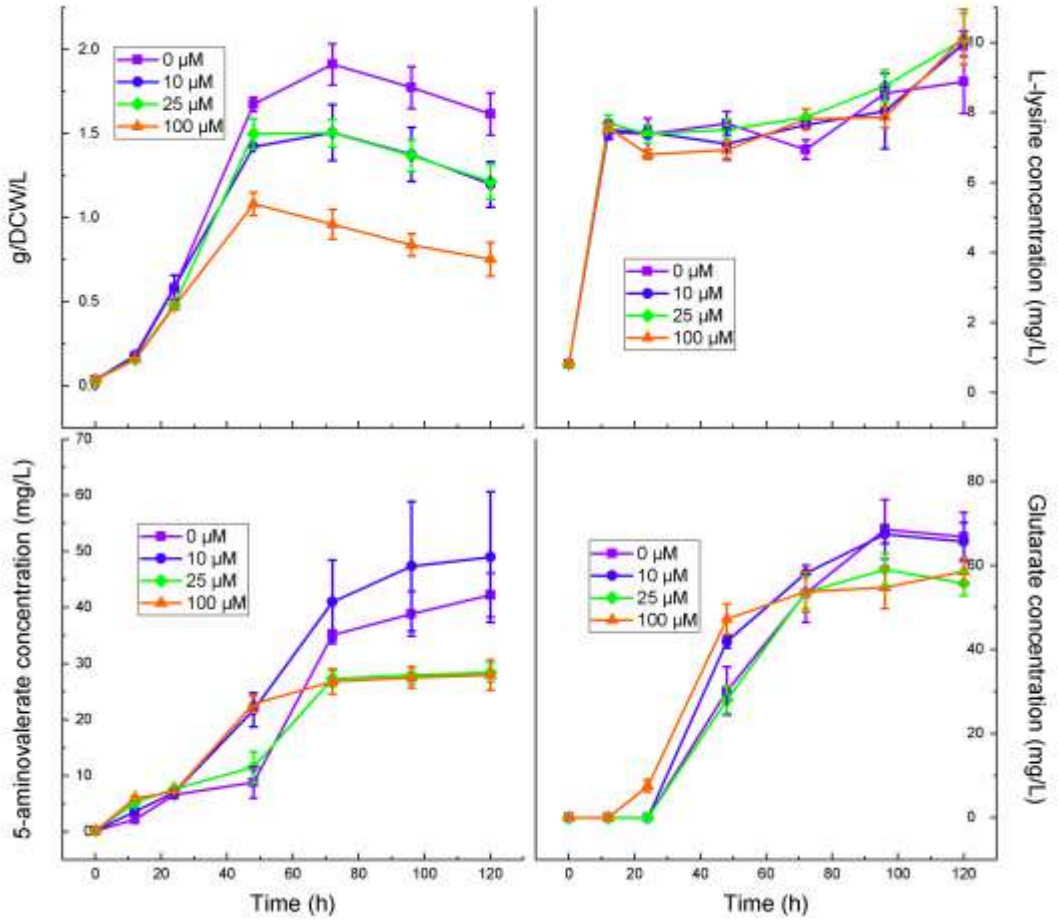

Figure 3.07. Glutarate Production by Engineered UTEX 2973.
Accumulation of biomass (top left), lysine (top right), 5-AMV (bottom left), and cadaverine (bottom right) by UTEX 2973 harboring pZD-LGC-32 in shake flasks containing 25 mL BG-11 at varying concentrations IPTG. IPTG concentrations used were 0 µM (purple squares), 10 µM (blue circles), 25 µM (green diamonds) and 100 µM (orange triangles). Error bars represent standard error from biological triplicates.

3.3.5 Expression of a Known Exporter in a Glutarate Production Strain

To investigate if glutarate export by native mechanism alone was perhaps a performance bottleneck, the recently discovered glutarate exporter encoded by *ynfM* from *C. glutamicum*[129,143] was lastly cloned and expressed via the

theophylline-inducible Riboswitch F (pZD-LGC-34). However, although this strain was capable of growth, it did not produce detectable levels of 5-AMV or glutarate over the course of 120 hours, even when maximally induced with theophylline (data not shown). It is possible that *ynfM*, a membrane gene which this study attempted to heterologously express from the gram-positive *C. glutamicum*, did not perform as hypothesized for reasons similar to those posited for the earlier failure of *cgmA* when expressed in UTEX 2973. The photoautotrophic activity of YnfM may change due to the higher pH relative to *C. glutamicum*, where the localized environment would be at least an order of magnitude more acidic. It is furthermore unclear whether *ynfM* is exporting dicarboxylic acids from the TCA cycle at the expense of OAA-dependent pathways. While biomass fell for increasing theophylline concentrations (Appendix D), at no level of induction was there evidence of significant succinate or α-ketoglutarate in the culture medium of pZD-LGC-34-harboring UTEX 2973 samples, both of which previously have been demonstrably selected for export by *ynfM*'s gene product[143]. By what mechanism low expression of *ynfM* is completely arresting 5-AMV and glutaric acid production whilst leaving cell fitness and intracellular dicarboxylic acid metabolism intact remains to be interrogated.

3.4 Future Work

The persistence of the intermediate 5-AMV during glutarate production was not alleviated by choices made to change the design, including overexpression of *davBA* and the addition of *ynfM* to potentially export the target

molecule. Another potential strategy is the heterologous expression of *E. coli*'s *gabP* importer gene, which has been demonstrated to transport 5-AMV back into the cytosol[142]. This putative construct would however likely trade off better conversion efficiency for cell fitness, as evidenced by the growth of UTEX 2973 overexpressing $lysC^{fbr}$ in the absence of the exporter *ybjE*.

Furthermore, while the photoautotrophic production of 5-AMV is as novel as cadaverine and glutarate in this work, the former molecule was not the target species during the expression of the *davDT* operon. It would be worthwhile to simplify the pathway by omitting the *davBA* operon, both to maximize 5-AMV titers, as well as to potentially further troubleshoot the glutarate pathway design through optimization of flux through the intermediate.

CHAPTER 4

CARBON FLUX INCREASE STRATEGIES THROUGH THE ADDITION OF AMINES TO CYANOBACTERIAL GROWTH MEDIA

ABSTRACT

Alkanoamines are a class of molecule with a functional group that allows them to catalyze the conversion of aqueous CO_2 into bicarbonate. This behavior makes alkanoamines a solvent commonly utilized for the scrubbing of industrial processes which output excess CO_2. The implementation of this class of chemical in photoautotrophic culture media is potentially favorable to cyanobacteria, which take up bicarbonate and eventually incorporate it into their central carbon metabolism. The amine loading strategy was tested through a set of mass experiments conducted in BG-11 medium, typically used when culturing freshwater cyanobacteria. Five amines – monoethanolamine (MEA), diethanolamine (DEA), triethanolamine (TEA), putrescine, and cadaverine, were tested across a range of concentrations as CO_2 was bubbled through abiotic media. The latter three molecules were determined to be roughly two-fold over the first two in terms of capture efficiency. PCC 6803 was grown in the presence of these three candidate amines at various concentrations. In all cases, cultures fared worse relative to no-amine controls, indicating serious challenges for the success of this strategy without major engineering of cyanobacteria due to potential toxicity effects.

4.1 Introduction

As the genotype of UTEX 2973 predispose it towards efficient uptake and conversion of CO_2[33], it stands to reason that the most impactful engineering of carbon flux through the system occurs upstream, with the mass transfer processes associated with CO_2 delivery. In fact, growth of UTEX 2973 at non-optimal CO_2 conditions can cause it to accumulate biomass at worse rates than its parent strain, PCC 7942, under those same conditions[30].

The equation governing mass transfer of CO_2 into media over time is:

$$\frac{dC_{CO_2}}{dt} = K_L a\left(C_{CO_2}{}^{*} - C_{CO_2}\right) \quad (1)$$

Where $\frac{dC_{CO_2}}{dt}$ represents the accumulation over time of dissolved CO_2 species in liquid, $K_L a$ the lumped volumetric mass transfer coefficient, C_{CO_2} the concentration of dissolved CO_2 species, and $C_{CO_2}{}^{*}$ the equilibrium concentration of dissolved CO_2 species (as determined by Henry's Law). The following set of reversible equilibrium relationships then describe the absorption and dissociation of CO_2 in aqueous media:

$$CO_2(g) \leftrightarrow CO_2(aq) \quad (2)$$

$$CO_2(aq) + H_2O \leftrightarrow H_2CO_3 \quad (3)$$

$$H_2CO_3 \leftrightarrow H^+ + HCO_3^- \quad (4)$$

$$HCO_3^- \leftrightarrow H^+ + CO_3^{2-} \quad (5)$$

$$H_2O \leftrightarrow H^+ + OH^- \quad (6)$$

With the concentration of total inorganic carbon (TIC) dissolved in water determined to be:

$$[TIC] = [CO_2(aq)] + [H_2CO_3] + [HCO_3^-] + [CO_3^{2-}] \quad (7)$$

When equilibrated with air at standard conditions and neutral pH, C_i in water is only 3.2 mg/L (0.07 mM), and 82% of it exists as bicarbonate, the preferred form of C_i for cyanobacterial uptake[151].

Rates of CO_2 absorption can be enhanced by increasing $K_L a$ and/or CO_2 solubility. $K_L a$ can be increased through greater mixing of the medium; though this quickly becomes energy-intensive and economically infeasible. Increasing CO_2 solubility, meanwhile, this can be achieved by maintaining a higher pH, to encourage the conversion to bicarbonate[36,152,153], or through the addition of CO_2 reactive, amine solvents. In the latter case, alkanolamines are routinely employed as scrubbing agents for industrial processes that would otherwise emit large quantities of CO_2 via flue gas exhaust. Common alkanoamines used in traditional CO_2 capture systems include the primary monoethanolamine (MEA), secondary diethanolamine (DEA), tertiary triethanolamine (TEA) and methyldiethanolamine (MDEA), and related compounds with bulky alkyl groups such as 2-amino-2-methyl-1-propanol (AMP)[37,154,155]. When describing aqueous media in the presence of amine solvents, the following series of reversible reactions occur[156,157] (except for tertiary amines which, owing to their lack of an N-H bond, do not form the carbamate ions seen in Equations (8) and (10)):

Carbamate formation: $CO_2(aq) + 2RNH_2 \leftrightarrow RNHCOO^- + RNH_3^+$ (8)

Bicarbonate formation: $CO_2(aq) + RNH_2 + H_2O \leftrightarrow HCO_3^- + RNH_3^+$ (9)

Carbamate reversion: $RNHCOO^- + H_2O \leftrightarrow RNH_2 + HCO_3^-$ (10)

In this case, the TIC expression also reflects the additional formation of the additional carbamate molecule, and is now determined as such:

$$[TIC] = [CO_2(aq)] + [H_2CO_3] + [HCO_3^-] + [CO_3^{2-}] + [RNHCOO^-] \quad (11)$$

Thus, addition of an alkanolamine to the solution can be seen as positively impacting CO_2 absorption through the increase in solubility of TIC species compared to Equation (7). The stoichiometry involved in Equations (8-10) require a 2:1 molar ratio of non-tertiary amine to CO_2, which limits the maximum CO2 loading to 0.5 mol CO_2 / mol amine[157]. Carbamate formation is believed to occur through a two-step zwitterion mechanism (not shown). The rate at which different amines catalyze conversion to bicarbonate depends somewhat on steric interactions, with secondary amines forming more unstable intermediates than primary ones. The instability of the carbamate intermediate leads the reversion reaction in Equation (10)[37,158]. Production of bicarbonate regenerates the amine, allowing for its reaction with additional CO_2 and thus significant enhancement in aqueous loading of C_i[156]. The chemical cost of regenerating primary and secondary amines from carbamate ions is high, as the latter's formation involves relatively high heat of absorption[157]. However, if the released bicarbonate were to be directly taken up by cyanobacteria, this would shift the equilibrium of C_i species in the media and make the carbamate reversion reaction in Equation (10) more favorable.

As the first to investigate the potential benefits of alkanolamine addition to cyanobacterial cultures, Kim and colleagues[37] added 100 mg/L of the amines MEA, DEA, TEA, and AMP to blank BG-11 medium bubbled with 5% CO_2 at 0.1

vol/vol/min, then measured C_i over time. In every case, the amines in solution demonstrated improved carbon capture over the medium with no amines. However, when *Scenedesmus accuminatus* AG10316, an algae species, was grown in the presence of the same set of amines, significant differences were noted between amine species. Specifically, with 2 mM MEA and 2 mM AMP, cultures performed worse than non-amine BG-11. However, 2 mM DEA and TEA cultures improved growth over the non-amine solution, suggesting that their ability to drive C_i into the medium outweighed possible toxicity effects. In a related study[154], *S. accuminatus* grown in the presence of 100 mg/L MEA reached a growth rate of 288.6 mg/L/d, compared to 177.1 mg/L/d with no amine. However, at higher concentrations of MEA, toxicity effects tend to emerge. At 300 mg/L, the growth rate was 202.9 mg/L/d.

Separate work involving *Spirulina* sp. LEB 18 further showed that the use of amine solvents to improve CO_2 mass transfer is a feasible strategy across algae species. A photobioreactor system that added MEA through recycle did not observe growth inhibition at concentrations up to 0.82 mmol/L, while roughly doubling C_i[159]. Employing such a system with an algal species engineered to convert this available carbon could therefore see strong improvements in bioproduction.

The amine cadaverine, produced in previous work, while not a conventional or common choice for scrubbing, possesses the amine chemistry required to affect the same result. Admittedly, tolerance assays and engineering conducted in Chapter 3 demonstrate that cadaverine interacting with

cyanobacteria leads to toxicity that confounds the potential benefits of improved CO_2 mass transfer. Regardless, it was of interest to test the physicochemical properties of cadaverine and putrescine; another polyamine with similar potential for direct biosynthesis. These were compared against typical industrial scrubbing species: MEA, DEA, and TEA. These chemicals were tested in growth assays of the model cyanobacterium PCC 6803 to better determine the possibility of their use across photoautotrophic organisms.

4.2 Methods and Materials

4.2.1 Chemicals

Cadaverine and putrescine were purchased from TCI America (Portland, OR). All other chemicals were purchased at the highest available purities from Sigma-Aldrich (St. Louis, MO) or Santa Cruz Biotechnology (Dallas, TX), unless otherwise indicated.

4.2.2 Media and Amine-CO_2 Mass Transfer Assays

All strains were cultured in BG-11 medium at 30°C. Sterile BG-11 containing no cyanobacteria was also utilized in amine-CO_2 mass transfer studies (Figure 4.01). 80 mL of BG-11 medium in a 100 mL graduated cylinder was bubbled with air at a rate of 80 mL/min, equal to 1 volume/volume/min (vvm). At the beginning of a mass transfer experiment, a known amount of amine was spiked into the medium, and the bubbling gas was changed to 0.5% CO_2 in air. Changes in CO_2 exiting the medium over time were recorded with a downstream Vaisala CO_2 probe GM70 CARBOCAP.

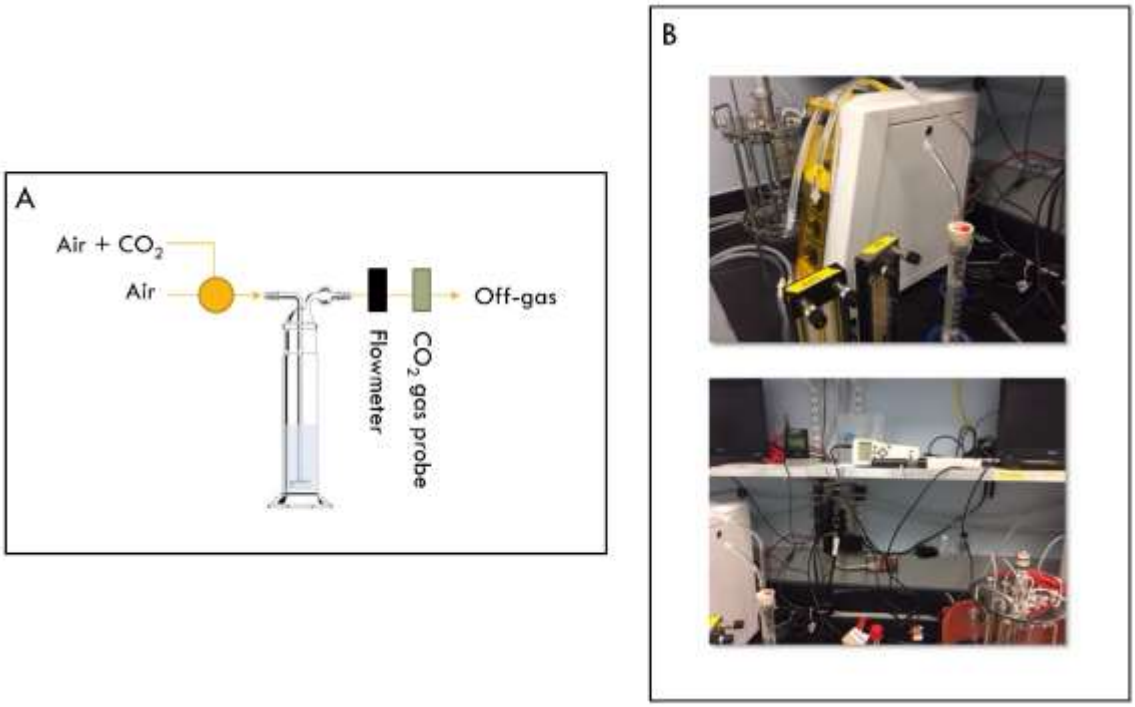

Figure 4.01 Apparatus Used for Amine Mass Transfer Experiments.
Diagram of the setup for the bubbling apparatus used in blank media experiments, composed of air and CO_2 flow channeled into rotameters in series to set the correct gas mixture, graduated cylinder fitted with a fritted glass bubbler, a flowmeter to set volumetric flow rate, and a CO_2 gas probe to determine CO_2 concentration (A). Pictured top: rotameters and bubbling cylinder; bottom: flowmeter and CO_2 probe (B).

With the CO_2 probe data output as ppm CO_2, the mass flowrate of CO_2 in the exit gas was determined via the following equation, assuming an ideal gas:

$$\dot{m}_{CO_2}\left[\text{ppm}_{CO_2}\right] = \frac{\frac{\left[\text{ppm}_{CO_2}\right]}{10^6}\cdot 101325\ \text{Pa}}{\left(8.314\cdot 10^6\ \frac{\text{Pa}\cdot\text{mL}}{\text{K}\cdot\text{mol}}\right)\cdot 303.15\ \text{K}} \cdot \frac{80\ \text{mL}}{60\ \text{s}} \cdot \left(\frac{44.01\cdot 10^3\ \text{mg}\ CO_2}{\text{mol}\ CO_2}\right) \qquad (12)$$

Using instantaneous CO2 vs time data from the outlet, the total mass of CO2 that left the system over the course of the experiment was determined using a Riemann sum at a resolution of 5 seconds intervals of the experiment:

$$m_{CO_2\,out} = \sum_{t=i}^{t_{final}} \frac{\left(\dot{m}_{CO_2 t} + \dot{m}_{CO_2 t+1}\right)\cdot 5\ \text{sec}}{2} \qquad (13)$$

The mass of CO_2 fed into the system in total was calculated by substituting in 5000 ppm for Equation (12) and multiplying it by the time of the experiment. The mass CO_2 captured was then determined as the difference between the total mass fed in less the total mass out.

4.2.3 Strains and Culture Conditions

PCC 6803 was obtained as a gift from the lab of Dr. Willem Vermaas (ASU, Tempe, AZ) and was used for growth studies in the presence of amines. 30 mL cultures of PCC 6803 in BG-11 were cultured in bubble tubes at an initial OD_{730} of 0.2 at 30°C, and 1 vol/vol/min of air. Light intensity varied from 30-100 $mE/m^2/s$ during the experiments. At an optical density of ~0.6-0.8, alkanoamines were added to the cultures. Each concentration of amine tested was done in duplicate.

4.3 Results and Discussion

4.3.1 Characterizing the relative impacts of different amine solvents on total CO2 solubility via breakthrough analysis

A range of different molecules were interrogated for their ability to retain aqueous CO_2 within the media as gas bubbles through it to saturation. A detector placed downstream of the bubbling system constantly measured CO_2 from the gas stream out. Increasing amounts of the same amine species generated a CO_2 breakthrough curve in which the total measured CO_2 out decreased despite inlet CO_2 being held constant, indicating that these species were “trapping” carbon

within the aqueous system in accordance with the TIC definition represented by equation (11).

The different types of species tested demonstrated some trends with respect to carbon retention (Figure 4.02 and 4.03). The same mass concentration of TEA tended to capture less CO_2 than DEA which in turn faired poorer than MEA, likely owing to the fact that equivalent masses of the amines with more ethanolic ligands possess less moles to react and perform the conversion to bicarbonate with. For example, for 40 mg/L of each ethanolamine, MEA captured 102.0 µmol CO_2, while DEA captured only 50.9 and TEA 41.5. Putrescine and cadaverine, the biogenic diamines, took longer to equilibrate (roughly 1000 seconds) to the final breakthroughs than the ethanolamines (600-900 seconds). While DEA and cadaverine are very similar in molecular weight, the latter chemical appeared to exhibit a stronger CO_2 capture effect for corresponding concentrations, capturing roughly double the amount of CO_2 at 40 mg/L. This is potentially a representation of the multiple amine sites on cadaverine playing a significant role in increasing the catalytic capacity of the molecule. While these species were not hypothesized to strictly double capacity, it was expected that they would demonstrate superior performance relative to the monoamine, especially since a single diamine molecule could potentially stabilize charge by acting as both the proton donor and acceptor in Equation (8) to create a zwitterion.

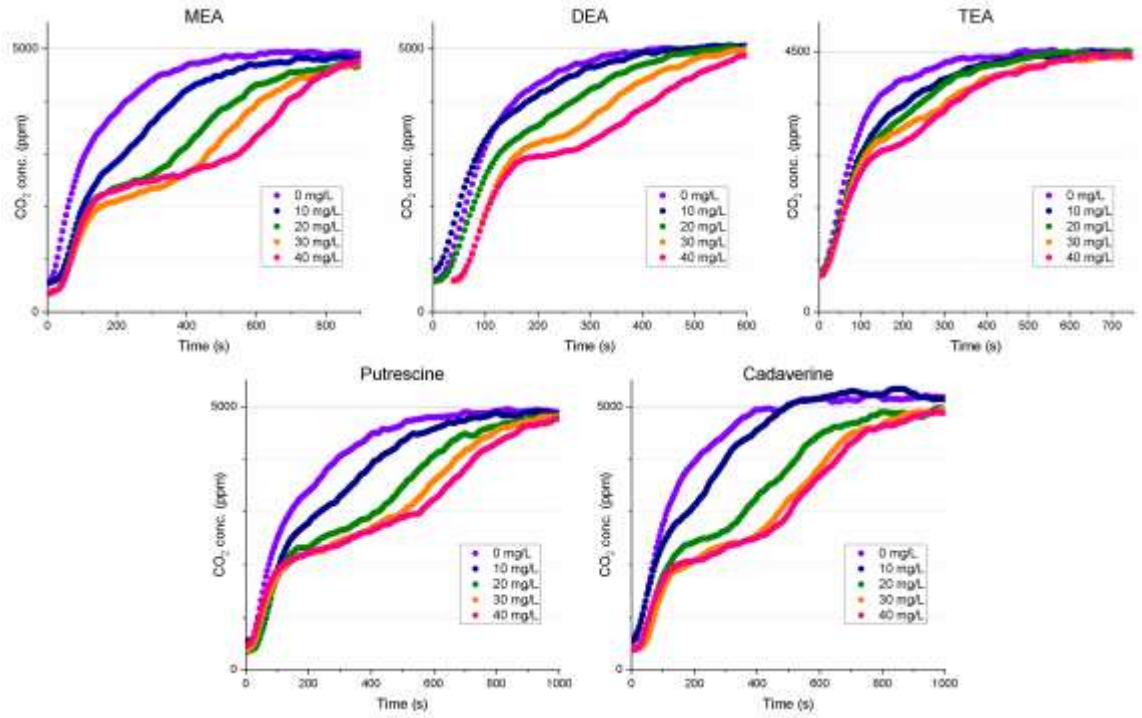

Figure 4.02. Breakthrough Curves for Various Amine Species.
CO_2 probe outlet readings of a system in which 0.5% CO_2 was bubbled through 80 mL BG-11 at a rate of 1 volume/volume/min. Known masses of various amines were spiked into the media to generate curves: 0 mg/L (purple), 10 mg/L (navy), 20 mg/L (green), 30 mg/L (orange), 40 mg/L (pink). Time=0 represents the point at which CO_2 began to bubble through the media. Endpoints were determined to be the time at which all curves appeared to converge. Each breakthrough curve was generated by a single time-course.

4.3.2 Comparison of CO_2 Capture Efficiency Between Amine Species

This behavior was somewhat validated by a per-mole basis examination of the total CO_2 uptake over the course of each experiment (Figure 4.03). When normalized for molar concentration of amine sites, it appears that MEA, cadaverine, and putrescine form one broad regime of capture profile, with maximum capture amounts in the range of roughly ~100-110 µmol CO_2, while DEA and TEA form another at a lower efficiency with maximum amounts of ~40-50. Cadaverine and putrescine, as explained above, likely benefit from their

enhanced ability to both donate and accept proton when forming carbamate ions. TEA's worse capacity results from its inability to form carbamate ion, leaving it with only hydrolysis of CO_2 to bicarbonate (Equation (9)), a much slower reaction150. Why MEA and DEA end up in the higher and lower capacity regimes respectively is a more speculative question. The major characteristic difference is that of primary vs. secondary amine, possibly indicating that the higher stability of the former type allows for higher carbon capacity of the doped media. Admittedly, the concentration range tested does not reach even half of the maximum concentration of the high-efficiency regime, forcing some amount of extrapolation with regards to what the lower regime would look like over the full range.

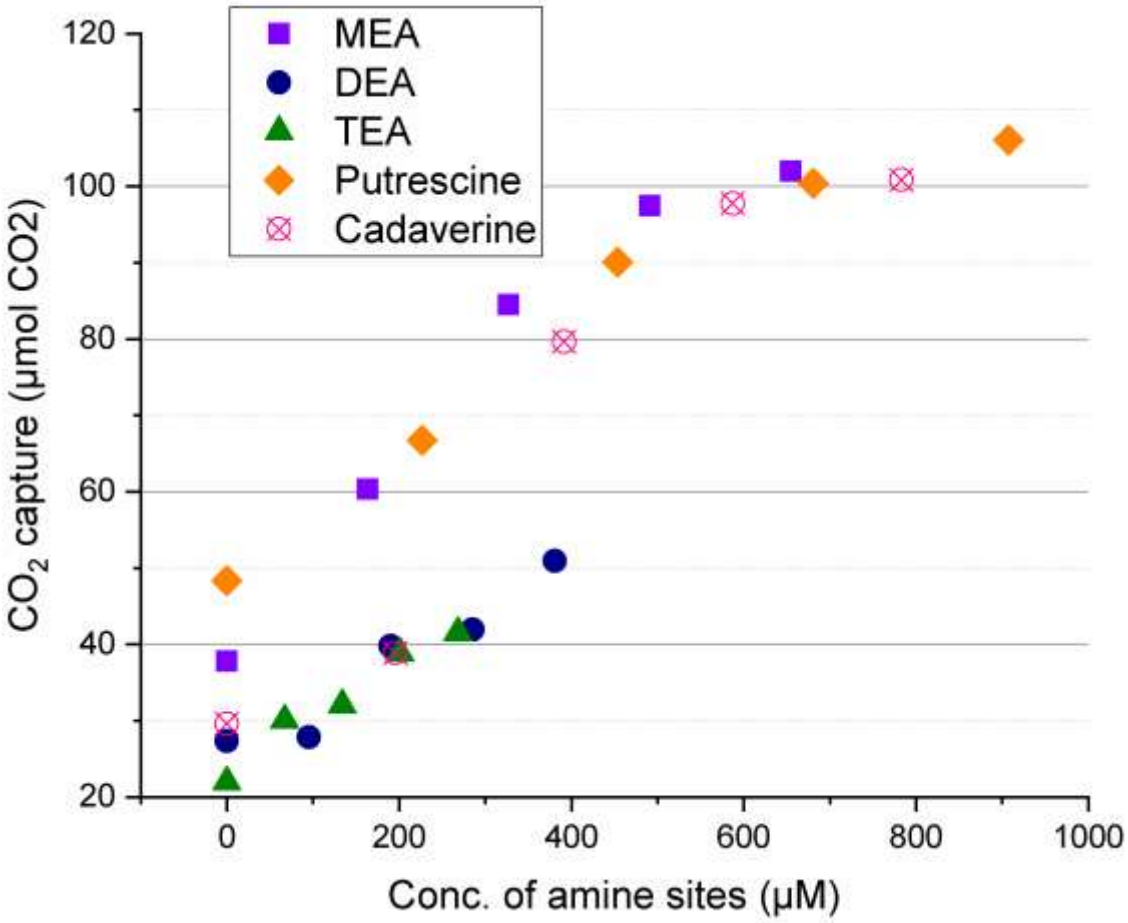

Figure 4.03 Amount of CO_2 Captured in Bubbling Experiments per Concentration of Amine Sites.
Total amounts of CO_2 captured for each experimental run were determined by calculating the difference between the constant feed in of 5000 ppm CO_2 and the measured CO_2 out, and subsequently generating a Riemann sum to integrate from the breakthrough curve time-course. Each different amine species was tested in increasing increments of mass concentration, of which the concentration of available amine sites for catalyzation of bicarbonate were determined. The amine species tested were MEA (purple squares), DEA (navy circles), TEA (green triangles), putrescine (orange diamonds), and cadaverine (pink bulleyes).

When the difference is taken between CO_2 captured at a given concentration of amine and the no-amine control (Figure 4.04), similar trends are observed for a high-efficiency and low-efficiency regime. Charting these values

against the maximum theoretical carbamate loading for each amine further reveals that the high-efficiency amines are absorbing significant carbon into the medium beyond what they can directly form an ion with, implicating significant bicarbonate formation. TEA, which can only form bicarbonate, is unable to meet even the theoretical loading of high-efficiency amines past 10 mg/L. The best fold improvement of DEA's total carbon difference against loading is ~1.55-fold, while the minimum fold improvement among high-efficiency amines above 10 mg/L is ~1.59-fold. Across the entire experiment, the best fold change is ~3.44-fold for MEA at 10 mg/L, indicating that low amounts of amine can still demonstrate a strong improvement in CO_2 solubility despite low potential for direct bicarbonate formation.

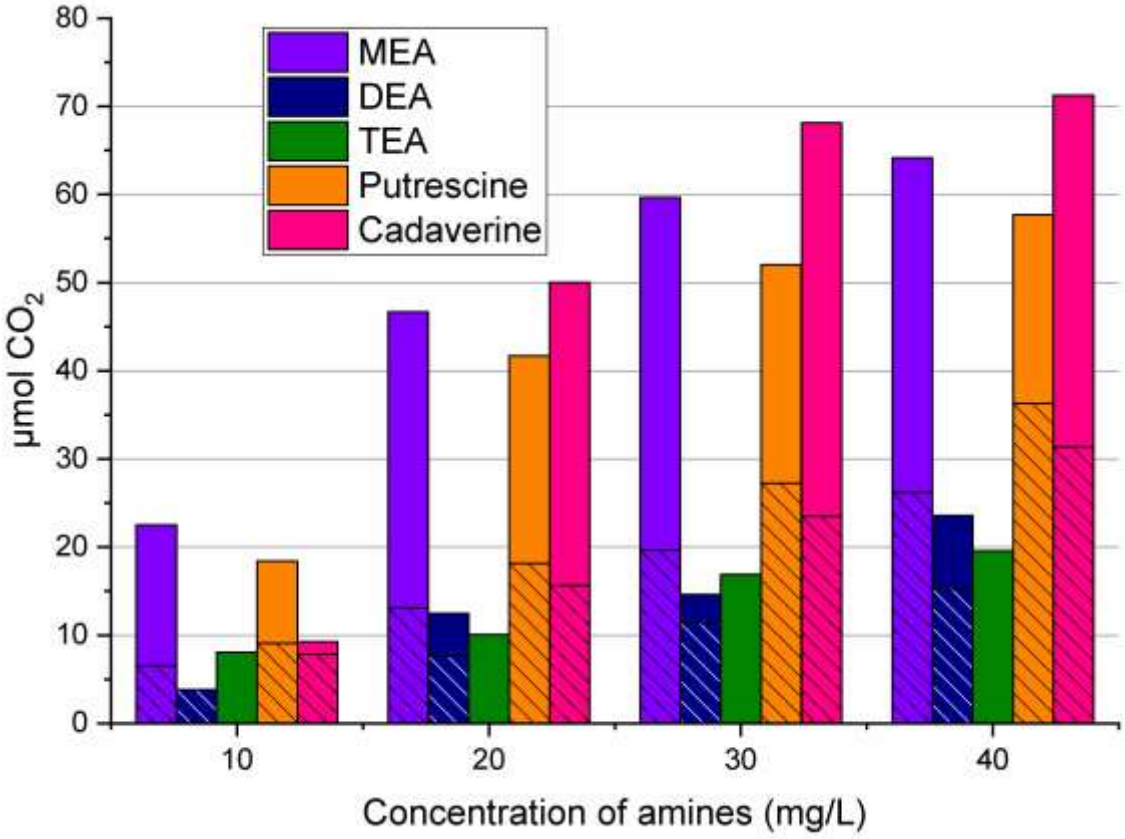

Figure 4.04 CO_2 Captured by Amines in Bubbling Compared to Maximum Theoretical Carbamate Loading.
Difference in CO_2 captured by each amine at each concentration tested relative to the corresponding no-amine control. The amine species tested were MEA (purple), DEA (navy), TEA (green), putrescine (orange), and cadaverine (pink). Striped regions of each bar represent the maximum theoretical amount of carbamate each amine could form for the given concentration. Each bar was determined from the breakthrough curve of a single time-course.

Comparison of the carbon capture efficiency between amines importantly demonstrated the interchangeability of MEA, cadaverine, and putrescine, which all exhibited similar capacity when amine site numbers were normalized. Furthermore, these three candidate amines are all potential decarboxylation products of biogenic amino acids (L-serine, L-lysine, and L-arginine respectively). All three candidate amines were then tested in the presence of PCC 6803

cultures to determine their effect on photosynthetic growth (Figure 4.05). Based on the results, it appears that trends noticed in the cadaverine tolerance assays described in Chapter 3 are more broadly applicable to cyanobacteria-amine interactions. PCC 6803 growth in the absence of cadaverine was roughly an order of magnitude improved from cultures exposed to as little as 30 mg/L, representing an even more severe loss of fitness than trends observed in wild-type UTEX 2973 (Figure 3.02). While the other two chemicals tested, MEA and putrescine, were not as intensely deleterious at low concentrations, neither showed any ability to confer positive growth attributes for PCC 6803 cultures at any point in the experiments. It appears that significant engineering of tolerance is a necessity in PCC 6803 in order to have a chance to reap the potential benefits of enhanced bicarbonate loading of media. However, based on the measured improvements in C_i solubility from amine concentrations in the 10-20 mg/L range, it appears that lower concentrations are worth testing in the presence of cyanobacterial cultures. Furthermore, cyanobacteria engineered to potentially overproduce these chemicals may benefit from an organic phase overlay in the culture to pull amines out of the aqueous media, although this would complicate the goal of CO_2 saturation.

An alternate strategy could be the marriage of amine synthesis pathways heterologously expressed in non-photoautotrophic bacteria with mutations endowing the host strain with a functional carbon concentration mechanism[160]. While the resulting mutant would certainly grow slowly, it would not experience the severity of toxic effects observed upon photoautotrophs in this work[115,161].

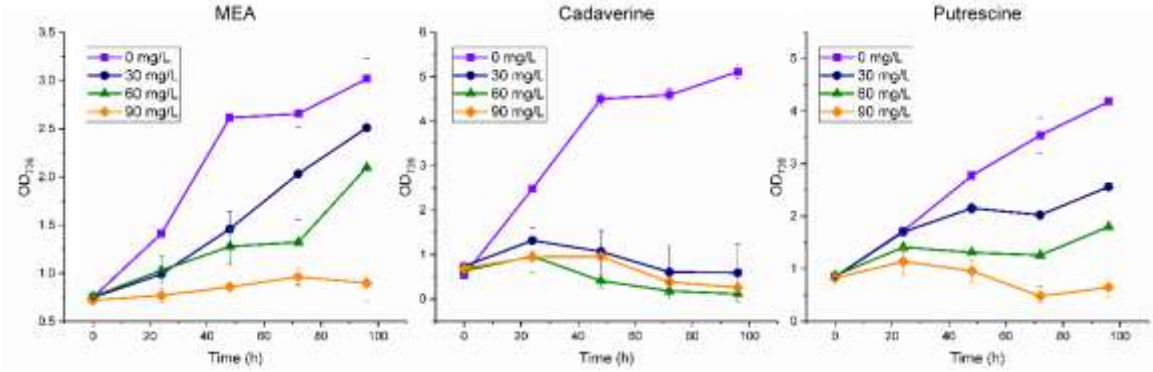

Figure 4.05 Growth Tolerance of PCC 6803 towards Different Amine Species.

Optical densities of wild-type PCC 6803 when grown in the presence of various amine species. Duplicate 30 mL culture tubes containing BG-11 at were seeded to an initial OD_{730} of 0.2, then grown at 30°C and 30-100 mE/m^2/s under 1 v/v/min air to an OD_{730} of roughly 0.6-0.8, at which point exogenous amine was added to each tube. Growth was then measured for 96 hours under these conditions. Amine concentrations were 0 mg/L (purple squares), 30 mg/L (navy circles), 60 mg/L (green triangles) and 90 mg/L (orange diamonds). Error bars represent standard error from biological triplicates.

4.4 Future Work

Running the breakthrough curves for higher concentrations of MEA and DEA would help to further fill out the trends seen in Figure 4.03. Additional amines are also worth testing for mass transfer properties, including industrially relevant species such as 2-amino-2-methyl-1-propanol[37], as well as other species that can potentially be overproduced in cyanobacteria, such as spermine and spermidine[162,163].

Redoing the set of tolerance assays in UTEX 2973 would be another worthwhile set of experiments. As can be clearly seen in comparisons of the growth profiles between Figures 3.02 and 4.05, wild-type UTEX 2973 fares better

than PCC 6803 at equivalent concentrations of cadaverine. It stands to reason that a similar trend would be observed with regards to putrescine, which is chemically quite similar to cadaverine.

CONCLUSIONS

Fast-growing cyanobacteria, including UTEX 2973, represent an opportunity to improve upon slower model photoautotrophs and achieve industrial photosynthesis of valuable chemicals. The relative lack of validated genetic parts in these strains, however, is a significant obstacle towards their wider implementation, even at lab scale. This body of work first aimed to produce L-lysine in UTEX 2973; a feat made possible through the characterization of a range of promoters in pAM4788-Km^R, a shuttle vector previously validated for expression and stability in PCC 7942, and NS3, an underexplored neutral site in UTEX 2973. Plasmid-based expression of a gene cassette containing aspartokinase *lysC*^{fbr} and the exporter *ybjE* led to a maximum L-lysine production that surpassed that of the only previous report of its photoautotrophic production. This pathway was then leveraged to produce two more compounds of relevance to bioplastics production, namely cadaverine and glutarate. The former involved engineering tolerance to the product through the expression of the ABC transporter *sapBCDF*, as well as carefully titrated expression of lysine decarboxylase *cadA*. The latter, meanwhile, was reached through heterologous expression of the entire *davBA*/*davDT* cassette. Finally, a range of amines, which increase available inorganic in aqueous environments through their direct reaction with CO_2, were tested for their ability to enhance mass transfer in BG-11 medium, as well as their effect on the growth of wild-type 6803. While toxicity phenomena appeared to dominate in cyanobacterial cultures in agreement with

the previous cadaverine studies, amine propensity for aqueous carbon capture was confirmed.

REFERENCES

1. Deng, M. de & Coleman, J. R. Ethanol synthesis by genetic engineering in cyanobacteria. *Applied and Environmental Microbiology* **65**, 523–528 (1999).

2. Gao, Z., Zhao, H., Li, Z., Tan, X. & Lu, X. Photosynthetic production of ethanol from carbon dioxide in genetically engineered cyanobacteria. *Energy and Environmental Science* **5**, 9857–9865 (2012).

3. Miao, R., Liu, X., Englund, E., Lindberg, P. & Lindblad, P. Isobutanol production in Synechocystis PCC 6803 using heterologous and endogenous alcohol dehydrogenases. *Metabolic Engineering Communications* **5**, 45–53 (2017).

4. Ruffing, A. M. Improved free fatty acid production in cyanobacteria with Synechococcus sp. PCC 7002 as host. *Frontiers in Bioengineering and Biotechnology* **2**, 1–10 (2014).

5. Liu, X., Sheng, J. & Curtiss, R. Fatty acid production in genetically modified cyanobacteria. *Proceedings of the National Academy of Sciences of the United States of America* **108**, 6899–6904 (2011).

6. Wang, W., Liu, X. & Lu, X. Engineering cyanobacteria to improve photosynthetic production of alka(e)nes. *Biotechnology for Biofuels* **6**, 1–9 (2013).

7. Gao, X. *et al.* Engineering the methylerythritol phosphate pathway in cyanobacteria for photosynthetic isoprene production from CO2. *Energy and Environmental Science* **9**, 1400–1411 (2016).

8. Choi, S. Y. *et al.* Improvement of Squalene Production from CO2 in Synechococcus elongatus PCC 7942 by Metabolic Engineering and Scalable Production in a Photobioreactor. *ACS Synthetic Biology* **6**, 1289–1295 (2017).

9. Lin, P. C., Saha, R., Zhang, F. & Pakrasi, H. B. Metabolic engineering of the pentose phosphate pathway for enhanced limonene production in the cyanobacterium Synechocysti s sp. PCC. *Scientific Reports* **7**, 1–10 (2017).

10. Brey, L. F. *et al.* Metabolic engineering of Synechocystis sp. PCC 6803 for the production of aromatic amino acids and derived phenylpropanoids. *Metabolic Engineering* **57**, 129–139 (2020).

11. Deshpande, A., Vue, J. & Morgan, J. Combining Random Mutagenesis and Metabolic Engineering for Enhanced Tryptophan Production in Synechocystis sp. Strain PCC 6803. *Applied and Environmental Microbiology* **86**, 1–11 (2020).

12. Korosh, T. C. *et al.* Engineering photosynthetic production of L-lysine. *Metabolic Engineering* **44**, 273–283 (2017).

13. Ungerer, J. *et al.* Sustained photosynthetic conversion of CO2 to ethylene in recombinant cyanobacterium Synechocystis 6803. *Energy and Environmental Science* **5**, 8998–9006 (2012).

14. Angermayr, S. A., Paszota, M. & Hellingwerf, K. J. Engineering a cyanobacterial cell factory for production of lactic acid. *Applied and Environmental Microbiology* **78**, 7098–7106 (2012).

15. Varman, A. M., Yu, Y., You, L. & Tang, Y. J. Photoautotrophic production of D-lactic acid in an engineered cyanobacterium. *Microbial Cell Factories* **12**, 1–8 (2013).

16. Wang, Y. *et al.* Biosynthesis of platform chemical 3-hydroxypropionic acid (3-HP) directly from CO2 in cyanobacterium Synechocystis sp. PCC 6803. *Metabolic Engineering* **34**, 60–70 (2016).

17. Wang, B., Pugh, S., Nielsen, D. R., Zhang, W. & Meldrum, D. R. Engineering cyanobacteria for photosynthetic production of 3-hydroxybutyrate directly from CO2. *Metabolic Engineering* **16**, 68–77 (2013).

18. Niederholtmeyer, H., Wolfstädter, B. T., Savage, D. F., Silver, P. A. & Way, J. C. Engineering cyanobacteria to synthesize and export hydrophilic products. *Applied and Environmental Microbiology* **76**, 3462–3466 (2010).

19. Lan, E. I. & Wei, C. T. Metabolic engineering of cyanobacteria for the photosynthetic production of succinate. *Metabolic Engineering* **38**, 483–493 (2016).

20. Lan, E. I. *et al.* Metabolic engineering of cyanobacteria for photosynthetic 3-hydroxypropionic acid production from CO2 using Synechococcus elongatus PCC 7942. *Metabolic Engineering* **31**, 163–170 (2015).

21. Yao, J. *et al.* Engineering a Xylose-Utilizing Synechococcus elongatus UTEX 2973 Chassis for 3-Hydroxypropionic Acid Biosynthesis under Photomixotrophic Conditions . *ACS Synthetic Biology* (2022) doi:10.1021/acssynbio.1c00364.

22. Atsumi, S., Higashide, W. & Liao, J. C. Direct photosynthetic recycling of carbon dioxide to isobutyraldehyde. *Nature Biotechnology* **27**, 1177–1180 (2009).

23. Roussou, S., Albergati, A., Liang, F. & Lindblad, P. Engineered cyanobacteria with additional overexpression of selected Calvin-Benson-Bassham enzymes show further increased ethanol production. *Metabolic Engineering Communications* **12**, e00161 (2021).

24. Eungrasamee, K., Incharoensakdi, A., Lindblad, P. & Jantaro, S. Synechocystis sp. PCC 6803 overexpressing genes involved in CBB cycle and free fatty acid cycling enhances the significant levels of intracellular lipids and secreted free fatty acids. *Scientific Reports* **10**, 1–13 (2020).

25. Zhu, X. G., Long, S. P. & Ort, D. R. Improving photosynthetic efficiency for greater yield. *Annual Review of Plant Biology* **61**, 235–261 (2010).

26. Clark, R. L. *et al.* High-CO2 Requirement as a Mechanism for the Containment of Genetically Modified Cyanobacteria. *ACS Synthetic Biology* **7**, 384–391 (2018).

27. Kamennaya, N. A. *et al.* Installing extra bicarbonate transporters in the cyanobacterium Synechocystis sp. PCC6803 enhances biomass production. *Metabolic Engineering* **29**, 76–85 (2015).

28. Price, G. D. Inorganic carbon transporters of the cyanobacterial CO2 concentrating mechanism. *Photosynthesis Research* **109**, 47–57 (2011).

29. Yu, J. *et al.* Synechococcus elongatus UTEX 2973, a fast growing cyanobacterial chassis for biosynthesis using light and CO_2. *Scientific reports* **5**, 8132 (2015).

30. Włodarczyk, A., Selão, T. T., Norling, B. & Nixon, P. J. Newly discovered Synechococcus sp. PCC 11901 is a robust cyanobacterial strain for high biomass production. *Communications Biology* **3**, (2020).

31. Young, J. D., Shastri, A. A., Stephanopoulos, G. & Morgan, J. A. Mapping photoautotrophic metabolism with isotopically nonstationary 13C flux analysis. *Metabolic Engineering* **13**, 656–665 (2011).

32. Jazmin, L. J. *et al.* Isotopically nonstationary 13C flux analysis of cyanobacterial isobutyraldehyde production. *Metabolic Engineering* **42**, 9–18 (2017).

33. Abernathy, M. H. *et al.* Deciphering cyanobacterial phenotypes for fast photoautotrophic growth via isotopically nonstationary metabolic flux analysis. *Biotechnology for Biofuels* **10**, 1–13 (2017).

34. Knoot, C. J., Ungerer, J., Wangikar, P. P. & Pakrasi, H. B. Cyanobacteria: Promising biocatalysts for sustainable chemical production. *Journal of Biological Chemistry* **293**, 5044–5052 (2018).

35. Kim, H. W., Cheng, J. & Rittmann, B. E. Direct membrane-carbonation photobioreactor producing photoautotrophic biomass via carbon dioxide transfer and nutrient removal. *Bioresource Technology* **204**, 32–37 (2016).

36. Zeng, X. *et al.* Autotrophic cultivation of Spirulina platensis for CO 2 fixation and phycocyanin production. *Chemical Engineering Journal* **183**, 192–197 (2012).

37. Kim, G., Choi, W., Lee, C. H. & Lee, K. Enhancement of dissolved inorganic carbon and carbon fixation by green alga Scenedesmus sp. in the presence of alkanolamine CO2 absorbents. *Biochemical Engineering Journal* **78**, 18–23 (2013).

38. Knoot, C. J., Khatri, Y., Hohlman, R. M., Sherman, D. H. & Pakrasi, H. B. Engineered Production of Hapalindole Alkaloids in the Cyanobacterium Synechococcus sp. UTEX 2973. *ACS Synthetic Biology* **8**, 1941–1951 (2019).

39. Lin, P. C., Zhang, F. & Pakrasi, H. B. Enhanced production of sucrose in the fast-growing cyanobacterium Synechococcus elongatus UTEX 2973. *Scientific Reports* **10**, 1–8 (2020).

40. Song, K., Tan, X., Liang, Y. & Lu, X. The potential of Synechococcus elongatus UTEX 2973 for sugar feedstock production. *Applied Microbiology and Biotechnology* **100**, 7865–7875 (2016).

41. Ungerer, J., Lin, P. C., Chen, H. Y. & Pakrasi, H. B. Adjustments to photosystem stoichiometry and electron transfer proteins are key to the remarkably fast growth of the Cyanobacterium synechococcus elongatus UTEX 2973. *mBio* **9**, 1–12 (2018).

42. Xia, P. F., Ling, H., Foo, J. L. & Chang, M. W. Synthetic Biology Toolkits for Metabolic Engineering of Cyanobacteria. *Biotechnology Journal* **14**, 1–11 (2019).

43. Liu, R., Bassalo, M. C., Zeitoun, R. I. & Gill, R. T. Genome scale engineering techniques for metabolic engineering. *Metabolic Engineering* **32**, 143–154 (2015).

44. Mileyko, Y., Joh, R. I. & Weitz, J. S. Small-scale copy number variation and large-scale changes in gene expression. *Proceedings of the National Academy of Sciences of the United States of America* **105**, 16659–16664 (2008).

45. Sergeyenko, T. v & Los, D. a. Identification of secreted proteins of the cyanobacterium. *FEMS Microbiology Letters* **193**, 213–216 (2000).

46. Matthias, K. *et al.* Comparative analysis of the primary transcriptome of synechocystis sp. PCC 6803. *DNA Research* **21**, 527–539 (2014).

47. Aoki, R., Goto, T. & Fujita, Y. A heme oxygenase isoform is essential for aerobic growth in the cyanobacterium synechocystis sp. PCC 6803: Modes of differential operation of two isoforms/enzymes to adapt to low oxygen environments in cyanobacteria. *Plant and Cell Physiology* **52**, 1744–1756 (2011).

48. Marbouty, M., Mazouni, K., Saguez, C., Cassier-Chauvat, C. & Chauvat, F. Characterization of the Synechocystis strain PCC 6803 penicillin-binding proteins and cytokinetic proteins FtsQ and FtsW and their network of interactions with ZipN. *Journal of Bacteriology* **191**, 5123–5133 (2009).

49. Pinto, F. *et al.* Improving a Synechocystis-based photoautotrophic chassis through systematic genome mapping and validation of neutral sites. *DNA Research* **22**, 425–437 (2015).

50. Sakamoto, T., Shen, G., Higashi, S., Murata, N. & Bryant, D. A. Alteration of low-temperature susceptibility of the cyanobacterium Synechococcus sp. PCC 7002 by genetic manipulation of membrane lipid unsaturation. *Archives of Microbiology* **169**, 20–28 (1997).

51. Begemann, M. B. *et al.* An Organic Acid Based Counter Selection System for Cyanobacteria. *PLoS ONE* **8**, 1–12 (2013).

52. Davies, F. K., Work, V. H., Beliaev, A. S. & Posewitz, M. C. Engineering limonene and bisabolene production in wild type and a glycogen-deficient mutant of Synechococcus sp. PCC 7002. *Frontiers in Bioengineering and Biotechnology* **2**, 1–11 (2014).

53. Ruffing, A. M., Jensen, T. J. & Strickland, L. M. Genetic tools for advancement of Synechococcus sp. PCC 7002 as a cyanobacterial chassis. *Microbial Cell Factories* **15**, 1–14 (2016).

54. Wang, M., Luan, G. & Lu, X. Systematic identification of a neutral site on chromosome of Synechococcus sp. PCC7002, a promising photosynthetic chassis strain. *Journal of Biotechnology* **295**, 37–40 (2019).

55. Bustos, S. A. & Golden, S. S. Light-regulated expression of the psbD gene family in Synechococcus sp . strain PCC 7942 : evidence for the role of duplicated psbD genes in cyanobacteria. 221–230 (1992).

56. Andersson, C. R. *et al.* Application of Bioluminescence to the Study of Circadian Rhythms in Cyanobacteria. **305**, 527–542 (2000).

57. Kim, W. J., Lee, S., Um, Y., Sim, S. J. & Woo, H. M. Development of SyneBrick Vectors As a Synthetic Biology Platform for Gene Expression in Synechococcus elongatus PCC 7942. **8**, 1–9 (2017).

58. Guerry, P., Embden, J. A. N. V. A. N. & Falkow, S. Molecular Nature of Two Nonconjugative Plasmids Carrying Drug Resistance Genes. **117**, 619–630 (1974).

59. Sode, K., Tatara, M., Takeyama, H., Burgess, J. G. & Matsunaga, T. Applied Af robiology S chnotogy Conjugative gene transfer in marine cyanobacteria : 369–373 (1992).

60. Meyer, R. Plasmid Replication and conjugative mobilization of broad host-range IncQ plasmids. **62**, 57–70 (2009).

61. Ferreira, E. A. *et al.* Expanding the toolbox for Synechocystis sp . PCC 6803 : validation of replicative vectors and characterization of a novel set of promoters. **3**, 1–15 (2018).

62. Taton, A. *et al.* Broad-host-range vector system for synthetic biology and biotechnology in cyanobacteria. **42**, 1–16 (2014).

63. Bishe, B., Taton, A., Golden, J. W. & Bishe, B. Modification of RSF1010-Based Broad-Host-Range Plasmids for Improved Conjugation and Cyanobacterial Bioprospecting Modification of RSF1010-Based Broad-Host-Range Plasmids for Improved Conjugation and Cyanobacterial Bioprospecting. 216–228 (2019) doi:10.1016/j.isci.2019.09.002.

64. Ng, A. H., Berla, B. M. & Pakrasi, H. B. Fine-tuning of photoautotrophic protein production by combining promoters and neutral sites in the cyanobacterium Synechocystis sp. strain PCC 6803. *Applied and Environmental Microbiology* **81**, 6857–6863 (2015).

65. Jones, C. M., Parrish, S. & Nielsen, D. R. Exploiting Polyploidy for Markerless and Plasmid-Free Genome Engineering in Cyanobacteria. *ACS Synthetic Biology* **10**, 2371–2382 (2021).

66. Liu, D. & Pakrasi, H. B. Exploring native genetic elements as plug - in tools for synthetic biology in the cyanobacterium Synechocystis sp . PCC. *Microbial Cell Factories* 1–8 (2018) doi:10.1186/s12934-018-0897-8.

67. Xu, Y. *et al.* Expression of genes in cyanobacteria: adaptation of endogenous plasmids as platforms for high-level gene expression in Synechococcus sp. PCC 7002. *Methods in molecular biology (Clifton, N.J.)* **684**, 273–293 (2011).

68. Miyasaka, H., Nakano, H., Akiyama, H., Kanai, S. & Hirano, M. Production of PHA (poly hydroxyalkanoate) by genetically engineered marine cyanobacterium. *Studies in Surface Science and Catalysis* **114**, 1–6 (1998).

69. Ikeda, K. *et al.* Transformation of the fresh water cyanobacterium Synechococcus PCC7942 with the shuttle-vector pAQ-EX1 developed for the marine cyanobacterium Synechococcus PCC7002. *World Journal of Microbiology and Biotechnology* **18**, 55–56 (2002).

70. Chen, Y. *et al.* Self-replicating shuttle vectors based on pANS, a small endogenous plasmid of the unicellular cyanobacterium Synechococcus elongatus PCC 7942. *Microbiology (United Kingdom)* **162**, 2029–2041 (2016).

71. Markley, A. L., Begemann, M. B., Clarke, R. E., Gordon, G. C. & Pfleger, B. F. Synthetic Biology Toolbox for Controlling Gene Expression in the Cyanobacterium Synechococcus sp. strain PCC 7002. *ACS Synthetic Biology* **4**, 595–603 (2015).

72. Zess, E. K., Begemann, M. B. & Pfleger, B. F. Construction of new synthetic biology tools for the control of gene expression in the cyanobacterium Synechococcus sp. strain PCC 7002. *Biotechnology and Bioengineering* **113**, 424–432 (2016).

73. Sengupta, A., Sunder, A. V., Sohoni, S. v. & Wangikar, P. P. Fine-Tuning Native Promoters of Synechococcus elongatus PCC 7942 to Develop a Synthetic Toolbox for Heterologous Protein Expression. *ACS Synthetic Biology* **8**, 1219–1223 (2019).

74. Zhou, J. *et al.* Discovery of a super-strong promoter enables efficient production of heterologous proteins in cyanobacteria. *Scientific Reports* **4**, 1–6 (2014).

75. Englund, E., Liang, F. & Lindberg, P. Evaluation of promoters and ribosome binding sites for biotechnological applications in the unicellular cyanobacterium Synechocystis sp . PCC 6803. 1–12 (2016) doi:10.1038/srep36640.

76. Peca, L., Kós, P. B. & Vass, I. Characterization of the activity of heavy metal-responsive promoters in the cyanobacterium Synechocystis PCC 6803. *Acta Biologica Hungarica* **58**, 11–22 (2007).

77. Guerrero, F., Carbonell, V., Cossu, M., Correddu, D. & Jones, P. R. Ethylene Synthesis and Regulated Expression of Recombinant Protein in Synechocystis sp. PCC 6803. *PLoS ONE* **7**, (2012).

78. Imamura, S. & Asayama, M. Sigma Factors for Cyanobacterial Transcription. *Gene Regulation and Systems Biology* **3**, GRSB.S2090 (2009).

79. Camsund, D., Heidorn, T. & Lindblad, P. Design and analysis of LacI-repressed promoters and DNA-looping in a cyanobacterium. *Journal of Biological Engineering* **8**, 1–23 (2014).

80. Huang, H. H. & Lindblad, P. Wide-dynamic-range promoters engineered for cyanobacteria. *Journal of Biological Engineering* **7**, 1–11 (2013).

81. Berla, B. M. *et al.* Synthetic biology of cyanobacteria: Unique challenges and opportunities. *Frontiers in Microbiology* **4**, 1–14 (2013).

82. Jones, C. M., Korosh, T. C., Nielsen, D. R. & Pfleger, B. F. Optimization of a T7-RNA polymerase system in Synechococcus sp. PCC 7002 mirrors the protein overproduction phenotype from E. coli BL21(DE3). *Applied Microbiology and Biotechnology* **105**, 1147–1158 (2021).

83. Li, S., Sun, T., Xu, C., Chen, L. & Zhang, W. Development and optimization of genetic toolboxes for a fast-growing cyanobacterium Synechococcus elongatus UTEX 2973. *Metabolic Engineering* **48**, 163–174 (2018).

84. Nakahira, Y., Ogawa, A., Asano, H., Oyama, T. & Tozawa, Y. Theophylline-dependent riboswitch as a novel genetic tool for strict regulation of protein expression in cyanobacterium synechococcus elongatus PCC 7942. *Plant and Cell Physiology* **54**, 1724–1735 (2013).

85. Ma, A. T., Schmidt, C. M. & Golden, J. W. Regulation of gene expression in diverse cyanobacterial species by using theophylline-responsive

riboswitches. *Applied and Environmental Microbiology* **80**, 6704–6713 (2014).

86. Wang, X. *et al.* Enhanced limonene production in cyanobacteria reveals photosynthesis limitations. *Proceedings of the National Academy of Sciences of the United States of America* **113**, 14225–14230 (2016).

87. Kinoshita, S., Udaka, S. & Shimono, M. Studies on the amino acid fermentation Part 1. Production of L-glutamic acid by various microorganisms. *The Journal of general and applied microbiology* **3**, 193–205 (1957).

88. Kinoshita, S., Nakayama, K. & Akita, S. Taxonomical study of glutamic acid accumulating bacteria, micrococcus glutamicus nov. Sp. *Journal of the Agricultural Chemical Society of Japan* **22**, 176–185 (1958).

89. Kinoshita, S. The Production of Amino Acids by Fermentation Processes. *Advances in Applied Microbiology* **1**, 201–214 (1959).

90. Kalinowski, J. *et al.* Genetic and biochemical analysis of the aspartokinase from Corynebacterium glutamicum. *Molecular Microbiology* **5**, 1197–1204 (1991).

91. Vrljic, M., Sahm, H. & Eggeling, L. A new type of transporter with a new type of cellular function: L-lysine export from Corynebacterium glutamicum. *Molecular Microbiology* **22**, 815–826 (1996).

92. Peters-Wendisch, P., Schiel-Bengelsdorf, B. M. & Wendisch, V. F. *Pyruvate Carboxylase is a Major Bottleneck for Glutamate and Lysine Production by Corynebacterium glutamicum*. *Article in Journal of Molecular Microbiology and Biotechnology* https://www.researchgate.net/publication/12013735 (2001).

93. Wittmann, C. & Becker, J. The L-lysine story: from metabolic pathways to industrial production. in *Amino Acid Biosynthesis~ Pathways, Regulation and Metabolic Engineering* (Springer, 2007).

94. Thierbach, G., Kalinowski, J., Bachmann, B. & Pühler, A. Cloning of a DNA fragment from Corynebacterium glutamicum conferring aminoethyl cysteine resistance and feedback resistance to aspartokinase. *Applied Microbiology and Biotechnology* **32**, 443–448 (1990).

95. Kelle, R., Hermann, T. & Bathe, B. *20 L-Lysine Production*.

96. van Ooyen, J., Noack, S., Bott, M., Reth, A. & Eggeling, L. Improved L-lysine production with Corynebacterium glutamicum and systemic insight

into citrate synthase flux and activity. *Biotechnology and Bioengineering* **109**, 2070–2081 (2012).

97. Buchholz, J. *et al.* Platform engineering of corynebacterium glutamicum with reduced pyruvate dehydrogenase complex activity for improved production of l-lysine, l-valine, and 2-ketoisovalerate. *Applied and Environmental Microbiology* **79**, 5566–5575 (2013).

98. Contador, C. A., Rizk, M. L., Asenjo, J. A. & Liao, J. C. Ensemble modeling for strain development of l-lysine-producing Escherichia coli. *Metabolic Engineering* **11**, 221–233 (2009).

99. Xu, J., Han, M., Ren, X. & Zhang, W. Modification of aspartokinase III and dihydrodipicolinate synthetase increases the production of L-lysine in Escherichia coli. *Biochemical Engineering Journal* **114**, 79–86 (2016).

100. Vrljic, M. *et al.* The LysE superfamily: Topology of the lysine exporter LysE of Corynebacterium glutamicum, a paradyme for a novel superfamily of transmembrane solute translocators. *Journal of Molecular Microbiology and Biotechnology* **1**, 327–336 (1999).

101. Bellman, A. *et al.* Expression control and specificity of the basic amino acid exporter lysE of Corynebacterium glutamicum. *Microbiology* **147**, 1765–1774 (2001).

102. Eggeling, L. & Bott, M. A giant market and a powerful metabolism: l-lysine provided by Corynebacterium glutamicum. *Applied Microbiology and Biotechnology* vol. 99 3387–3394 (2015).

103. Gunji, Y. & Yasueda, H. Enhancement of l-lysine production in methylotroph Methylophilus methylotrophus by introducing a mutant LysE exporter. *Journal of Biotechnology* **127**, 1–13 (2006).

104. Xu, J. Z., Ruan, H. Z., Yu, H. B., Liu, L. M. & Zhang, W. Metabolic engineering of carbohydrate metabolism systems in Corynebacterium glutamicum for improving the efficiency of l-lysine production from mixed sugar. *Microbial Cell Factories* **19**, (2020).

105. Kind, S., Becker, J. & Wittmann, C. Increased lysine production by flux coupling of the tricarboxylic acid cycle and the lysine biosynthetic pathway-Metabolic engineering of the availability of succinyl-CoA in Corynebacterium glutamicum. *Metabolic Engineering* **15**, 184–195 (2013).

106. Ying, H., He, X., Li, Y., Chen, K. & Ouyang, P. Optimization of culture conditions for enhanced lysine production using engineered Escherichia coli. *Applied Biochemistry and Biotechnology* **172**, 3835–3843 (2014).

107. Buschke, N., Schröder, H. & Wittmann, C. Metabolic engineering of Corynebacterium glutamicum for production of 1,5-diaminopentane from hemicellulose. *Biotechnology Journal* **6**, 306–317 (2011).

108. Gopinath, V., Meiswinkel, T. M., Wendisch, V. F. & Nampoothiri, K. M. Amino acid production from rice straw and wheat bran hydrolysates by recombinant pentose-utilizing Corynebacterium glutamicum. *Applied Microbiology and Biotechnology* **92**, 985–996 (2011).

109. Kawaguchi, H., Sasaki, M., Vertès, A. A., Inui, M. & Yukawa, H. Engineering of an L-arabinose metabolic pathway in Corynebacterium glutamicum. *Applied Microbiology and Biotechnology* **77**, 1053–1062 (2008).

110. Sasaki, M., Jojima, T., Inui, M. & Yukawa, H. Simultaneous utilization of d-cellobiose, d-glucose, and d-xylose by recombinant Corynebacterium glutamicum under oxygen-deprived conditions. *Applied Microbiology and Biotechnology* **81**, 691–699 (2008).

111. Hoffmann, S. L. *et al.* Lysine production from the sugar alcohol mannitol: Design of the cell factory Corynebacterium glutamicum SEA-3 through integrated analysis and engineering of metabolic pathway fluxes. *Metabolic Engineering* **47**, 475–487 (2018).

112. Pathania, A. & Sardesai, A. A. Distinct paths for basic amino acid export in Escherichia coli: YbjE (LysO) mediates export of L-lysine. *Journal of Bacteriology* **197**, 2036–2047 (2015).

113. Gibson, D. G. *et al.* Enzymatic assembly of DNA molecules up to several hundred kilobases. *Nature Methods* **6**, 343–345 (2009).

114. Englund, E., Andersen-Ranberg, J., Miao, R., Hamberger, B. & Lindberg, P. Metabolic Engineering of Synechocystis sp. PCC 6803 for Production of the Plant Diterpenoid Manoyl Oxide. *ACS Synthetic Biology* **4**, 1270–1278 (2015).

115. Adkins, J., Jordan, J. & Nielsen, D. R. Engineering Escherichia coli for Renewable Production of the 5-Carbon Polyamide Building-Blocks 5-Aminovalerate and Glutarate. *Biotechnol. Bioeng* **110**, 1726–1734 (2013).

116. Kim, Y. H. *et al.* Application of diethyl ethoxymethylenemalonate (DEEMM) derivatization for monitoring of lysine decarboxylase activity. *Journal of Molecular Catalysis B: Enzymatic* **115**, 151–154 (2015).

117. Kittleson, J. T., Wu, G. C. & Anderson, J. C. Successes and failures in modular genetic engineering. *Current Opinion in Chemical Biology* **16**, 329–336 (2012).

118. Segall-Shapiro, T. H., Sontag, E. D. & Voigt, C. A. Engineered promoters enable constant gene expression at any copy number in bacteria. *Nature Biotechnology* **36**, 352–358 (2018).

119. Topp, S. *et al.* Synthetic riboswitches that induce gene expression in diverse bacterial species. *Applied and Environmental Microbiology* **76**, 7881–7884 (2010).

120. Becker, J., Zelder, O., Häfner, S., Schröder, H. & Wittmann, C. From zero to hero-Design-based systems metabolic engineering of Corynebacterium glutamicum for l-lysine production. *Metabolic Engineering* **13**, 159–168 (2011).

121. Steinhauser, D., Fernie, A. R. & Araújo, W. L. Unusual cyanobacterial TCA cycles: Not broken just different. *Trends in Plant Science* **17**, 503–509 (2012).

122. Schwarz, D. *et al.* Metabolic and transcriptomic phenotyping of inorganic carbon acclimation in the cyanobacterium Synechococcus elongatus PCC 7942. *Plant Physiology* **155**, 1640–1655 (2011).

123. Ciebiada, M., Kubiak, K. & Daroch, M. Modifying the cyanobacterial metabolism as a key to efficient biopolymer production in photosynthetic microorganisms. *International Journal of Molecular Sciences* **21**, 1–24 (2020).

124. Xiong, W., Brune, D. & Vermaas, W. F. J. The γ-aminobutyric acid shunt contributes to closing the tricarboxylic acid cycle in Synechocystis sp. PCC 6803. *Molecular Microbiology* **93**, 786–796 (2014).

125. Zhang, S. & Bryant, D. A. The tricarboxylic acid cycle in cyanobacteria. *Science* **334**, 1551–1553 (2011).

126. Zhang, S., Qian, X., Chang, S., Dismukes, G. C. & Bryant, D. A. Natural and synthetic variants of the tricarboxylic acid cycle in cyanobacteria: Introduction of the GABA Shunt into Synechococcus sp. PCC 7002. *Frontiers in Microbiology* **7**, 1–13 (2016).

127. Malla, S. *et al.* A Novel Efficient L-Lysine Exporter Identified by Functional Metagenomics. (2020) doi:10.1101/2020.04.30.071142.

128. Zhou, L. & Zeng, A. Engineering a Lysine-ON Riboswitch for Metabolic Control of Lysine Production in Corynebacterium glutamicum. (2015) doi:10.1021/acssynbio.5b00075.

129. Han, T., Kim, G. B. & Lee, S. Y. Glutaric acid production by systems metabolic engineering of an L-lysine–overproducing Corynebacterium glutamicum. *Proceedings of the National Academy of Sciences of the United States of America* **117**, 30328–30334 (2020).

130. Kwak, D. H., Lim, H. G., Yang, J., Seo, S. W. & Jung, G. Y. Synthetic redesign of Escherichia coli for cadaverine production from galactose. *Biotechnology for Biofuels* **10**, 1–9 (2017).

131. Li, M. *et al.* Improving the secretion of cadaverine in Corynebacterium glutamicum by cadaverine-lysine antiporter. *Journal of Industrial Microbiology and Biotechnology* **41**, 701–709 (2014).

132. Kind, S. *et al.* From zero to hero - Production of bio-based nylon from renewable resources using engineered Corynebacterium glutamicum. *Metabolic Engineering* **25**, 113–123 (2014).

133. Mi, J. *et al.* Cellular Engineering and Biocatalysis Strategies toward Sustainable Cadaverine Production: State of the Art and Perspectives. *ACS Sustainable Chemistry and Engineering* **9**, 1061–1072 (2021).

134. Knorr, S. *et al.* Widespread bacterial lysine degradation proceeding via glutarate and L-2-hydroxyglutarate. *Nature Communications* **9**, 2–11 (2018).

135. Yamamoto, Y., Miwa, Y., Miyoshi, K., Furuyama, J. I. & Ohmori, H. The Escherichia coli ldcC gene encodes another lysine decarboxylase, probably a constitutive enzyme. *Genes and Genetic Systems* **72**, 167–172 (1997).

136. Kikuchi, Y., Kojima, H., Tanaka, T., Takatsuka, Y. & Kamio, Y. Characterization of a second lysine decarboxylase isolated from Escherichia coli. *Journal of Bacteriology* **179**, 4486–4492 (1997).

137. Kim, H. T. *et al.* Metabolic Engineering of Corynebacterium glutamicum for the High-Level Production of Cadaverine That Can Be Used for the Synthesis of Biopolyamide 510. *ACS Sustainable Chemistry and Engineering* **6**, 5296–5305 (2018).

138. Revelles, O., Espinosa-Urgel, M., Molin, S. & Ramos, J. L. The davDT operon of Pseudomonas putida, involved in lysine catabolism, is induced in response to the pathway intermediate δ-aminovaleric acid. *Journal of Bacteriology* **186**, 3439–3446 (2004).

139. Revelles, O., Espinosa-Urgel, M., Fuhrer, T., Sauer, U. & Ramos, J. L. Multiple and interconnected pathways for l-lysine catabolism in Pseudomonas putida KT2440. *Journal of Bacteriology* **187**, 7500–7510 (2005).

140. Park, S. J. *et al.* Metabolic engineering of Escherichia coli for the production of 5-aminovalerate and glutarate as C5 platform chemicals. *Metabolic Engineering* **16**, 42–47 (2013).

141. Rohles, C. M., Gießelmann, G., Kohlstedt, M., Wittmann, C. & Becker, J. Systems metabolic engineering of Corynebacterium glutamicum for the production of the carbon-5 platform chemicals 5-aminovalerate and glutarate. *Microbial Cell Factories* **15**, 1–13 (2016).

142. Li, W. *et al.* Targeting metabolic driving and intermediate influx in lysine catabolism for high-level glutarate production. *Nature Communications* **10**, (2019).

143. Fukui, K. *et al.* Corynebacterium glutamicum CgynfM encodes a dicarboxylate transporter applicable to succinate production. *Journal of Bioscience and Bioengineering* **127**, 465–471 (2019).

144. Mullineaux, C. W. The thylakoid membranes of cyanobacteria: Structure, dynamics and function. *Australian Journal of Plant Physiology* **26**, 671–677 (1999).

145. Mukhopadhyay, A. Tolerance engineering in bacteria for the production of advanced biofuels and chemicals. *Trends in Microbiology* **23**, 498–508 (2015).

146. Soksawatmaekhin, W., Kuraishi, A., Sakata, K., Kashiwagi, K. & Igarashi, K. Excretion and uptake of cadaverine by CadB and its physiological functions in Escherichia coli. *Molecular Microbiology* **51**, 1401–1412 (2004).

147. Kind, S., Kreye, S. & Wittmann, C. Metabolic engineering of cellular transport for overproduction of the platform chemical 1,5-diaminopentane in Corynebacterium glutamicum. *Metabolic Engineering* **13**, 617–627 (2011).

148. Sugiyama, Y. *et al.* A novel putrescine exporter SapBCDF of Escherichia coli. *Journal of Biological Chemistry* **291**, 26343–26351 (2016).

149. Onyeabor, M., Martinez, R., Kurgan, G. & Wang, X. *Engineering transport systems for microbial production*. *Advances in Applied Microbiology* vol. 111 (Elsevier Inc., 2020).

150. Machas, M. *et al.* Emerging tools, enabling technologies, and future opportunities for the bioproduction of aromatic chemicals. *Journal of Chemical Technology and Biotechnology* **94**, 38–52 (2019).

151. Burnap, R. L., Hagemann, M. & Kaplan, A. Regulation of CO2concentrating mechanism in cyanobacteria. *Life* **5**, 348–371 (2015).

152. Song, C. *et al.* Microalgae carbon fixation integrated with organic matters recycling from soybean wastewater: Effect of pH on the performance of hybrid system. *Chemosphere* **248**, 126094 (2020).

153. Costa, J. & Camerini, F. Relation between Transfer of CO2 and the pH of the Medium. *American Chemical Science Journal* **6**, 51–57 (2015).

154. Choi, W., Kim, G. & Lee, K. Influence of the CO 2 absorbent monoethanolamine on growth and carbon fixation by the green alga Scenedesmus sp. *Bioresource Technology* **120**, 295–299 (2012).

155. Rosa, G. M. da, Morais, M. G. de & Costa, J. A. V. Green alga cultivation with monoethanolamine: Evaluation of CO2 fixation and macromolecule production. *Bioresource Technology* **261**, 206–212 (2018).

156. Garca-Abuin, A., Gomez-Diaz, D., Navaza, J. M. & Rumbo, A. CO2 Capture by Pyrrolidine: Reaction Mechanism and Mass Transfer. *AIChE Journal* **60**, 1098–1106 (2014).

157. Rinker, E. B., Ashour, S. S. & Sandall, O. C. Absorption of Carbon Dioxide into Aqueous Blends of Diethanolamine and Methyldiethanolamine. *Industrial & Engineering Chemistry Research* **39**, 4346–4356 (2000).

158. Hook, R. J. An Investigation of Some Sterically Hindered Amines as Potential Carbon Dioxide Scrubbing Compounds. *Industrial and Engineering Chemistry Research* **36**, 1779–1790 (1997).

159. Rosa, G. M. da, Moraes, L., Cardias, B. B., Souza, M. da R. A. Z. de & Costa, J. A. V. Chemical absorption and CO2 biofixation via the cultivation of Spirulina in semicontinuous mode with nutrient recycle. *Bioresource Technology* **192**, 321–327 (2015).

160. Flamholz, A. I. *et al.* Functional reconstitution of a bacterial co2 concentrating mechanism in e. Coli. *eLife* **9**, 1–57 (2020).

161. Foti, M., Médici, R. & Ruijssenaars, H. J. Biological production of monoethanolamine by engineered Pseudomonas putida S12. *Journal of Biotechnology* **167**, 344–349 (2013).

162. Michael, A. J. Polyamine function in archaea and bacteria. *Journal of Biological Chemistry* **293**, 18693–18701 (2018).

163. Kera, K. *et al.* Reduction of spermidine content resulting from inactivation of two arginine decarboxylases increases biofilm formation in Synechocystis sp. strain PCC 6803. *Journal of Bacteriology* **200**, 1–15 (2018).

164. Shastri, A. A. & Morgan, J. A. Flux balance analysis of photoautotrophic metabolism. *Biotechnology Progress* **21**, 1617–1626 (2005).

APPENDIX A

LIST OF PRIMERS USED IN THE STUDIES OF CHAPTER 2 AND CHAPTER 3

Name	Sequence	Assembly	Sequencing
ZDC-001	taggcgggctggccggccttggatccctcgagtcccgtca	pAM4788-Km^R, pZDC-LGC-01, pZD-LGC-03	
ZDC-002	gccctaaaacaaagttaaacatctcatgaacaataaaactgtctgc	pAM4788-Km^R, pZDC-LGC-21	
ZDC-003	gcagacagttttattgttcatgagatgttaactttgttttagggc	pAM4788-Km^R, pZDC-LGC-21	
ZDC-004	tgacgggactcgagggatccaaggccggccagcccgccta	pAM4788-Km^R, pZDC-LGC-01, pZD-LGC-03	
ZDC-005	cgccgccgccggataccggtcccgtcagtcagagcttcac	pZD-LGC-02	
ZDC-006	gtcattcaaccagtctcctgaaccttatccagttgccttg	pZD-LGC-02	
ZDC-007	caggagactggttgaatgacttttgatgctttcaccaaggtggtg	pZD-LGC-02	
ZDC-008	caccaccttggtgaaagcatcaaaagtcattcaaccagtctcctg	pZD-LGC-02	
ZDC-012	gtgaagctctgactgacgggaccggtatccggcggcggcg	pZD-LGC-02	
ZDC-013	ttgatgctttcaccaaggtggtgttttctggctgttaatcattc	pZD-LGC-15	
ZDC-016	atgctttcaccaaggtggtgtctaaaggtgaagaattattcactg	pZD-LGC-02	
ZDC-024	tttgtacaagaaagctgggtttacgcagagaaaaaggcga	pZD-LGC-15	
ZDC-025	tcgccttttttctctgcgtaaacccagctttcttgtacaaa	pZD-LGC-15	
ZDC-026	gagagttatagttgtattccaatttgtgacc		yemGFP
ZDC-045	cgccgccgccggataccggtgacgtctaagaaaccattattatca	pZD-LGC-04	
ZDC-046	tgaataattcttcacctttagacatctagtatttctcctcttttctagtatg	pZD-LGC-04	
ZDC-047	catactagaaaagaggagaaatactagatgtctaaaggtgaagaattattca	pZD-LGC-04	
ZDC-048	tgataataatggtttcttagacgtcaccggtatccggcggcggcg	pZD-LGC-04	
ZDC-049	GTATTGAAAGAAGAAAGCAAAAAATAAacccagctttcttgtacaaa	pZD-LGC-29	
ZDC-050	GTATTGAAAGAAGAAAGCAAAAAATAAacccagctttcttgtacaaa	pZD-LGC-29	
ZDC-057	CTTCCTTTCGGGCTTTGTTAccgagtttgtacaagaaagc	pZD-LGC-04, pZD-LGC-16	
ZDC-058	gctttcttgtacaaactcggTAACAA	pZD-LGC-04, pZD-LGC-16	

	AGCCCGAAAGGAAG		
ZDC-059	ccgctcactgaggctgtcagAACCG GAAGGAGCTGACTGG	pZD-LGC-04	
ZDC-060	CCAGTCAGCTCCTTCCG GTTctgacagcctcagtgagcgg	pZD-LGC-04	
ZDC-062	caaagatgacggtaactacaagacc		yemGFP
ZDC-067	ccgctcactgaggctgtcagcccgtcag tcagagcttcac	pZD-LGC-13, pZD-LGC-16, pZD-LGC-26	
ZDC-070	CCAGTCAGCTCCTTCCG GTTgcgacgagagggctgcgagc	pZD-LGC-13, pZD-LGC-30	
ZDC-071	gctcgcagccctctcgtcgcAACCG GAAGGAGCTGACTGG	pZD-LGC-13, pZD-LGC-30	
ZDC-072	gtgaagctctgactgacgggctgacag cctcagtgagcgg	pZD-LGC-13, pZD-LGC-16, pZD-LGC-26	
ZDC-075	cagaaatcatccttagcgaaagctaag		P_{trc2O}
ZDC-080	tgaataattcttcacctttagacataccgg tatccggcggcggcg	pZD-LGC-01	
ZDC-081	cgccgccgccggataccggtatgtctaa aggtgaagaattattca	pZD-LGC-01	
ZDC-086	aggtgaagaattattcactggttctgaaat tgttgtctccaaat	pZD-LGC-14	
ZDC-087	tttgtacaagaaagctgggtttactcaaa caaattactatgcagt	pZD-LGC-14	
ZDC-088	actgcatagtaatttgtttgagtaaaccca gctttcttgtacaaa	pZD-LGC-14	
ZDC-089	atttggagacaacaatttcagaaccagtg aataattcttcacct	pZD-LGC-14	
ZDC-090	aggttcaggagactggttgaatgacttca gaaaccttacagg	pZD-LGC-22	
ZDC-091	ctaatgtcctgcagttggaactagtgcgc attattggctc	pZD-LGC-22	
ZDC-092	gagccaataatgcgcactagttccaact gcaggacattag	pZD-LGC-22	
ZDC-093	cctgtaaggtttctgaagtcattcaacca gtctcctgaacct	pZD-LGC-22	
ZDC-094	aggttcaggagactggttgaatgttttctg ggctgttaatc	pZD-LGC-15	
ZDC-095	ctaatgtcctgcagttggaattacgcaga gaaaaaggcga	pZD-LGC-13	
ZDC-096	tcgccttttctctgcgtaattccaactgca ggacattag	pZD-LGC-13	
ZDC-097	gattaacagcccagaaaacattcaacca gtctcctgaacct	pZD-LGC-15	
ZDC-102	atcttcttggcagaactcatgattccctatt tctctgaaaaaaggtctgttatctcaatcc cagtc	pZD-LGC-25	
ZDC-103	ctaatgtcctgcagttggaattaatgtgcg ttagacgcgg	pZD-LGC-25, pZD-LGC-27	

ZDC-104	ccgcgtctaacgcacattaattccaactg caggacattag	pZD-LGC-25, pZD-LGC-27	
ZDC-105	ccctatttctctgaaaaaaggtctgttatct caatcccagtcgatgattacgcagagaa aaaggcga	pZD-LGC-25, pZD-LGC-31	
ZDC-109	TTTGATGCCTGGCTCTAG TAttactcaaacaaattactatgcagt	pZD-LGC-28	
ZDC-110	actgcatagtaatttgtttgagtaaTAC TAGAGCCAGGCATCAAA	pZD-LGC-28	
ZDC-117	CACACTGGCTCACCTTC G		T_{rrnB}
ZDC-118	gcggcgcagcccagt		cadB
ZDC-119	ctgcggataccactgatggtcatgc		cadB
ZDC-122	tttgtacaagaaagctgggtGGTTTT AAAGAAAAAGGGCAG	pZD-LGC-28	
ZDC-123	CTGCCCTTTTTCTTTAAA ACCacccagctttcttgtacaaa	pZD-LGC-28	
ZDC-129	taggcgggctggccggcctttcagcca gctcgtcgtgatg	pZD-LGC-06	
ZDC-130	tgacgggactcgagggatccgaccgat caaccagtccctc	pZD-LGC-06, pZD-LGC-07, pZD-LGC-08, pZD-LGC-09, pZD-LGC-10, pZD-LGC-11, pZD-LGC-12	
ZDC-131	gagggactggttgatcggtcggatccct cgagtcccgtca	pZD-LGC-06, pZD-LGC-07, pZD-LGC-08, pZD-LGC-09, pZD-LGC-10, pZD-LGC-11, pZD-LGC-12	
ZDC-132	cacgtctgccccggcttgtccccgtcagt cagagcttcac	pZD-LGC-12	
ZDC-133	gtgaagctctgactgacggggacaagc cggggcagacgtg	pZD-LGC-12	
ZDC-134	ccgggcccggggatgagctcacagtcg gcgtcacggcaac	pZD-LGC-06	
ZDC-135	gttgccgtgacgccgactgtgagctcat ccccgggcccgg	pZD-LGC-06	
ZDC-136	catcacgacgagctggctgaaaggccg gccagcccgccta	pZD-LGC-06	
ZDC-137	gagcgatgcctggcgtcg		NS3 I
ZDC-138	cgaatgagccggatggcgag		NS3 II
ZDC-140	ctttttcagagaaatagggaatcatgcg cgttaacaatggttt	pZD-LGC-18	
ZDC-141	ctaatgtcctgcagttggaattacagtttc ggaccagccg	pZD-LGC-18	
ZDC-142	cggctggtccgaaactgtaattccaactg caggacattag	pZD-LGC-18	
ZDC-143	aaaccattgttaacgcgcatgattccctat ttctctgaaaaaag	pZD-LGC-18	
ZDC-154	ggataagaaacgcgggtgttctcg		pck

ZDC-155	cgctgaaaggtatcgcttctatgcac		pck
ZDC-165	cacgtctgccccggcttgtcAACCG GAAGGAGCTGACTGG	pZD-LGC-10, pZD-LGC-11	
ZDC-166	CCAGTCAGCTCCTTCCG GTTgacaagccggggcagacgtg	pZD-LGC-10, pZD-LGC-11	
ZDC-167	cacgtctgccccggcttgtcacatgtgg ccaatgctcgag	pZD-LGC-06, pZD-LGC-07, pZD-LGC-08, pZD-LGC-09	
ZDC-168	ctcgagcattggccacatgtgacaagcc ggggcagacgtg	pZD-LGC-06, pZD-LGC-07, pZD-LGC-08, pZD-LGC-09	
ZDC-169	ctcgccatccggctcattcg		NS3 II
ZDC-170	cgacgccaggcatcgctc		NS3 I
ZDC-178	aggttcaggagactggttgaatgaacaa gaagaaccgcca	pZD-LGC-32, pZD-LGC-34	
ZDC-179	ccctatttctctgaaaaaaggtctgttatct caatcccagtcgatgatcagcctttacgc aggtgca	pZD-LGC-32	
ZDC-180	gactgggattgagataacagacctttttc agagaaatagggaatcatgcagctcaa agacgctca	pZD-LGC-31, pZD-LGC-32	
ZDC-181	ctaatgtcctgcagttggaatcaggcgat ttcagcgaagc	pZD-LGC-31	
ZDC-182	gcttcgctgaaatcgcctgattccaactg caggacattag	pZD-LGC-31	
ZDC-183	tggcggttcttcttgttcattcaaccagtct cctgaacct	pZD-LGC-32, pZD-LGC-34	
ZDC-184	gaccaactgcgacgaccacc		davB
ZDC-185	ggtggtcgtcgcagttggtc		davB
ZDC-186	gcagacgtcgctgaatgcgg		davB
ZDC-187	ccgcattcagcgacgtctgc		davB
ZDC-188	gccctggtcgagctggc		davD
ZDC-189	gccagctcgaccagggc		davD
ZDC-190	gggccgcgaaggttccaag		davD
ZDC-191	cttggaaccttcgcggccc		davD
ZDC-192	ccatcgcctcggtcgagc		davT
ZDC-193	gctcgaccgaggcgatgg		davT
ZDC-194	ggatggcagcttgctggcc		davA
ZDC-195	ggccagcaagctgccatcc		davA
ZDC-196	ctttttttcagagaaatagggaatcatgaa cgaacaatattccgc	pZD-LGC-19	
ZDC-197	ctaatgtcctgcagttggaattagccggt attacgcatac	pZD-LGC-19	
ZDC-198	gtatgcgtaataccggctaattccaactg caggacattag	pZD-LGC-19	
ZDC-199	gcggaatattgttcgttcatgattccctatt tctctgaaaaaag	pZD-LGC-19	
ZDC-200	ctggaaagccaccgatttgttcctg		ppc

ZDC-201	caggaacaaatcggtggctttccag		ppc
ZDC-202	cctgcgcgtaaccgaacagg		ppc
ZDC-203	cctgttcggttacgcgcagg		ppc
ZDC-204	ctttttttcagagaaatagggaatcatgtcg actcacacatcttc	pZD-LGC-20	
ZDC-205	ctaatgtcctgcagttggaattaggaaac gacgacgatca	pZD-LGC-20	
ZDC-206	tgatcgtcgtcgtttcctaattccaactgc aggacattag	pZD-LGC-20	
ZDC-207	gaagatgtgtgagtcgacatgattcccta tttctctgaaaaaag	pZD-LGC-20	
ZDC-208	cgaaattgcgccagcacagc		pyc
ZDC-209	caaggatctgccactgccac		pyc
ZDC-210	ctgttgacggtgcttccgca		pyc
ZDC-211	ccactgcttgttcgcctggatg		pyc
ZDC-212	caacgaggtggagtgcgaggt		pyc
ZDC-213	cagcttccttaacaaacgcgcgg		pyc
ZDC-214	cgccagctccgcctgg		pyc
ZDC-215	caccggtgagatcaagaacctctgg		pyc
ZDC-216	ctttttcagagaaatagggaatcatgtct aaaggtgaagaattattca	pZD-LGC-17	
ZDC-217	ctaatgtcctgcagttggaattatttgtaca attcatccatacca	pZD-LGC-17	
ZDC-218	tggtatggatgaattgtacaaataattcca actgcaggacattag	pZD-LGC-17	
ZDC-219	tgaataattcttcacctttagacatgattcc ctatttctctgaaaaaag	pZD-LGC-17	
ZDC-220	ATAATGGTACCGGTGAT ACCAGCATCGTCTTGAT GCCCTTGGCAGCACCCT GCTAAGGAGGCAACAAG atgtctaaaggtgaagaattat	pZD-LGC-05	
ZDC-221	AAGGGCATCAAGACGAT GCTGGTATCACCGGTAC CATTATACGAGCCGATG ATTAATTGTCAATTCGA AACCGGTaccggtatccggcgg	pZD-LGC-05	
ZDC-222	GTATAATGGTACCGGTG ATACCAGCATCG		P_{conII}-Riboswitch-F
ZDC-223	CGATGCTGGTATCACCG GTACCATTATAC		P_{conII}-Riboswitch-F
ZDC-224	GCTAAGGAGGCAACAAG ATGAACGTTATTGCAAT ATTGAATCAC	pZD-LGC-29	
ZDC-225	GTGATTCAATATTGCAA TAACGTTCATCTTGTTGC CTCCTTAGC	pZD-LGC-29	

ZDC-226	CTGCCCTTTTTCTTTAAA ACCACCGGTTTCGAATT GACAAT	pZD-LGC-30, pZD-LGC-34	
ZDC-227	ATTGTCAATTCGAAACC GGTGGTTTTAAAGAAAA AGGGCAG	pZD-LGC-30, pZD-LGC-34	
ZDC-228	cgccgccgccggataccggtgcgacg agagggctgcgagc	pZD-LGC-26, pZD-LGC-27	
ZDC-229	gctcgcagccctctcgtcgcaccggtat ccggcggcggcg	pZD-LGC-26, pZD-LGC-27	
ZDC-230	aggttcaggagactggttgaatgattatc ttcaccttacgcc	pZD-LGC-23, pZD-LGC-30	
ZDC-231	ctaatgtcctgcagttggaattagcgatct ttacgccacg	pZD-LGC-23	
ZDC-232	cgtggcgtaaagatcgctaattccaactg caggacattag	pZD-LGC-23	
ZDC-233	ggcgtaaggtgaagataatcattcaacc agtctcctgaacct	pZD-LGC-23, pZD-LGC-30	
ZDC-234	gaaaactgtaagcccaggcgagg		sapB
ZDC-235	gttgggctgctaccggatcac		sapF
ZDC-242	ctcagtcctaggtataatgctagcatctat actggaagagagtcaattcagggtggtg aatatgtctaaaggtgaagaattattca	pZD-LGC-03	
ZDC-243	actctcttccagtatagatgctagcattat acctaggactgagctagctgtcaagaatt accggtatccggcggcg	pZD-LGC-03	
ZDC-244	gtcaattcagggtggtgaatatgagttct gccaagaagat	pZD-LGC-24	
ZDC-245	tttgtacaagaaagctgggtttaatgtgc gttagacgcgg	pZD-LGC-24	
ZDC-246	ccgcgtctaacgcacattaaacccagctt tcttgtacaaa	pZD-LGC-24	
ZDC-247	atcttcttggcagaactcatattcaccacc ctgaattgac	pZD-LGC-24	
ZDC-248	gtcaattcagggtggtgaatatgcagctc aaagacgctca	pZD-LGC-31, pZD-LGC-33	
ZDC-249	tttgtacaagaaagctgggttcaggcgat ttcagcgaagc	pZD-LGC-31	
ZDC-250	gcttcgctgaaatcgcctgaacccagctt tcttgtacaaa	pZD-LGC-31	
ZDC-251	tgagcgtctttgagctgcatattcaccac cctgaattgac	pZD-LGC-31, pZD-LGC-33	
ZDC-252	caccaccctgaattgactctcttcc		P_{J23119}
ZDC-253	tcgccttttttctctgcgtaaaattcttgaca gctagctca	pZD-LGC-27	
ZDC-254	tgagctagctgtcaagaattttacgcaga gaaaaaggcga	pZD-LGC-27	
ZDC-255	tgcacctgcgtaaaggctgaaattcttga	pZD-LGC-33	

	cagctagctca		
ZDC-256	tgagctagctgtcaagaatttcagccttta cgcaggtgca	pZD-LGC-33	
ZDC-257	CCTGCTAAGGAGGCAAC AAGatgaactccatgagccaagc	pZD-LGC-34	
ZDC-258	tttgtacaagaaagctgggtttaattggc gttgcgggcaa	pZD-LGC-34	
ZDC-259	ttgcccgcaacgccaattaaacccagctt tcttgtacaaa	pZD-LGC-34	
ZDC-260	gcttggctcatggagttcatCTTGTT GCCTCCTTAGCAGG	pZD-LGC-34	
ZDC-261	ggaaacccaaatagttgtacagcgacac		ynfM
ZDC-262	gggattaattttgccgcttgtcccc		ynfM
ZDC-263	gtcaattcagggtggtgaatatgtcgact cacacatcttc	pZD-LGC-21	
ZDC-264	gaagatgtgtgagtcgacatattcaccac cctgaattgac	pZD-LGC-21	
ZDC-267	ggaagagagtcaattcagggtggtg		P_{J23119}
ybjE_fwd_int _check	cacgttaattttgctacttttcc		ybjE
ybjE_rev_int _check	ggaaaagtagcaaaattaacgtg		ybjE
lysC_fwd_int _check	cgcgatgttcaggcacagtg		lysC
lysC_rev_int _check	cactgtgcctgaacatcgcg		lysC
cgmA_fwd_i nt_check	ctgcacgccatatgcctcttc		cgmA
cgmA_rev_in t_check	gaagaggcatatggcgtgcag		cgmA
yc054	tgctggtattacccatggtatggatg		yemGFP
yc057	tctacggagaccgcagcatgac		nonspecific
yc059	agggactggctttcagccatg		pANS

APPENDIX B

ESTIMATED NITROGEN PRESENT UNDER STANDARD MEDIA CONDITIONS AND NITROGEN CONSUMPTION AT 48 AND 120 HOURS INTO CULTURING UTEX 2973 HARBORING PZD-LGC-13

Nitrogen Inputs (BG-11)	mg/L N
17.6 mM $NaNO_3$	246.4
0.021 mM ferric ammonium citrate	1.5
Total:	247.9

Nitrogen Consumed (48 h)	mg/L N
2.36 g/L biomass‡	266.7
256.4 mg/L L-lysine	49.1
Total:	315.8

Nitrogen Consumed (120 h)	mg/L N
1.59 g/L biomass‡	179.7
556.3 mg/L L-lysine	106.5
Total:	286.2

‡ Percentage of nitrogen in biomass was estimated to be 11.3% based off of work involving PCC 6803[164].

APPENDIX C

GROWTH AND L-LYSINE PRODUCTION OF UTEX 2973 HARBORING PZD-LGC-13 UNDER NITROGEN-SUPPLEMENTED CONDITIONS

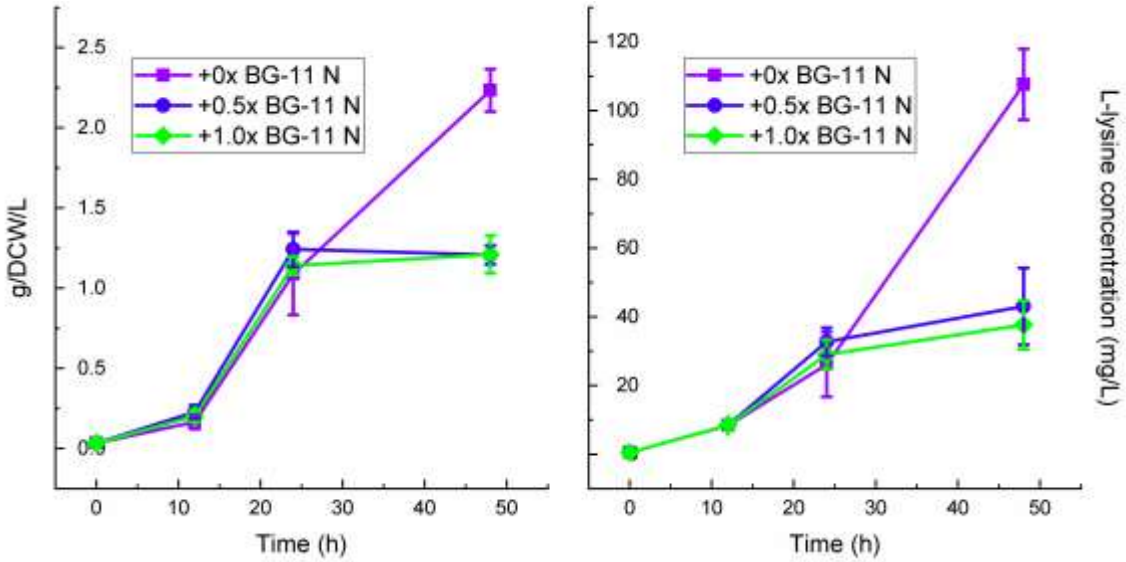

Comparing cell growth (left) and extracellular L-lysine accumulation (right) by engineered UTEX 2973 strains over the course of 120 hours when grown in shake flasks containing 25 mL BG-11 and varying amounts of nitrogen sulfate added to the media. Multipliers of BG-11 N represent molar equivalents of molecular nitrogen present in BG-11 (1 equivalent = 17.72 mmol N). Nitrogen equivalent amounts used were 0x (purple squares), 0.5x (blue circles), and 1.0x (green diamonds. Light intensity was increased from standard conditions to 500 µmol photon m^{-2} s^{-1} at 12 hours into culturing. Error bars represent standard error from biological triplicates.

APPENDIX D

GROWTH OF UTEX 2973 HARBORING PZD-LGC-34

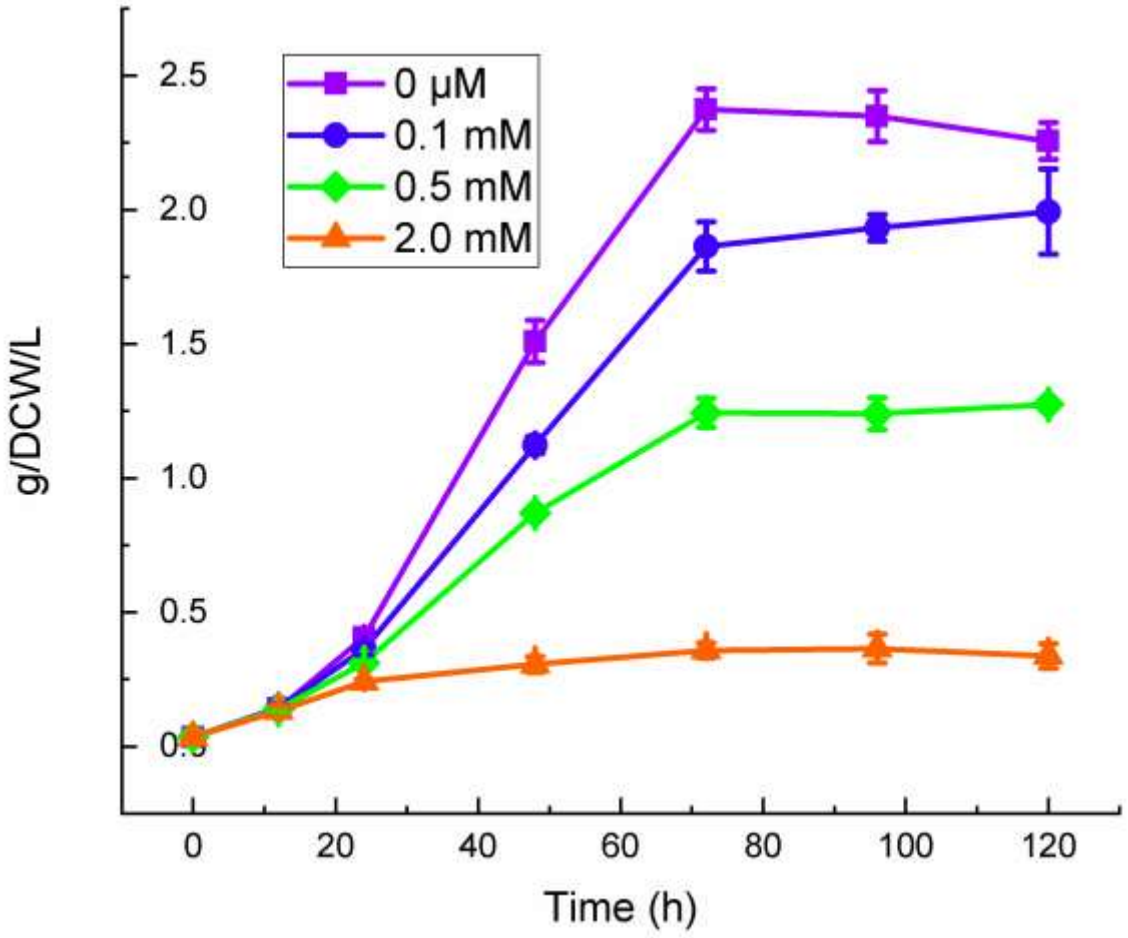

Accumulation of biomass by UTEX 2973 harboring pZD-LGC-34 in shake flasks containing 25 mL BG-11 at varying concentrations of theophylline. Theophylline concentrations used were 0 mM (purple squares), 0.1 mM (blue circles), 0.5 mM (green diamonds) and 2.0 mM (orange triangles). Theophylline was introduced into sample flasks at 12 hours into culturing. Error bars represent standard error from biological triplicates.